SAINT PETERSBURG STATE UNIVERSITY

PETERSBURG NUCLEAR PHYSICS INSTITUTE
NAMED BY B.P. KONSTANTINOV OF NATIONAL RESEARCH CENTRE
"KURCHATOV INSTITUTE"

Prosniak Sergei Dmitrievich

Quantum-mechanical study of atomic-molecular systems for nuclear properties analysis

Specialization 1.3.3. Theoretical physics

Dissertation is submitted for the degree
of Candidate of Physical and Mathematical Sciences
Translation from Russian

Scientific supervisor:
Skripnikov Leonid Vladimirovich
Cand. Sci. (Phys.-Math)

Saint Petersburg
2024

Contents

Introduction

Relevance of the research topic.

As a result of advances in the development of modern spectroscopy techniques in recent decades, the accuracy of experiments on atomic-molecular systems has been greatly improved. As a result, the requirements to the theoretical interpretation of such experiments have also increased, and there is a need for quantum-mechanical calculations at a new level of accuracy. One of the experiments where such calculations are required for the interpretation of measurement results are experiments aimed at determining nuclear magnetic dipole moments. Magnetic moments of nuclei are interesting for different fields of physics from several points of view. First, by comparing experimental values with the results of nuclear structure calculations, one can test the nuclear models. Furthermore, the value of the magnetic moment is necessary to calculate the hyperfine splitting in the spectra of ions, atoms, and molecules. Comparison of theoretical and experimental hyperfine structure constants is a reliable way to check the accuracy of the calculation of the electronic wave function near the nucleus for atoms [1–5] and molecules [6–14]. It is necessary for estimation of the calculation uncertainty of other quantities necessary for modern physics but inaccessible for direct measurement. Among such quantities are the enhancement factor of the electric dipole moment (EDM) of the electron, the scalar-pseudoscalar interaction constant, the parameters of the axionlike particle (ALP)-induced $\mathcal{T}$, $\mathcal{P}$-violating electron-nuclear interaction, and other characteristics describing possible sources of $\mathcal{T}$, $\mathcal{P}$-parity violation in atomic-molecular systems [1,5,15–23]. It is equally important to know the magnitude of the magnetic moment of the nucleus for testing quantum electrodynamics (QED) using experiments with highly charged ions [24]. For example, the inaccurate value of the magnetic moment of the Bi nucleus given in standard tables of nuclear data with an underestimated uncertainty led to the so-called “hyperfine puzzle” [25]. The specific difference, i.e. the combination of the

hyperfine structure (HFS) constants of the hydrogen-like and helium-like ions chosen to exclude the effects of finite nucleus size, measured in the experiment, turned out to be different from that predicted by QED theory for bound states. It has been suggested that there may even be "New Physics" behind it. However, the point turned out to be that in determining the magnetic moment of the ^{209}Bi nucleus, the shielding constant calculated in a rather rough approximation was used, which was not taken into account in the final uncertainty. In the paper [26] it was proposed to carry out an experiment on another system for which a reliable theoretical calculation was possible. As a result, with the refined magnetic moment, the theoretical and experimental specific differences coincided within the uncertainty limits. The puzzle was solved successfully.

One of the main methods for measuring the magnetic moment of stable nuclei is nuclear magnetic resonance (NMR) spectroscopy with atomic-molecular systems [27]. Since the nucleus in such a system is surrounded by electrons, it is partially shielded from the external magnetic field. Thus, in order to determine the magnetic moment from the experimental data, it is necessary to know the shielding constant. To calculate it from first principles, a precise quantum-chemical calculation [26, 28, 29] is necessary.

In the case of short-lived nuclei, it is difficult to perform NMR experiments. However, the magnetic moment of the short-lived isotope can be determined if the magnetic moment of the stable isotope is known, as well as theoretical and experimental data on the hyperfine splitting in the spectra of the considered atoms [30–37]. Furthermore, to achieve high accuracy, it is necessary to know with high precision the magnetic moment of the stable isotope, as well as to take into account the hyperfine magnetic anomaly, a special combination of the hyperfine constants and g-factors of the isotopes under consideration. The theoretical calculation of this quantity is a rather complicated problem and the result strongly depends on the choice of the nuclear model and its parameters. However, this problem can be

solved by measuring the hyperfine constants for the two electronic states of the isotopes under consideration and calculating the anomaly ratio for these states. The latter quantity turns out to be quite stable in theoretical calculations with different nuclear models. However, it is necessary to take into account the effects of interelectron correlation by performing a precise quantum-chemical calculation.

No less interesting property of the atomic nucleus is its rms charge radius. This quantity is widely used in various calculations, including quantum-chemical ones. Comparison of the experimental value and the result of theoretical calculations is a good test for methods of atomic nuclei structure modeling [38–41]. Moreover, the selected modeling method should not only reproduce absolute values with an acceptable uncertainty, but also make it possible to obtain the dependence of the radius on the number of neutrons observed in experiments for a chain of isotopes of one element. Based on the type of this dependence in a chain of isotopes of one element, it is possible to conclude about the changes in the shape and structure of the nucleus when the number of neutrons changes. The chain of mercury isotopes [42–46] is a notable example. For even number of neutrons ($N = 102, 104, 106$) the shape of the nucleus is close to spherical, and for odd number of neutrons ($N = 101, 103, 105$) it is strongly deformed (quadrupole deformation parameter $\beta \approx 0.3$). As a result, the dependence of the charge radius on the number of neutrons is "sawtooth". Observing a similar dependence for any other nucleus, it will be possible to conclude that there also exists "shape staggering". Moreover, it is possible to set constraints on the properties of nuclear matter [47] if the radii of the isotopes of some elements are known with high precision.

For stable nuclei, there are several methods for experimental determination of charge radii [48]. However, applying them to measure the radii of short-lived nuclei is currently difficult. In this case, the main method of determining charge radii is based on experiments that measure isotope shifts in the optical spectra of neutral atoms. To determine the radii from the obtained data, a precise quantum-chemical

calculation of the field and mass shift constants is required.

Another interesting property of the nucleus for physics is its sensitivity to axions and axionlike particles. These hypothetical particles can be a solution to many unsolved problems. For example, they appear in the Peccei – Quinn solution to the strong $\mathcal{CP}$ problem [49–51] and various compactifications of string theory [52, 53]. In addition, these particles are popular dark matter candidates [54–56], and may also be the source of $\mathcal{T}$, $\mathcal{P}$-parity violation in atomic-molecular systems. Therefore, a lot of theoretical and experimental studies have been devoted to their search. A summary of constraints on the properties of axions and axionlike particles obtained in laboratory and astrophysical experiments can be found in Ref. [57]. One of the experiments in which it is possible to set a constraint on the coupling constant of the nucleus-ALP interaction are experiments searching for the electron EDM [58]. More precisely, from the experimental data one can set a constraint on the product of the coupling constants of the ALP-nucleus interaction and the ALP-electron interaction. For this, however, it is necessary to calculate the molecular parameters of this interaction, determined by the electronic structure of the molecule used in the experiment, using the methods of quantum chemistry.

Elaboration of the topic.

The contribution of the finite charge distribution of the nucleus to the hyperfine structure constant was first considered in Ref. [59]. Then, in the paper of Bohr and Weisskopf [60], the contribution arising from a finite distribution of magnetization over the nucleus was theoretically investigated. Due to these corrections, the direct proportionality between the hyperfine structure constants and the nuclear g-factors is violated. This effect is widely known as the hyperfine magnetic anomaly. In many cases, when the measurement accuracy of hyperfine structure constants is not high enough, this effect is neglected. However, nowadays, for a number of systems such an approximation is not always accurate enough. As mentioned above, a direct theoretical calculation of the anomaly is rather complicated [61]. Therefore, in

Refs. [30,62], a method for determining the magnetic moment of a short-lived isotope using the magnetic moment of a stable isotope, which does not require calculation of the anomaly itself, was proposed. However, this method requires the calculation of the anomaly ratio for the two electronic states, as well as the measurement of the hyperfine structure constants of the two isotopes in the electronic states under consideration. For thallium isotopes, such an approach was applied, for example, in Ref. [33]. Another task in this study was to take into account the contribution of the finite nucleus magnetization distribution effect to the nuclear magnetic moment shielding constant in the NMR experiment. To our knowledge, this effect has not been previously considered anywhere in the framework of precision calculation using the coupled cluster method.

Advances in spectroscopy have greatly improved the accuracy of measuring isotope shifts in the optical spectra of neutral atoms. Modern experimental methods make it possible to measure them with a relative uncertainty ranging from 0.05% to 2% depending on the element under consideration (see, for example, Refs. [38–40, 63, 64]). However, field and mass shift constants are required to determine charge radii from experimental data. As a result, the calculation accuracy requirements for these constants have increased, and it became necessary to perform quantum-mechanical calculations with a detailed analysis of the uncertainty. Nevertheless, for numerous elements, values with no specified uncertainty at all are used in the interpretation of the experiment. The empirical uncertainty estimate for the field shift constant, namely "of 10% to 30%" proposed by Otten [65], far exceeds the experimental uncertainty achieved. The mass shift in many cases is only qualitatively estimated [48], and its uncertainty can exceed 100%. Although such an accuracy of constants calculation does not qualitatively change the physical picture when considering isotopic chains, the accuracy turns out to be important in other cases, for example, when considering isotonic chains. As a result, it became necessary to develop methods for calculating isotope shift constants with an accuracy correspon-

ding to that of modern experiments and a rigorous analysis of the theoretical uncertainty.

Another goal of this dissertation was to reinterpret experiments searching for a $\mathcal{T}$, $\mathcal{P}$-parity violating electron EDM in atoms and molecules in terms of constraints on the products of the interaction coupling constants of the ALP with the nucleus and with the electron. The experiment searching for the electron EDM with neutral atoms was first proposed by Salpeter in Ref. [66]. Then in the papers [67, 68] it was discovered that the observed effect can be enhanced in heavy atoms. So far many experiments have been carried out with various atoms and molecules [1]. A nonzero EDM was not detected, but the EDM constraint became increasingly stringent as they were performed. The most accurate electron EDM limitation to date was established in the experiment [69] with the molecular cation HfF^+: $|d_e| = 4.1 \times 10^{-30}\ e \cdot \text{cm}$. As mentioned above, electron-nuclear and electron-electron interactions induced by axions and axionlike particles can be another source of $\mathcal{T}$, $\mathcal{P}$-symmetries violation in atoms and molecules. The first direct calculations of this effect for atoms and atom-based estimates for molecules were carried out in Ref. [58]. First-principles calculations for the Fr atom and the YbOH molecule were performed in Refs. [70–72]. This allowed one to establish constraints on the products of the interaction coupling constants of the nucleus with the ALP and the electron with the ALP for different masses of the ALPs. Note that in the paper [71] devoted to the study of the YbOH molecule, calculations were performed only for ALP masses close to 1 MeV. For some ALP models, this is quite sufficient [73–75]. Nevertheless, all ALP masses are of interest from the physics point of view [76, 77]. Generalization of direct calculation methods of the effect for molecules in the case of ALPs heavier than 1 MeV has not been carried out up to the present thesis. The molecular cation HfF^+ is of particular interest for the theoretical study of the effect. For this system, direct molecular calculations of the $\mathcal{T}$, $\mathcal{P}$-parity violating interaction induced by the ALPs have not been performed before.

Goals and objectives of the paper. The main goal of the research is to develop methods for the theoretical study of atomic-molecular systems to analyze the properties of nuclei. The paper solved the following objectives:

1. Development of methods for calculating the correction for the finite distribution of the nucleus magnetization to the hyperfine splitting of atoms, which is necessary for the interpretation of experiments to determine the magnetic dipole moment of short-lived nuclei from spectroscopic experiments.

2. Development of methods for calculation of isotope shift constants for neutral atoms necessary for determination of charge radii of short-lived isotopes.

3. Simulation of $\mathcal{T}, \mathcal{P}$-violating axionlike-particle-mediated interactions in molecules. Determination of constraints on the product of the interaction coupling constants of axionlike particles with atomic nuclei and electrons.

Scientific novelty. In this work, we propose methods to calculate the Bohr – Weisskopf correction using various models of the magnetization of the nucleus with simultaneous consideration of interelectron correlation effects at the level of the relativistic coupled cluster method for neutral atoms. This allowed one, in particular, to demonstrate the correctness of the hypothesis about the sufficient independence of the ratio of hyperfine magnetic anomalies on the choice of the nuclear model based on the example of the thallium atom. This fact was used in the determination of magnetic moments of short-lived thallium isotopes. For the first time, within the framework of the relativistic coupled cluster method, the effect of finite magnetization distribution over the nucleus was taken into account in the calculation of the shielding constant of the nuclear magnetic moment in a molecule for the problems of interpretation of nuclear magnetic resonance experiments.

The methods used in the calculation of isotope shifts in highly charged ions have been adapted for application to neutral atoms using high-precision coupled

cluster methods up to accounting for quadruple amplitudes. This allowed one to perform relativistic calculations with simultaneous consideration of the interelectron correlation and detailed analysis of the theoretical uncertainty.

For the first time for the molecular cation HfF^+, the molecular parameters of the $\mathcal{T}$, $\mathcal{P}$-violating axionlike-particle-mediated interaction have been calculated from first principles using the relativistic coupled cluster method. The calculations were carried out for a wide range of axionlike particle masses. They allowed one to set more accurate constraints on the product of the interaction coupling constants of axionlike particles with nuclei and electrons.

Theoretical and practical significance. In the dissertation work we have developed methods of calculation of the hyperfine structure constant taking into account the finite distribution of the nucleus magnetization and interelectron correlation by the coupled cluster method for neutral atoms. They can be used to interpret future spectroscopic experiments aimed at determining the magnetic moments of short-lived nuclei. The theoretical approach used to calculate the finite magnetization distribution correction to the shielding constant of the magnetic moment of a nucleus in a molecular NMR experiment can be used to more accurately determine the magnetic moments of stable nuclei. In addition, the approaches developed for calculating isotope shift parameters can be applied to determine the charge radii of short-lived isotopes from spectroscopic experimental data. The programs written for modeling the electron-nucleus axionlike-particle-mediated $\mathcal{T}$, $\mathcal{P}$-violating interaction can be used to interpret new experiments searching for electron EDM in terms of constraints on the coupling constants of this interaction.

The reliability of the obtained results is confirmed by comparison with other theoretical works and experimental data, as well as by rigorous testing and verification of the programs developed to perform the calculations. The results of the research have been published in leading peer-reviewed journals and discussed at several national and international conferences.

Approbation of the research. The findings of the research were reported and discussed at the following conferences:

1. International Youth Conference PhysicA.SPb/2017, October 24 – 26, 2017, Saint Petersburg, Russia.
2. IV All-Russian Youth Scientific Forum "Open Science 2017", November 15 – 17, 2017, Gatchina, Leningrad Region, Russia.
3. 15th Russian Symposium "Foundations of Atomistic Multiscale Modeling and Simulation", August 15 – 26, 2018, New Athos, Abkhazia.
4. Workshop «Searching for New Physics with Cold and Controlled Molecules», November 26 – 30, 2018, Mainz, Germany.
5. 53-rd Winter School Petersburg Nuclear Physics Institute NRC "Kurchatov Institute", March 02 – 07, 2019, Roshchino, Leningrad Region, Russia.
6. XXVI International scientific conference of students and young scientists "Lomonosov-2019", 8 – 12 April 2019, Moscow, Russia.
7. International Conference on Precision Physics and Fundamental Physical Constants (FFK – 2019), June 9 – 14, 2019, Tihany, Hungary.
8. LXIX International Conference «Nucleus – 2019» on Nuclear Spectroscopy and Nuclear Structure «Fundamental Problems of Nuclear Physics, Nuclei at Borders of Nucleon Stability, High Technologies», July 1 – 5, 2019, Dubna, Moscow Region, Russia.
9. 16th Russian Symposium "Foundations of Atomistic Multiscale Modeling and Simulation", August 15 – 26, 2019, New Athos, Abkhazia.
10. VI All-Russian Youth Scientific Forum «Open Science 2019», November 13 – 15, 2019, Gatchina, Leningrad Region, Russia.
11. 54-th Winter School Petersburg Nuclear Physics Institute NRC "Kurchatov Institute", 10 – 15 March 2020, Roschino, Leningrad Region, Russia.

12. VII All-Russian Scientific Forum for Young Scientists “Open Science 2020”, 18 – 20 November 2020, Gatchina, Leningrad Region, Russia.
13. International Symposium on Molecular Spectroscopy, June 21 – June 25, 2021, (online)
14. The 3rd International Conference on HYPERFINE Interactions and their Applications (HYPERFINE 2021), 05 – 10 September 2021, poster (online)
15. VIII All-Russian Scientific Forum for Young Scientists “Open Science 2021”, 17 – 19 November 2021, Gatchina, Leningrad Region, Russia.
16. School-conference “Modern problems of Chemical Physics and Theoretical Chemistry”, 25 – 29 July 2022, Bolshye Koty, Irkutsk Region, Russia.
17. IV All-Russian Scientific Forum for Young Scientists with International Participation “Open Science 2022”, 16 – 18 November 2021, Gatchina, Leningrad Region, Russia.
18. All-Russian Scientific and Practical School-Conference with International Participation “Modern problems of Chemical physics, Theoretical Chemistry and experimental methods of materials research of modern power engineering”, 03 – 07 July 2023, Saint Petersburg, Russia.
19. XXXV Symposium “Modern Chemical Physics”, 18 – 28 September 2023, Tuapse, Krasnodar Krai, Russia.
20. The XXVII International Scientific Conference of Young Scientists and Specialists (AYSS-2023), 30 October – 03 November 2023, Dubna, Moscow Region, Russia.
21. X All-Russian Scientific Forum for Young Scientists with International Participation “Open Science 2023”, 15 – 17 November 2023, Gatchina, Leningrad Region, Russia.
22. 56-th Winter School Petersburg Nuclear Physics Institute NRC «Kurchatov Institute», March 17 – 22, 2024, Luga, Leningrad Region, Russia.

In addition, the intermediate results of the study were presented at scientific seminars of the Division of Quantum Mechanics, Department of Physics, Saint Petersburg State University and the Quantum Physics and Chemistry Department of the Advanced Development Division, NRC "Kurchatov Institute" – PNPI.

On the topic of the dissertation work, 4 computer programs are registered:

1. Computer program No. 2019613002 "Program for calculation of matrix elements of the Bohr – Weisskopf correction of the hyperfine splitting in atoms in the model of a uniformly magnetized nucleus". Date of registration: 05.03.2019.
   Right holder: NRC "Kurchatov Institute" – PNPI.
   Author: Prosnyak Sergey Dmitrievich.

2. Computer program No. 2020666971 "Program for calculation of matrix elements of the magnetization distribution correction to the hyperfine structure of heavy atoms in the one-particle nucleus model with Woods – Saxon potential". Date of registration: 18.12.2020. Right holder: NRC "Kurchatov Institute" – PNPI.
   Author: Prosnyak Sergey Dmitrievich.

3. Computer program No. 2024610108 "Program for calculation of matrix elements of normal mass shift operator". Date of registration: 09.01.2024.
   Right holder: NRC "Kurchatov Institute" – PNPI.
   Author: Prosnyak Sergey Dmitrievich.

4. Computer program No. 2024612074 "Program for calculating the specific mass shift correction to the nuclear recoil operator". Date of registration: 29.01.2024.
   Right holder: NRC "Kurchatov Institute" – PNPI.
   Author: Prosnyak Sergey Dmitrievich.

The results obtained within this research were presented in 8 articles in the peer-reviewed scientific journals recommended by the Higher Attestation Commission of the Russian Federation and/or included in the RSCI, Web of Science and Scopus databases:

1. Prosnyak S. D., Maison D. E., Skripnikov L. V. *Hyperfine structure in thallium atom: Study of nuclear magnetization distribution effects* // J. Chem. Phys. — 2020. — V. 152, no. 4. — P. 044301.

2. Prosnyak S. D., Skripnikov L. V. *Effect of nuclear magnetization distribution within the Woods-Saxon model: Hyperfine splitting in neutral Tl* // Phys. Rev. C. — 2021. — Mar. — V. 103. — P. 034314.

3. Prosnyak S. D., Maison D. E., Skripnikov L. V. *Updated Constraints on $\mathcal{T}$,$\mathcal{P}$-Violating Axionlike-Particle-Mediated Electron-Electron and Electron-Nucleus Interactions from HfF^+ Experiment* // Symmetry. — 2023. — V. 15, no. 5 — P. 1043.

4. Prosnyak S. D., Skripnikov L. V. *Axion-mediated electron-nucleus and electron-electron interactions in the barium monofluoride molecule* // Phys. Rev. A. — 2024. — V. 109, no. 4 — P. 042821.

5. Skripnikov L. V., Prosnyak S. D. *Refined nuclear magnetic dipole moment of rhenium:* ^{185}Re *and* ^{187}Re. // Phys. Rev. C. — 2022. — Nov. — V. 106., no. 5. — P. 054303.

6. Penyazkov G., Prosnyak S. D., Barzakh A. E. et al. *Refined theoretical values of field and mass isotope shifts in thallium to extract charge radii of Tl isotopes* // J. Chem. Phys. — 2023. — V. 158, no. 11. — P. 114110.

7. Cubiss J. G., Andreyev A. N., Barzakh A. E., Van Duppen P., Hilaire S., Péru S., Goriely S., Al Monthery M., Althubiti N. A., Andel B., Antalic S.,

Atanasov D., Blaum K., Cocolios T. E., Day Goodacre T., de Roubin A., Farooq-Smith G. J., Fedorov D. V., Fedosseev V. N., Fink D. A., Gaffney L. P., Ghys L., Harding R. D., Huyse M., Imai N., Joss D. T., Kreim S., Lunney D., Lynch K. M., Manea V., Marsh B. A., Martinez Palenzuela Y., Molkanov P. L., Neidherr D., O'Neill G. G., Page R. D., Prosnyak S. D., Rosenbusch M., Rossel R. E., Rothe S., Schweikhard L., Seliverstov M. D., Sels S., Skripnikov L. V., Stott A., Van Beveren C., Verstraelen E., Welker A., Wienholtz F., Wolf R. N., Zuber K. *Deformation versus Sphericity in the Ground States of the Lightest Gold Isotopes* // Phys. Rev. Lett. — 2023 — V. 131 — P. 202501.

8. Yue Z., Andreyev A. N., Barzakh A. E., Borzov I. N., Cubiss J. G., Algora A., Au M., Balogh M., Bara S., Bark R. A., Bernerd C., Borge M. J. G., Brugnara D., Chrysalidis K., Cocolios T. E., De Witte H., Favier Z., Fraile L. M., Fynbo H. O. U., Gottardo A., Grzywacz R., Heinke R., Illana A., Jones P. M., Judson D. S., Korgul A., Köster U., Labiche M., Le L., Lica R., Madurga M., Marginean N., Marsh B., Mihai C., Nácher E., Neacsu C., Nita C., Olaizola B., Orce J. N., Page C. A. A., Page R. D., Pakarinen J., Papadakis P., Penyazkov G., Perea A., Piersa-Siłkowska M., Podolyák Zs., Prosnyak S. D., Reis E., Rothe S., Sedlak M., Skripnikov L. V., Sotty C., Stegemann S., Tengblad O., Tolokonnikov S. V., Udías J. M., Van Duppen P., Warr N., Wojtaczka W. *Magnetic moments of thallium isotopes in the vicinity of magic* $N = 126$ // Phys. Lett. B. — 2024 — V. 849 — P. 138452.

Personal contribution of the author. The research was carried out on the basis of Saint Petersburg State University and NRC "Kurchatov Institute" – PNPI. All of the main findings submitted for defense were obtained personally by the applicant. If the used data were obtained during the joint work, to avoid ambiguity the author of the corresponding result is explicitly mentioned.

Structure of the thesis.

The thesis consists of Introduction, 4 Chapters, Conclusion, Acknowledgments, List of abbreviations and designations, Bibliography. The thesis contains 113 pages, 2 figures, 24 tables. The bibliography includes 214 items.

- The **introduction** describes the relevance of the research topic, the degree of its development, the goals and objectives of the dissertation work, its scientific significance and novelty, the applied research methods, as well as discusses the approbation of the work. In addition, the section concludes with the main scientific results and formulates the statements to be defended.
- In **Chapter 1** the methods used in this work for modeling the electronic structure of atoms and molecules are described, namely, the Dirac – Hartree – Fock method and the coupled cluster method. In addition, a description of the finite-field method used to calculate the properties of the systems under consideration is given.
- In **Chapter 2** we consider the calculation of the finite magnetization distribution correction to the hyperfine splitting in the optical spectra of neutral atoms. Various models of the nuclear magnetization distribution are used for the calculations. The obtained calculation results are used to refine the magnetic moments of short-lived thallium isotopes. In addition, the influence of the nuclear magnetization distribution on the shielding constant of the magnetic moment of the nucleus by electrons in the NMR experiment with the molecular anion ReO_4^- is estimated.
- In **Chapter 3** the calculation of constants characterizing isotope shifts in the optical spectra of neutral atoms is considered. The detailed description of the calculations for the gold atom is provided and the results for the thallium atom are briefly presented. The use of the results obtained for the interpretation of experiments on the refinement of charge radii is discussed.

- In **Chapter 4** the calculation of molecular parameters of the electron-nuclear and electron-electron $\mathcal{T}$, $\mathcal{P}$-violating axionlike-particle-mediated interactions is considered. Using the results of calculations and the data of experiments searching for the electron electric dipole moment on the molecular cation HfF^+, we improve the constraints on the product of the interaction coupling constants of axionlike particles with electrons and nuclei.
- The **conclusion** summarizes the main results and findings obtained in this dissertation work.

Principal scientific results.

1. The hyperfine structure constants were calculated taking into account the effect of a finite distribution of the magnetization of the nucleus within the framework of the model of a uniformly magnetized ball (Ref. [34], pp. 4 – 5; program [78]) and the single-particle model of the nucleus with the Woods – Saxon potential (Ref. [37], pp. 4 – 5; program [79]) with simultaneous consideration for the effects of electron correlation within the framework of the relativistic coupled cluster method for the $6p^2P_{1/2}$ and $6p^2P_{3/2}$ states of the neutral atom ^{205}Tl. All calculations, except for the Gaunt interaction contribution, were performed by the author of this thesis. The correction for the Gaunt interaction was calculated by D. E. Maison. Using the example of the $6p^2P_{3/2}$ state, it is shown that due to the effects of interelectron correlation, the Bohr – Weisskopf effect can make a significant contribution (more than 10%) to the hyperfine structure constant.
2. Using several models of the nuclear magnetization distribution, the ratio of hyperfine magnetic anomalies for the $7s^2S_{1/2}$ and $6p^2P_{1/2}$ states of several isotopes of the thallium atom has been calculated (paper [37], p. 5). Using the value obtained in the framework of the one-particle model with the Woods –

Saxon potential, the values of magnetic moments of short-lived thallium isotopes were determined (Ref. [37], p. 6; work [80], pp. 3 – 4 of main text and p. 2 of supplemental material).

3. In the framework of the one-particle model of the nucleus with the Woods – Saxon potential, a correction for the magnetization distribution over the nucleus to the magnetic moment shielding constant in the NMR experiment with the molecular anion ReO_4^- (Ref. [81], p. 4) has been calculated. The matrix elements of the interaction operator corresponding to this correction were calculated by the author of this thesis. Calculations of the electronic structure were carried out by L. V. Skripnikov. It is shown that this correction can be comparable or even exceed the contribution to the shielding constant from the solvent effect.

4. A scheme of high-precision calculations of isotope shift constants in neutral atoms and a detailed analysis of the theoretical uncertainty, as well as computer programs necessary for this purpose, have been developed (Ref. [82], pp. 2 – 6; programs [83, 84]). Using these programs, calculations of isotope shift parameters for the $6s^2S_{1/2} \to 6p^2P_{1/2}$ transition of gold atom and transitions $6p^2P_{3/2} \to 7s^2S_{1/2}$, $6p^2P_{1/2} \to 6d^2D_{3/2}$, $6p^2P_{1/2} \to 7s^2S_{1/2}$ of the thallium atom have been performed. The theoretical scheme and program code were designed by the author of the thesis. Numerical calculations of the isotope shift for the thallium atom were performed by G. Penyazkov.

5. The field and mass isotope shift constants for the gold atom $6s^2S_{1/2} \to 6p^2P_{1/2}$ transition were calculated, as well as the theoretical uncertainty of the obtained results was estimated (paper [85], p. 3 of main text and pp. 2 – 3 of supplemental material).

6. The molecular parameters of the $\mathcal{T}$, $\mathcal{P}$-violating axionlike-particle-mediated interactions in HfF^+ molecular cation have been calculated (paper [86], pp. 8 – 9;

paper [87], p. 3 of main text and p. 1 of supplemental material). Using these results, constraints on the product of the interaction coupling constants of axionlike particles with electrons and nuclei are established (paper [86], pp. 8 – 10; paper [87], p. 4 of main text and p. 1 of supplemental material). The calculation of the matrix elements of the operator of the $\mathcal{T}$, $\mathcal{P}$-violating axionlike-particle-mediated electron-nucleus interaction in the point nucleus approximation was carried out by D. E. Maison. A much more complicated calculation of the matrix elements of the $\mathcal{T}$, $\mathcal{P}$-violating electron-electron interaction operator, as well as the correction for the finite nucleus size of the electron-nuclear interaction operator was performed by the author of this dissertation. Correlation calculations were also performed by D. E. Maison.

In all the mentioned above articles, one of the co-authors is L. V. Skripnikov. He supervised the calculations, read and edited the texts of the articles before their publication.

Thesis statements to be defended.

1. It is demonstrated that the correction for the nucleus magnetization distribution to the hyperfine splitting in atoms and molecules can be calculated using a finite Gaussian basis set with sufficient accuracy for applications. This makes it possible to use modern quantum-chemical software packages using this type of basis sets to calculate the Bohr – Weisskopf correction. The first calculations were performed in which the Woods – Saxon model of magnetization distribution and the effects of electron correlation in the framework of the relativistic coupled cluster method were simultaneously considered.

2. The sufficient stability of the results of the calculation of the hyperfine magnetic anomalies ratio for the electronic states $7s^2S_{1/2}$ and $6p^2P_{1/2}$ of the Tl atom with respect to the choice of the model of magnetization distribution over the nucleus using the relativistic coupled cluster method has been numerically

demonstrated. Using the calculated ratio of hyperfine anomalies, the magnetic moments of short-lived isotopes of Tl have been refined.

3. For the first time for a molecule at the level of the relativistic coupled cluster method, the contribution of the effect of the finite distribution of the magnetization of the nucleus to the shielding constant of the magnetic moment of the nucleus by the electrons of the molecule in the NMR experiment has been calculated. Based on the example of the molecular anion ReO_4^-, it was found that this effect can give a significant contribution to the shielding constant (at the level of two percent).

4. Using the method developed in this study for calculating isotope shift constants and analyzing theoretical uncertainties, the values of atomic isotope shift parameters were obtained for the $6s^2S_{1/2} \to 6p^2P_{1/2}$ of the Au atom and transitions $6p^2P_{3/2} \to 7s^2S_{1/2}$, $6p^2P_{1/2} \to 6d^2D_{3/2}$, $6p^2P_{1/2} \to 7s^2S_{1/2}$ of the Tl atom with an accuracy that exceeds that of all previous theoretical studies.

5. Using the isotope shift constants calculated in this work for the $6s^2S_{1/2} \to 6p^2P_{1/2}$ transition of the Au atom, the charge radii of a number of short-lived Au isotopes have been determined, and the uncertainty due to the uncertainty of theoretical calculations has been estimated.

6. The experiment on the search for electron EDM on the molecular cation HfF^+ has been interpreted in terms of constraints on the product of the interaction coupling constants of axionlike particles with nuclei and electrons. A scheme for calculating the matrix elements of the $\mathcal{T}$, $\mathcal{P}$-violating electron-electron interaction operator has been developed, which also allows one to calculate the effect of $\mathcal{T}$, $\mathcal{P}$-violating electron-nucleus interaction induced by the exchange of an axionlike particle, taking into account the effect of the finite size of the nucleus.

Chapter 1.
Electronic structure modeling

Chapter 1 presents a brief review of the main methods used in this work to perform quantum chemical calculations. First, the Dirac – Hartree – Fock method [88] with the use of a Gaussian finite basis set is discussed, which provides an initial approximation for the electronic wave function as well as a set of virtual orbitals. Then, a brief introduction is given to the relativistic coupled cluster method [89,90], which can be used to model interelectron correlation effects with high accuracy. Next, the finite field method [91] is discussed, which allows one to calculate various properties of atoms and molecules. A detailed review of these methods can be found in the books [92–94].

1.1. Dirac – Hartree – Fock method

The most of considered in this dissertation atoms and molecules contain nuclei of heavy elements. In order to achieve the accuracy corresponding to modern experiments, it is necessary to take into account relativistic effects when modeling the electronic structure of such systems. In this regard, the Dirac – Hartree – Fock (DHF) method instead of the Hartree – Fock (HF) method, which is widely used for light elements, was applied to obtain the electronic wave function in the first approximation. One important difference between these two methods should be noted: when solving the Dirac equation using the DHF method, it is required to avoid "variational collapse" caused by the presence of a negative spectrum. For this purpose, when transforming the system of equations into a matrix problem, it is necessary to project the solutions onto a subspace with a positive spectrum.

The Hamiltonian of the electronic problem can be written in the following form:

$$\hat{H} = \Lambda_+ \left[\sum_{i=1}^{N} \hat{h} + \frac{1}{2} \sum_{i,j=1}^{N} V(\boldsymbol{r}_i - \boldsymbol{r}_j) \right] \Lambda_+, \tag{1.1}$$

where,

- $\hat{h}$ — one-electron Dirac Hamiltonian, taking into account the kinetic energy of electrons and their interaction with the nucleus;
- $V(\boldsymbol{r}_i - \boldsymbol{r}_j)$ — interelectron interaction potential (can be chosen either in the Coulomb, Gaunt or Breit approximation);
- Λ_+ — projector on positive spectrum states.

As in the case of the nonrelativistic problem, it is necessary to solve a system of integro-differential equations to obtain an approximate electron wave function:

$$\hat{h}^{DHF}(\boldsymbol{r})\psi_n(\boldsymbol{r}) = \varepsilon_n \psi_n(\boldsymbol{r}), \tag{1.2}$$

$$\hat{h}^{DHF}(\boldsymbol{r}) = \hat{h}(\boldsymbol{r}) + \hat{J}(\boldsymbol{r}) - \hat{K}(\boldsymbol{r}), \tag{1.3}$$

where ψ_n is a one-particle four-component spinor and the Coulomb and exchange terms are given by the following expressions:

$$\hat{J}(\boldsymbol{r})f(\boldsymbol{r}) = \sum_{m=1}^{N} \int d\boldsymbol{r'} \psi_m^\dagger(\boldsymbol{r'}) V(\boldsymbol{r} - \boldsymbol{r'}) \psi_m(\boldsymbol{r'}) f(\boldsymbol{r}), \tag{1.4}$$

$$\hat{K}(\boldsymbol{r})f(\boldsymbol{r}) = \sum_{m=1}^{N} \int d\boldsymbol{r'} \psi_m^\dagger(\boldsymbol{r'}) V(\boldsymbol{r} - \boldsymbol{r'}) f(\boldsymbol{r'}) \psi_m(\boldsymbol{r}). \tag{1.5}$$

The first N eigenfunctions of the Fock operator $\hat{h}^{DHF}$ with the lowest energy correspond to occupied electron orbitals, while the remaining ones correspond to

vacant ones. The unoccupied orbitals in the DHF approximation do not contribute to the ground state wave function, but they are used in the further accounting of interelectron correlation effects.

As a computational implementation of the DHF method, a relativistic analogue of the Rutan method was used. This method consists of expanding one-electron orbitals into a finite set of basis functions. The introduction of a finite basis set allows us to proceed from the solution of the system of integro-differential equations to the matrix spectral problem. Since the problem is relativistic and the solution is sought in the form of a bispinor, all its components are decomposed by basis functions. For the calculations in this thesis, Gaussian basis sets are used, which allows us to compute the two-electron integrals quite simply. In most cases, these sets were obtained by adding diffuse functions to the Dyall basis sets [95–100]. The method of constructing compact Gaussian basis sets (primarily for harmonics with $L = 4, 5, 6$) is described in detail in [14, 101]. We note separately that we used the Kramers-restricted version of the DHF method [88, 102, 103].

1.2. Coupled cluster method

In most cases in this thesis, the single-reference coupled cluster method is used to account for interelectron correlation effects. This method allows us to perform precision calculations for electronic states that can be described well enough by a single Slater determinant in the zero-order approximation. The method is based on the exponential ansatz:

$$|\Phi\rangle = \exp(\hat{T})|\Psi\rangle, \tag{1.6}$$

where:

- $|\Psi\rangle$ — reference determinant;
- $\hat{T}$ — total excitation operator;

- $|\Phi\rangle$ — wave function with electron correlation effects taken into account.

The excitation operator $\hat{T}$ can be written in the following form:

$$\hat{T} = \hat{T}_1 + \hat{T}_2 + \hat{T}_3 + \dots, \tag{1.7}$$

where the terms $\hat{T}_1$, $\hat{T}_2$,... denote the excitation operators of different orders:

$$\hat{T}_1 = \sum_{\substack{i \in occ \\ b \in virt}} t_i^b a_b^\dagger a_i; \quad \hat{T}_2 = \frac{1}{2!} \sum_{\substack{i_1 < i_2 \in occ \\ b_1 < b_2 \in virt}} t_{i_1 i_2}^{b_1 b_2} a_{b_1}^\dagger a_{b_2}^\dagger a_{i_2} a_{i_1}.$$

The scalar coefficients $t_{\dots}^{\dots}$ are called cluster amplitudes. They can be obtained by solving the cluster amplitude equations [89, 90]. $a_b^\dagger$ and a_i denote the creation and annihilation operators of the one-electron states b and i. The indices i_1, i_2... refer to occupied states, i.e., those included in the reference determinant $|\Psi\rangle$, and the indices $b_1, b_2, \dots$ refer to vacant (virtual) orbitals.

To obtain an explicit form of the wave function, the exponent must be decomposed into a series:

$$|\Phi\rangle = (1 + \hat{T}_1 + \hat{T}_2 + \dots + \frac{1}{2}(\hat{T}_1^2 + \hat{T}_2^2 + 2\hat{T}_1\hat{T}_2 + \dots) + \dots)|\Psi\rangle. \tag{1.8}$$

For convenience, the terms of the series corresponding to excitations of the same order are usually grouped together:

$$|\Phi\rangle = (1 + \hat{T}_1 + \frac{1}{2}\hat{T}_1^2 + \hat{T}_2 + \dots)|\Psi\rangle. \tag{1.9}$$

This series contains a huge but still finite number of terms, since it is impossible to excite more than N electrons in a system with N electrons. In practice, due to the computational complexity of the problem, it is usually limited to a small number of excitation orders to be considered. The most commonly used approximations are

denoted as follows:

- CCSD — Coupled cluster method with single and double excitations ($\hat{T} \approx \hat{T}_1 + \hat{T}_2$);
- CCSD(T) — Coupled cluster method with single and double excitations, as well as taking into account corrections to energy from triply excited states according to perturbation theory.

One of the main advantages of the coupled cluster method over other methods of accounting for electron correlation is its size consistency. It means that no matter how many terms of the series $\hat{T}_n$ are taken into account, the energy of a system consisting of several independent subsystems is equal to the sum of the energies of these subsystems.

In the case where the single-reference coupled cluster method is not applicable because the electronic state under consideration is described by a combination of determinants, we used the relativistic Fock space coupled cluster method (FS-CC). A detailed review of this method is presented in papers [104–107].

In practice, we used locally modified versions of the programs DIRAC15 [103, 108], MRCC [109–111], Exp-T [112,113] and HFD [114–116], which allow the calculation of various one-electron and two-electron properties using the finite field method.

1.3. Calculation of properties using the finite-field method

In this thesis, a finite-field method [91] is used to compute the expectation values of various operators. This method is based on the Hellmann – Feynman theorem, which can be formulated as follows. Consider a one-parameter set of Hamiltonians $\hat{H}(\lambda)$. Suppose that each Hamiltonian has a normalized to unity wave function and ground state energy:

$$\hat{H}(\lambda)\Psi_\lambda(x) = E(\lambda)\Psi_\lambda(x). \tag{1.10}$$

Then the energy derivative of λ can be calculated as follows:

$$\frac{\partial E(\lambda)}{\partial \lambda}\bigg|_{\lambda=0} = \langle\Psi|\frac{\partial \hat{H}(\lambda)}{\partial \lambda}|\Psi\rangle\bigg|_{\lambda=0}. \tag{1.11}$$

We can use this theorem to calculate the properties as follows. Let us add to the Hamiltonian of the system under consideration $\hat{H}_0$ a property operator $\hat{A}$ with an arbitrary factor λ: $\hat{H}(\lambda) = \hat{H}_0 + \lambda\hat{A}$. Then the expectation value of the operator can be calculated using the following formula:

$$\overline{A} = \frac{\partial E(\lambda)}{\partial \lambda}\bigg|_{\lambda=0}. \tag{1.12}$$

It should be noted that for nonvariational approximate wave functions the formula (1.12) is not absolutely accurate. The advantage of this method in comparison with the calculation using a one-electron density matrix is the simplicity of implementation. In the calculation by the finite-field method it is necessary to calculate only energy values at different values of the parameter λ, while in the calculation by means of the density matrix it is necessary to calculate it beforehand, which is a difficult task in the relativistic case.

Chapter 2.

Correction for the finite distribution of magnetization over the nucleus to the hyperfine structure

In Chapter 2 the influence of the effect of the finite distribution of the nucleus magnetization on the hyperfine splitting in atomic spectra is considered. First, tests for various hydrogen-like ions are provided. They showed good agreement with earlier studies [117, 118]. We then performed the calculation for the neutral Tl atom. The obtained hyperfine structure constants for the $6p^2P_{1/2}$ and $6p^2P_{3/2}$ states agree well with the experimental data from the papers [119, 120]. We then investigated the hyperfine magnetic anomaly. Using a direct calculation, we showed that the anomaly ratio for the electronic states $7s^2S_{1/2}$ and $6p^2P_{1/2}$ is quite stable with respect to the choice of the nuclear magnetization distribution model. The calculated value of the anomaly ratio was used to determine the magnetic moments of short-lived Tl isotopes. These results, obtained using the programs [78, 79], were first published in Refs. [34, 37, 80].

Then the contribution of the finite distribution of the nucleus magnetization to the shielding constant in the NMR experiment was investigated. On the example of the molecular anion ReO_4^- it was shown that the contribution of this effect is significant, it is larger than the solvent effect, which is often taken into account in theoretical studies. At the same time, the considered effect due to the finite magnetization distribution for molecules was not taken into account earlier in the framework of the precision calculation by the relativistic coupled cluster method. With the help of the shielding constant, taking into account the correction for the finite magnetization distribution, the magnetic moment of ^{185}Re and ^{187}Re nuclei

was refined. The results of the study were first published in the paper [81].

2.1. General theoretical information

2.1.1. Hyperfine splitting in the spectrum of hydrogen-like ions

Before proceeding to the consideration of the hyperfine structure in the spectra of neutral atoms, let us consider the hyperfine splitting in the spectrum of hydrogen-like ions. For this system, the hyperfine splitting energy of the ground electronic state can be written as follows [118]:

$$\Delta E = \frac{4}{3}\alpha(\alpha Z)^3 \frac{\mu}{\mu_N}\frac{m}{m_p}\frac{2I+1}{2I} mc^2\big(G(\alpha Z)(1-\delta)(1-\varepsilon)+x_{rad}\big) \qquad (2.1)$$

where α is the fine structure constant, Z — nuclear charge, μ — nuclear magnetic moment, μ_N — nuclear magneton, m — electron mass, m_p — proton mass, I — spin of the nucleus, c — speed of light, $G(\alpha Z)$ — relativistic factor [121, 122] and x_{rad} — correction due to QED effects. In addition, the equation (2.1) includes the Breit – Rosenthal (BR) correction δ due to the finite charge distribution over the nucleus and the Bohr – Weisskopf (BW) correction ε due to the finite magnetization distribution. In the model of a uniformly charged nucleus, the following analytical expression [121, 123] was obtained for the BR correction:

$$\delta = b_N \cdot R_c^{2\gamma-1}\ ,\ \gamma = \sqrt{\kappa^2-(\alpha Z)^2}, \qquad (2.2)$$

where b_N is a parameter independent of the structure of the nucleus, κ is the relativistic quantum number, R_c is the charge radius of the ball, related to the mean-square radius r_c by the relation $R_c = \sqrt{\frac{5}{3}}\cdot r_c$. Note that the dependence (2.2) can be applied to test the used numerical methods. The calculation of the BW correction is a more challenging problem, let's consider it in more detail.

To calculate the BW correction, it is necessary to choose a model of the magnetization distribution over the nucleus. In the single-particle approximation, the magnetization distribution is determined by a single valence nucleon. In the one-particle Woods – Saxon (WS) model, the wave function of a valence nucleon is defined as a solution of the Schrödinger equation with the WS potential [124, 125]:

$$U(r) = V(r) + V_C(r) + V_{SO}(r), \tag{2.3}$$

where

$$V(r) = -\frac{V_0}{1 + e^{(r-R_0)/a}}, \tag{2.4}$$

$$V_C(r) \;=\; \begin{cases} (Z-1)/r & r \geqslant R_C \\ (Z-1)(3 - r^2/R_C^2)/2R_C & r \leqslant R_C \end{cases}, \tag{2.5}$$

$$V_{SO}(r) = \lambda(\frac{\hbar}{2m_p c})^2 \frac{1}{r}\frac{d}{dr}\frac{V_0}{1 + e^{(r-R_{SO})/a}}\, \boldsymbol{\sigma} \cdot \boldsymbol{l}. \tag{2.6}$$

Here $R_C = \sqrt{5/3}\langle r_c^2\rangle^{1/2}$ is the charge radius of the nucleus, and $\langle r_c^2\rangle^{1/2}$ is the rms charge radius. Table 2.1 presents the WS potential parameters R_0, R_{SO}, a, V_0, and λ used in this work. The Coulomb term V_C must be excluded if the valence nucleon is a neutron. For further consideration, let us denote the orbital momentum of the valence nucleon by the letter L.

Table 2.1. The WS potential parameters [125] used in the calculations. The radii were given by the relations $R_0 = r_0 A^{1/3}$ and $R_{SO} = r_{SO} A^{1/3}$, where A is the mass number.

	r_0 (fm)	r_{SO} (fm)	a (fm)	V_0 (MeV)	λ
Proton	1.275	0.932	0.70	58.7	17.8
Neutron	1.347	1.280	0.70	40.6	31.5

In the single-particle WS model, the BW correction can be calculated using

the following relations [60, 126, 127]:

$$\varepsilon = \frac{g_S}{g_I}\left[\frac{1}{2I}\langle K_S\rangle + \frac{(2I-1)}{8I(I+1)}\langle K_S - K_L\rangle\right] + \frac{g_L}{g_I}\left[\frac{(2I-1)}{2I}\langle K_L\rangle + \frac{(2I+1)}{4I(I+1)}\frac{m_p}{\hbar^2}\langle \phi_{SO} r^2 K_L\rangle\right] \tag{2.7}$$

in the case $I = L + 1/2$ and

$$\varepsilon = \frac{g_S}{g_I}\left[-\frac{1}{2(I+1)}\langle K_S\rangle - \frac{(2I+3)}{8I(I+1)}\langle K_S - K_L\rangle\right] + \frac{g_L}{g_I}\left[\frac{(2I+3)}{2(I+1)}\langle K_L\rangle - \frac{(2I+1)}{4I(I+1)}\frac{m_p}{\hbar^2}\langle \phi_{SO} r^2 K_L\rangle\right] \tag{2.8}$$

in the case $I = L - 1/2$. In these equations, ϕ_{SO} denotes the radial part of the spin-orbit interaction $V_{SO} = \phi_{SO}\,\boldsymbol{\sigma}\cdot\boldsymbol{l}$, and g_I is the g-factor of the nucleus. The value $g_L = 1$ was used for the valence proton, and the value $g_L = 0$ was used for the valence neutron. The following relations were applied to determine g_S:

$$\frac{\mu}{\mu_N} = \frac{1}{2}g_S + \left[I - \frac{1}{2} + \frac{2I+1}{4(I+1)}\frac{m_p}{\hbar^2}\langle \phi_{SO} r^2\rangle\right] g_L \tag{2.9}$$

in the case $I = L + 1/2$ and

$$\frac{\mu}{\mu_N} = -\frac{I}{2(I+1)}g_S + \left[\frac{I(2I+3)}{2(I+1)} - \frac{2I+1}{4(I+1)}\frac{m_p}{\hbar^2}\langle \phi_{SO} r^2\rangle\right] g_L \tag{2.10}$$

in the case $I = L - 1/2$. The values of $\langle K_S\rangle$ and $\langle K_L\rangle$ were obtained by averaging the electronic functions $K_S(r)$ and $K_L(r)$ with the valence nucleon distribution density $|u(r)|^2$:

$$\langle K_{S,L}\rangle = \int_0^\infty K_{S,L}(r)\,|u(r)|^2\,r^2\,dr. \tag{2.11}$$

Since hydrogen-like ions are spherically symmetric, the functions $K_S(r)$ and

$K_L(r)$ can be calculated as follows:

$$K_S(r) = \frac{\int_0^r fg\, dr_{el}}{\int_0^\infty fg\, dr_{el}}, \tag{2.12}$$

$$K_L(r) = \frac{\int_0^r (1 - r_{el}^3/r^3) fg\, dr_{el}}{\int_0^\infty fg\, dr_{el}}, \tag{2.13}$$

where g and f are the radial components of the Dirac electron wave function. For the ground state of the $1s$ hydrogen-like ion, the following approximate expressions can be used [60, 121]:

$$K_S(r) = b\left[\frac{a_1}{2}\Big(\frac{r}{R_C}\Big)^2 + \frac{a_2}{4}\Big(\frac{r}{R_C}\Big)^4 + \frac{a_3}{6}\Big(\frac{r}{R_C}\Big)^6\right], \tag{2.14}$$

$$K_L(r) = 3b\left[\frac{a_1}{10}\Big(\frac{r}{R_C}\Big)^2 + \frac{a_2}{28}\Big(\frac{r}{R_C}\Big)^4 + \frac{a_3}{54}\Big(\frac{r}{R_C}\Big)^6\right]. \tag{2.15}$$

The expansion coefficients b and $a_{i=1,2,3}$ are given in the paper [121].

In addition to the WS model, the model of uniform distribution (UD) of the valence nucleon can be applied in the single-particle approximation. In this model, the nucleon distribution can be written as follows:

$$|u(r)|^2 = \frac{3}{R_C^3}\theta(R_C - r), \tag{2.16}$$

where $\theta(R_C - r)$ – Heaviside function:

$$\theta(R_C - r) = \begin{cases} 1, & \text{if } r < R_C; \\ 0, & \text{if } r > R_C. \end{cases} \tag{2.17}$$

The equations (2.7) and (2.8) are also used to calculate the BW correction in this

model, but in this case the spin-orbit interaction terms must be excluded.

2.1.2. Hyperfine structure in the spectrum of neutral atoms

In consideration of the hyperfine splitting in the spectrum of neutral atoms it is convenient to use the hyperfine structure constant A. Using this quantity, the energy of the hyperfine sublevel $E(F)$ with total momentum F can be written as follows:

$$E(F) = \frac{1}{2}\big(F(F+1) - I(I+1) - J(J+1)\big)A, \tag{2.18}$$

where I is the spin of the nucleus and J is the total momentum of all electrons of the atom. The transition energy between two neighboring sublevels ΔE can be written in the following form:

$$\Delta E = E(F) - E(F-1) = F \cdot A. \tag{2.19}$$

The hyperfine structure constant can be calculated by averaging the hyperfine interaction operator $\mathrm{H_{HFS}}$ with the electronic wave function Ψ:

$$A = \frac{1}{I \cdot M_J}\langle\Psi|\mathrm{H_{HFS}}|\Psi\rangle, \tag{2.20}$$

where M_J is the projection of the total electronic momentum J on the quantization axis.

In the theoretical study of the hyperfine constant A, a parameterization similar to that used in the consideration of the splitting energy of hydrogen-like ions can be used:

$$A = A'_0(1-\varepsilon)(1-\delta) + \Delta A_{QED}, \tag{2.21}$$

where A'_0 is the HFS constant for the point nucleus, ε is the Bohr – Weisskopf correction, δ is the Breit – Rosenthal correction, and ΔA_{QED} is the correction due

to QED effects.

When performing relativistic calculations in neutral atoms, it is more convenient to use a model of the nucleus with a finite charge distribution from the beginning. Therefore, in the present work the HFS constants in all cases have been calculated for a finite charge distribution of the nucleus. Thus, the calculations were performed without separation into the HFS constant in the point nucleus model A'_0 and the factor $(1-\delta)$, i.e., the following parameterization was used:

$$A = A_0(1-\varepsilon). \tag{2.22}$$

The ΔA_{QED} term is not included in this expression, since we neglected this contribution in the calculations of neutral atoms.

In addition, the approach proposed in Ref. [128] can be used to parameterize the HFS constant:

$$A = A_0(1-(b_N + b_M d_{nuc})R_c^{2\gamma-1}), \tag{2.23}$$

$$\varepsilon(R_c, d_{nuc}) = b_M d_{nuc} R_c^{2\gamma-1}, \tag{2.24}$$

where b_M is the electronic parameter independent of the model of the magnetization distribution over the nucleus, and d_{nuc} is the nuclear factor depending only on the properties of the considered nucleus.

In the point magnetic dipole (PMD) approximation, the hyperfine interaction of the electron with the magnetic moment of the nucleus $\boldsymbol{\mu}$ is given by the following operator:

$$\mathrm{H_{HFS}} = \frac{1}{c}\boldsymbol{\mu}\cdot\frac{(\boldsymbol{r}\times\boldsymbol{\alpha})}{r^3}, \tag{2.25}$$

where $\boldsymbol{r}$ is the electron radius-vector, $\boldsymbol{\alpha}$ are the Dirac matrices.

The following substitution [118, 129, 130] can be used to account for the finite

nuclear magnetization distribution:

$$\boldsymbol{\mu} \to \boldsymbol{\mu}(r) = \boldsymbol{\mu} F(r). \tag{2.26}$$

As can be noticed, in the PMD approximation $F(r) = 1$. In the case of a finite magnetization distribution over the nucleus, the function $F(r)$ inside the nucleus itself can be significantly different from 1. In the works [129–133] explicit expressions for various models of the magnetization distribution are given. The simplest model of a uniformly magnetized ball [34, 134–137] is most commonly used in the calculation of the BW correction in neutral atoms. In this model, inside a ball with radius $r_n = \sqrt{5/3}\, r_c$ (r_c — the root-mean-square charge radius) the function F is defined by the formula $F(r) = (r/r_n)^3$, and the outside remains equal to 1, as for the point dipole [131].

In the present dissertation, the single-particle model of the nucleus with the WS potential, discussed in detail above for hydrogen-like ions, has been used to perform calculations in neutral atoms. In this model the function $F(r)$ has the following form [129]:

$$\begin{aligned} F(r') = \frac{\mu_N}{\mu} \Bigg\{ & \int_0^{r'} r^2 |u(r)|^2 dr \left[\frac{1}{2} g_S + \right. \\ & \left. \left(I - \frac{1}{2} + \frac{2I+1}{4(I+1)} m_p \phi_{SO}(r) r^2 \right) g_L \right] + \\ & \int_{r'}^{\infty} r^2 \left(\frac{r'}{r} \right)^3 |u(r)|^2 dr \left[-\frac{2I-1}{8(I+1)} g_S + \right. \\ & \left. \left. \left(I - \frac{1}{2} + \frac{2I+1}{4(I+1)} m_p \phi_{SO}(r) r^2 \right) g_L \right] \right\} \end{aligned} \tag{2.27}$$

in the case $I = L + 1/2$ and

$$F(r') = \frac{\mu_N}{\mu}\left\{\int_0^{r'} dr r^2 |u(r)|^2 \left[-\frac{I}{2(I+1)} g_S + \left(\frac{I(2I+3)}{2(I+1)} - \frac{2I+1}{4(I+1)} m_p \phi_{SO}(r) r^2\right) g_L\right] + \int_{r'}^{\infty} r^2 \left(\frac{r'}{r}\right)^3 |u(r)|^2 dr \left[\frac{2I+3}{8(I+1)} g_S + \left(\frac{I(2I+3)}{2(I+1)} - \frac{2I+1}{4(I+1)} m_p \phi_{SO}(r) r^2\right) g_L\right]\right\} \tag{2.28}$$

in the case $I = L - 1/2$. Also, as for hydrogen-like ions, the calculation of the BW correction requires solving the Schrödinger equation for the valence nucleon with the WS potential (see details in subsection 2.1.1). As before, we assume $g_L = 1$ for the valence proton and $g_L = 0$ for the valence neutron. The parameter g_s is determined by the equations (2.9) – (2.10).

In addition to the one-particle model with the WS potential, we have considered a one-particle model with a uniform distribution of valence nucleon for neutral atoms. In this model, the valence nucleon density $|u(r)|^2$ is a constant inside the nucleus (see equations (2.16) – (2.17)), and when performing calculations using the equations (2.9) – (2.10) and (2.27) – (2.28) it is necessary to exclude the terms with spin-orbit interaction [121].

It should be noted that the BW contribution to the hyperfine structure constant of an atom or *molecule* has one interesting property. According to Ref. [14], the BW contribution to the HFS constant induced by a heavy nucleus can be factorized with very high accuracy (see equation (29) in Ref. [14]) into an electronic factor, E, and a factor depending on the nuclear magnetization distribution, N. As shown in Ref. [14], this factorization is valid for almost any electronic state, regardless of the methods used to account for electron correlation effects. In this case, the electronic factor depends only on the electronic state under consideration. At the same time,

the factor depending on the nuclear magnetization distribution does not depend on the electronic state. For example, in Ref. [14], the matrix element of the BW contribution operator over the $1s$-function of the corresponding hydrogen-like ion B_s was used as the nuclear factor. From the existence of factorization, it follows that at a given level of electronic structure theory the ratio of the two BW contributions calculated using two different models of the nuclear magnetization distribution is equal to the ratio of the nuclear parts and should not depend on the method of calculation of the electronic structure. Moreover, this ratio should not depend on the real electronic and charge states of the open-shell system under consideration (we do not consider here the situation when the HFS constant is determined exclusively by the electron in the electronic state with $j \geq 3/2$).

2.1.3. Hyperfine magnetic anomaly

In the point nucleus approximation, the ratio of the hyperfine structure constants of two different isotopes (denoted by numbers 1 and 2) in the same electronic state is proportional to the ratio of the nuclear g-factors of the isotopes. However, beyond this approximation, i.e., taking into account the finite size of the nucleus, this is not the case because of the BW and BR effects. The corresponding correction ${}^1\Delta^2$ is called the hyperfine magnetic anomaly:

$$ {}^1\Delta^2 = \frac{A_1 g_2}{A_2 g_1} - 1, \tag{2.29} $$

where A_1 and A_2 are the HFS constants [see equation (2.20)] for the considered electronic state, g_1 and g_2 are the nuclear g-factors of isotopes 1 and 2.

Let us consider how the hyperfine magnetic anomaly can be taken into account when determining the magnetic moments of short-lived isotopes [31–33, 35]. Let us denote the stable isotope by number 1 and the short-lived isotope — by number 2. If the magnetic moment of the stable isotope μ_1 and the hyperfine magnetic anomaly

${}^1\Delta^2[b]$ for some electronic state b are known, then the magnetic moment μ_2 of the short-lived isotope can be determined using the measured HFS constants A_1 and A_2 for this electronic state b:

$$\mu_2 = \mu_1 \cdot \frac{A_2[b]}{A_1[b]} \cdot \frac{I_2}{I_1} \cdot (1 + {}^1\Delta^2[b]). \tag{2.30}$$

The calculation of the anomaly ${}^1\Delta^2[b]$ directly is rather challenging, since the result obtained strongly depends on the nuclear model used and its parameters. Nevertheless, as we will see in the following, the result of calculating the anomaly ratio

$${}^1k^2[a,b] = {}^1\Delta^2[a]/{}^1\Delta^2[b] \tag{2.31}$$

for the two electronic states a and b turns out to be quite stable. Due to this fact, it is possible to determine the magnetic moment of a short-lived isotope. For this purpose, besides the theoretically calculated anomaly ratio ${}^1k^2[a,b]$, one needs experimental values of the hyperfine constants $A_{1,2}[a]$ and $A_{1,2}[b]$ for the electronic states a and b of the considered nuclei, as well as the magnetic moment of the stable isotope μ_1. For convenience, we introduce a quantity called the differential hyperfine magnetic anomaly ${}^1\theta^2[a,b]$ [30, 33]:

$${}^1\theta^2[a,b] = \frac{A_1[a]}{A_2[b]}\frac{A_2[a]}{A_1[b]} - 1 = \frac{1 + {}^1\Delta^2[a]}{1 + {}^1\Delta^2[b]} - 1. \tag{2.32}$$

Note that ${}^1\theta^2[a,b]$ does not depend on the spins and magnetic moments of the considered nuclei. As follows from the first equality in the equations (2.32), only experimental values of the hyperfine constants are required to determine ${}^1\theta^2[a,b]$. Using simple algebraic transformations, the following relation [31–33] can be obtained

from the equation (2.32):

$$^1\Delta^2[b] = \frac{^1\theta^2[a,b]}{^1k^2[a,b] - ^1\theta^2[a,b] - 1}. \tag{2.33}$$

The required magnetic moment of the short-lived isotope μ_2 can be determined by substituting the obtained value $^1\Delta^2[b]$ into equation (2.30).

Using the theory formulated in the paper [14], one can qualitatively describe the dependence of the anomaly ratio and differential anomaly on the choice of the nuclear magnetization distribution model. For convenience, let us rewrite the equation (2.22), emphasizing the correction for the finite charge distribution over the nucleus δ:

$$A = A_0(1-\varepsilon) = A'_0(1-\delta)(1-\varepsilon), \tag{2.34}$$

where A'_0 is the HFS constant in the point nucleus approximation. In this case, in the main order, the magnetic anomaly is determined by two terms arising from differences in the distribution of magnetization and charge over the nucleus:

$$^1\Delta^2 \approx {}^1\Delta^2_m + {}^1\Delta^2_c = \varepsilon_2 - \varepsilon_1 + \delta_2 - \delta_1. \tag{2.35}$$

For isotopes with different valence nucleon states, the magnetic term $(\varepsilon_2 - \varepsilon_1)$ gives the main contribution to the anomaly, while the charge term $(\delta_2 - \delta_1)$ can be neglected in this case, i.e., $^1\Delta^2 \approx \varepsilon_2 - \varepsilon_1$. Using factorization of the BW corrections [14] for heavy elements by the electronic factor E and the nuclear N, the following relation can be obtained:

$$^1\Delta^2[a] \approx \varepsilon_2[a] - \varepsilon_1[a] = E[a](N_2 - N_1). \tag{2.36}$$

As can be seen, the ratio of anomalies for the two electronic states depends on

the ratio of electronic factors:

$$^1k^2[a,b] = \frac{^1\Delta^2[a]}{^1\Delta^2[b]} \approx \frac{E[a]}{E[b]}. \tag{2.37}$$

In practice, small deviations from this equality can be observed, since it is obtained by neglecting the BR effect, which can be valuable if the BW corrections for the two considered isotopes are similar. Nevertheless, it can be assumed that the main contribution to the uncertainty in the calculation of the anomaly ratio comes from the uncertainty in the modeling of the electronic structure. Note also that the differential anomaly depends on both electronic and nuclear factors:

$$^1\theta^2[a,b] \approx {}^1\Delta^2[a] - {}^1\Delta^2[b] = (E[a] - E[b])(N_2 - N_1). \tag{2.38}$$

2.1.4. Contribution of the Bohr – Weisskopf effect to the nuclear magnetic moment shielding constant

Using molecular NMR experiment, the magnetic moment of the nucleus can be determined with high accuracy. However, due to shielding of the external magnetic field by the electrons of the molecule, the result of the measurements is the so-called uncorrected magnetic moment $\mu^{\text{uncorr.}}$. It is related to the magnetic moment of the nucleus μ by the following expression:

$$\mu = \mu^{\text{uncorr.}}/(1-\sigma), \tag{2.39}$$

where σ is the shielding constant. This constant is the isotropic part of the shielding tensor: $\sigma = 1/3 \sum_a \sigma_{a,a}$. The following expression can be used to determine the shielding tensor corresponding to the nucleus j in the considered molecule:

$$\sigma^j_{a,b} = \left.\frac{\partial^2 E}{\partial \mu_{j,a} \partial \mathrm{B}_b}\right|_{\boldsymbol{\mu}_j=0,\mathbf{B}=0}, \tag{2.40}$$

where E is the energy of the system, $\mu_{j,a}$ is the a component of the magnetic moment vector $\boldsymbol{\mu}_j$ of the j-th nucleus, B_b is the b component of the homogeneous external magnetic field vector $\mathbf{B}$.

In practical calculations, the interaction of electrons with the external magnetic field $\mathbf{B}$ and the hyperfine interaction with the magnetic moments of nuclei must be included in the Hamiltonian of the system. The interaction of electrons in a molecule with an external homogeneous magnetic field $\mathbf{B}$ can be described by the following operator included in the Dirac – Coulomb Hamiltonian:

$$\mathrm{H}_B = \mathbf{B} \cdot \frac{c}{2}(\boldsymbol{r}_G \times \boldsymbol{\alpha}), \tag{2.41}$$

where $\boldsymbol{\alpha}$ are the Dirac matrices, and $\boldsymbol{r}_G = \boldsymbol{r} - \boldsymbol{R}_G$, $\boldsymbol{R}_G$ is the coordinate system origin [93] from which the electron radius-vector in this equation originates. The hyperfine interaction between the electron and the magnetic moment $\boldsymbol{\mu}_j$ of the j-th nucleus in the PMD approximation can be written as follows:

$$\mathrm{H}_{\mathrm{HFS}} = \frac{1}{c}\boldsymbol{\mu}_j \cdot \frac{(\boldsymbol{r}_j \times \boldsymbol{\alpha})}{r_j^3}, \tag{2.42}$$

where $\boldsymbol{r}_j = \boldsymbol{r} - \boldsymbol{R}_j$, $\boldsymbol{R}_j$ is the coordinate of the j-th nucleus. Note that the interaction (2.25) does not account for the effect of the finite distribution of nuclear magnetization. However, using the same substitution [118, 129, 130] as for neutral atoms, the BW effect can be accounted for: $\boldsymbol{\mu} \to \boldsymbol{\mu}(r) = \boldsymbol{\mu}F(r)$.

2.2. Calculation of the finite magnetization distribution correction for the thallium atom

2.2.1. Calculation details

We used the charge radii for stable nuclei from the data tables [48]. For short-lived thallium isotopes, we used the radius values given in Ref. [138]. The magnetic moments of stable nuclei were found in the data tables [27], and those of short-lived thallium isotopes in Ref. [34]. For convenience, the values of all the above parameters are summarized in Table 2.2.

Table 2.2. The nuclear parameters used in the calculations are: valence nucleon state, magnetic dipole moment [26–28,34,81,139], and rms charge radius [48,138]. The values of magnetic moments used in previous works are presented in square brackets; they have been revised in recent works [26, 28, 81, 139].

Nucleus	State	μ_I/μ_N	$\langle r_c^2\rangle^{1/2}$ (fm)
^{185}Re	$2d_{5/2}$	3.1567(3)(12) [3.1871(3)]	5.3596
^{191}Tl^m	$1h_{9/2}$	3.79(2)	5.4310
^{193}Tl^m	$1h_{9/2}$	3.84(3)	5.4382
^{203}Tl	$3s_{1/2}$	1.62225787(12)	5.4666
^{205}Tl	$3s_{1/2}$	1.63821461(12)	5.4759
^{209}Bi	$1h_{9/2}$	4.092(2) [4.1106(2)]	5.5211

To obtain the wave function of the valence nucleon in the one-particle model of the nucleus with the WS potential, we numerically solved the radial Schrödinger equation on a grid. The program necessary for this was developed by the author of this thesis. The probability densities of the valence nucleon distribution for different nuclei obtained as a result of the solution are shown in Fig. 2.1. To obtain the electronic wave functions of hydrogen-like ions, we numerically solved the Dirac equation using a finite basis set of Gaussian functions. This set included 50 s-type functions with exponential parameters forming a geometric progression. The common ratio of this progression is 1.8, and the largest element – $5 \cdot 10^8$.

In the calculations of the HFS of a neutral thallium atom, the QED effects

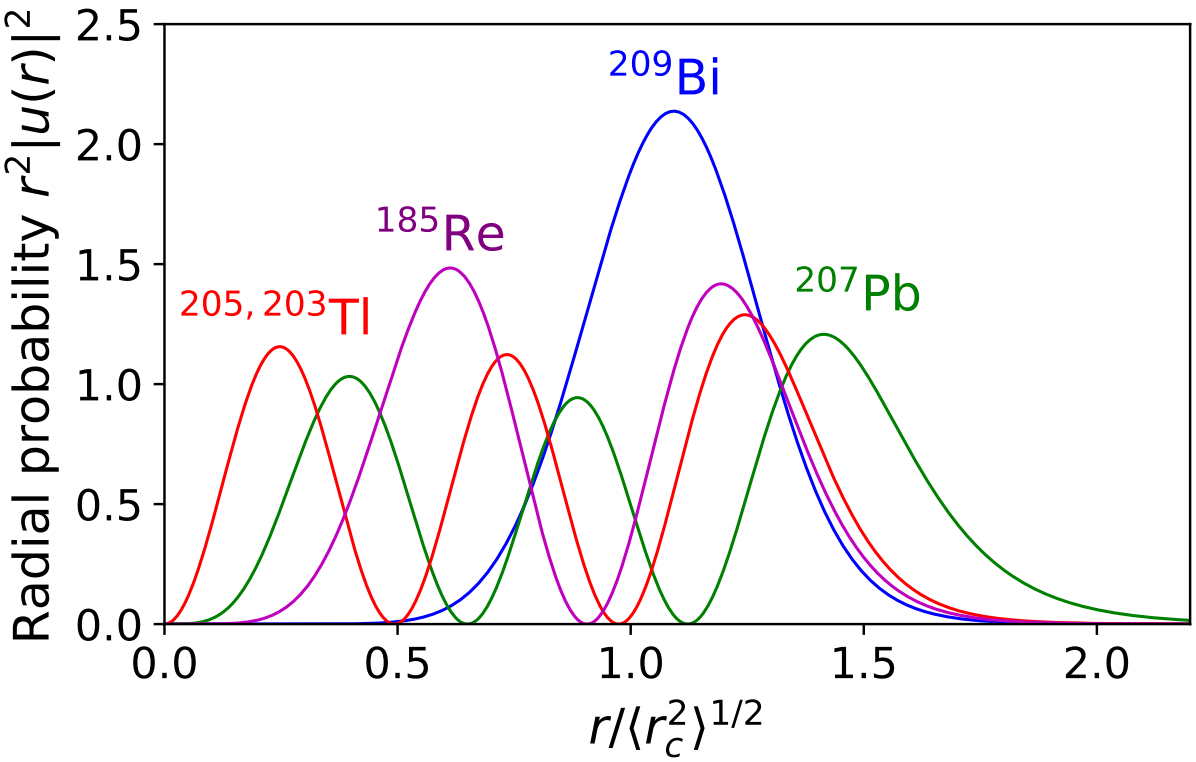

Figure 2.1. Radial probability densities of the valence nucleon distribution calculated for different nuclei. The densities of the isotopes ^{203}Tl and ^{205}Tl are labeled with one line because they are almost identical in the scale of the figure.

were not taken into account. The atomic orbitals necessary for the correlation calculations were obtained within the framework of the DHF method, where the Fock operator was determined by averaging over the $6p^1_{j=1/2}$ and $6p^1_{j=3/2}$ electron shell configurations for the $6p^2P_{1/2}$ and $6p^2P_{3/2}$ electronic states. The main correlation all-electron calculations were performed within the CCSD(T) [89, 90] method with the Dirac – Coulomb Hamiltonian. In these calculations we used the uncontracted basis set Dyall AAE4Z [98] augmented with one h and one i function. In total, this set consisted of $35s$, $32p$, $22d$, $16f$, $10g$, $5h$, and $2i$ functions. We will denote it by LBas later in this chapter. The energy of the virtual orbitals in these calculations was limited to 10000 E_h. Such a high energy constraint is important for a correct description of the behavior of the electron wave function near the atomic nucleus,

which was demonstrated in Refs. [10, 18]. After the main calculation, we calculated corrections for the incompleteness of the basis set and the effects of interelectron correlation beyond the CCSD(T) method. The correction for the finite basis set size was calculated within the CCSD(T) method using an extended basis set consisting of $44s$, $40p$, $31d$, $24f$, $15g$, $9h$, and $8i$ functions. In these calculations, the $1s - 3d$-electrons were excluded from the solution of the correlation problem, and the virtual orbitals were constrained from above to energies of 150 E_h. To evaluate the contribution of correlation effects to the HFS constant beyond the CCSD(T) method, we performed calculations using the CCSDT(Q) [110, 111, 140] method. In these calculations, we used the SBas basis set, which includes $30s$, $26p$, $15d$, and $9f$ functions. This set is an extended version of the CVDZ [95, 97] basis set, augmented with several diffuse functions. As in the calculation of the finite-size basis set correction, $1s - 3d$-electrons were excluded from the solution of the electron problem. The contribution of the Gaunt interaction to the hyperfine splitting was calculated by D. E. Maison with the CCSD(T) method using the SBas basis set in Ref. [34]. The code developed by L. V. Skripnikov in Ref. [141] was used to calculate the matrix elements of the hyperfine interaction operator in the PMD approximation. The code for performing calculations of HFS with finite nucleus magnetization distribution was developed by the author of this dissertation.

2.2.2. Hydrogen-like thallium ion

To verify the developed methods for calculating the BW correction in the single-particle model of the nucleus with the WS potential, calculations were carried out for a number of hydrogen-like ions. Table 2.3 summarizes the obtained values and compares them with the results obtained in previous works [117, 118]. As can be seen, the difference between the current and previous results is rather small. The difference can be explained by the use of different models of the charge distribution of

Table 2.3. Calculated values of the BW correction ε (in %) using the single-particle WS model for various hydrogen-like ions in the $1s$ ground electronic state. Without or with SO denotes whether or not the spin-orbit interaction is taken into account in the solution of the nuclear problem.

	$^{185}Re^{74+}$	$^{203}Tl^{80+}$	$^{205}Tl^{80+}$	$^{209}Bi^{82+}$
Ref. [117]	1.18	1.74	1.74	1.31
Ref. [118], eqs. (2.14), (2.15), without SO	1.20	1.77	1.77	1.33
Ref. [118], eqs. (2.14), (2.15), with SO	1.22	1.79	1.79	1.18
This work, eqs. (2.14), (2.15), without SO	1.20	1.78	1.78	1.29
This work, eqs. (2.14), (2.15), with SO	1.22	1.80	1.79	1.17
This work, eqs. (2.12), (2.13), without SO	1.30	1.87	1.87	1.43
This work, eqs. (2.12), (2.13), with SO	1.32	1.89	1.89	1.30
Experiment	1.34	2.21	2.23	1.02

the nucleus. In this research, the Gaussian charge distribution model was used [142], while in the previous ones the Fermi distribution model was used. The reason for using the Gaussian model in this work is that it allows one to perform calculations of HFS not only for neutral atoms, but also for molecules.

In addition to the theoretical results, Table 2.3 also presents the BW correction values obtained from the experimental data [143,144] using the following expression:

$$\varepsilon_{\rm exp} = 1 - \frac{(A^{\rm exp} - \Delta A^{\rm QED})}{\frac{\mu}{I\cdot M_J}\langle \Psi_{JM_J}|\frac{[\mathbf{r}_{el}\times\boldsymbol{\alpha}]_z}{r_{el}^3}|\Psi_{JM_J}\rangle}. \tag{2.43}$$

To calculate the denominator in this expression, we used the data from [118], as well as the latest values of nuclear magnetic moments. The contribution of QED effects was found in Refs. [118,145,146]. It should be noted that for the single-particle model there is a small dependence of the BW correction calculation result on the magnetic moment, since the parameter g_S depends on its value [see equations (2.7) – (2.10)]. Therefore, in order to compare the results, we used the same values of magnetic moments as used in previous works to calculate the BW correction for hydrogen-like ions. However, to determine the experimental value of the BW correction, we used the present-day values of the nuclear magnetic moments [26, 28, 139] (see

Table 2.2). In addition, we note that Table 2.3 shows that the approximate equations (2.14) and (2.15) provide a reasonably good approximation to the more accurate equations (2.12) and (2.13).

2.2.3. Hyperfine structure in a neutral thallium atom

Tables 2.4 and 2.5 present the results of the calculation of the HFS constants for the neutral ^{205}Tl atom in the $6p^2P_{1/2}$ ground electronic state and the $6p^2P_{3/2}$ first excited state. The second column presents the results in the PMD approximation. The third column presents the results in the uniformly magnetized ball model [34]. The last column presents the results obtained within the single-particle model with the WS potential. These values were obtained using the equation (2.27) for one-electron matrix elements. From Tables 2.4 and 2.5, a good agreement between the results obtained in the uniformly magnetized ball model and the single-particle WS model can be found for ^{205}Tl. In addition to the full value of the HFS constants, the BW contribution, $-A^{\rm BW}$, is given separately in Tables 2.4 and 2.5 (see numbers in parentheses). As noted above, due to the factorization of the BW contribution by the electronic and nuclear factors, the ratio of the BW contributions calculated in different models of the magnetization distribution should not depend on the electronic state under consideration and the method of electronic structure modeling. According to our results, for the $6p^2P_{1/2}$ and $6p^2P_{3/2}$ states of neutral Tl and $1s^2S_{1/2}$ states of hydrogen-like Tl, this hypothesis is indeed confirmed (with an uncertainty less than 1%).

The main source of the uncertainty in the calculation of the HFS constant for the $6p^2P_{1/2}$ state is the neglect of QED effects. For the ground state of hydrogen-like Tl [118, 143], as well as for the already studied heavy neutral systems [3], the QED contribution to the HFS constant is less than 1%. Based on this, one can expect that the contribution of QED effects to the HFS constant for the $6p^2P_{1/2}$ state is

Table 2.4. Calculated values of the hyperfine structure constant (in MHz) of a neutral thallium atom ^{205}Tl in the $6p^2P_{1/2}$ electronic state using various nuclear models and electronic theory methods. The contribution of the BW effect $-A^{\rm BW}$ is given in parentheses.

Method	PMD	Ball	WS
DHF	18805	18681	18696
		(−124)	(−109)
CCSD	21965	21807	21826
		(−158)	(−139)
CCSD(T)	21524	21372	21390
		(−152)	(−134)
+Basis corr.	−21	–	–
+CCSDT − CCSD(T)	+73	–	–
+CCSDT(Q) − CCSDT	−5	–	–
+Gaunt	−83	–	–
Total[a]	21488	21337	21354

[a]Instead of missing corrections, the values of contributions obtained in the point dipole model were used (given in the first column).

of the same order of magnitude. The uncertainty in accounting for interelectron correlation effects can be estimated as the contribution of perturbative quadruple cluster amplitudes. The contribution to the uncertainty due to the incompleteness of the basis set can be estimated as the value of the basis set correction. Taking into account all the contributions discussed above, the final theoretical uncertainty for the $6p^2P_{1/2}$ state is no more than 1% of the full value of the HFS constant. Thus, the results of calculations using the uniformly magnetized ball model and the single-particle WS model agree well with the experimental value of 21310.835(5) MHz [119] within the estimated uncertainty.

From Table 2.5 follows that in the case of the $6p^2P_{3/2}$ state, the *relative* contribution of correlation effects to the hyperfine structure constant is quite large, in contrast to the $6p^2P_{1/2}$ state. Nevertheless, the convergence in the level of accounting for the interelectron correlation effects was achieved in the calculations. Previous studies have also noted a strong *relative* contribution of correlation effects [135,147].

As can be seen from Table 2.5, the contribution of the perturbative quadruple cluster amplitudes to the HFS constant cannot be neglected. In addition, the significant correlation contribution explains the worse agreement between different theoretical values of the hyperfine structure constant (see Table 2.6). In the case of the $6p^2P_{1/2}$ state, the *relative* interelectron correlation contribution is much smaller (see Tables 2.4 and 2.5). Qualitatively, such a significant contribution of correlation effects to the HFS constant for the $6p^2P_{3/2}$ state can be explained by a small correlation admixture of configurations having much larger matrix elements of the hyperfine interaction operator compared to the leading configuration corresponding to the singly occupied $6p_{3/2}$ orbital. The latter matrix element is rather small, since the amplitude of the $6p_{3/2}$ orbital in the vicinity of the Tl nucleus is small. Note also that for the $6p^2P_{3/2}$ state the *absolute* value of the correlation effects contribution to the HFS constant is 1167 MHz. This is less than the absolute value of the contribution of correlation effects to the HFS constant of state $6p^2P_{1/2}$: 2651 MHz. However, in the case of the $6p^2P_{1/2}$ state, the contribution of correlation effects is not dominating, since the matrix element of the leading configuration corresponding to the singly occupied $6p_{1/2}$ orbital is much larger.

The calculated value of the BW correction for the ^{205}Tl atom in the $6p^2P_{3/2}$ state is -14% in the uniformly magnetized ball model and -12% in the WS model. Nevertheless, for both models the obtained value has the opposite sign with respect to the BW correction to the $6p^2P_{1/2}$ state hyperfine structure constant (see Table 2.7). Qualitatively, the following considerations can be used to explain such a significant magnitude of the BW correction and its sign. In the framework of the Kramers-restricted DHF method used in the present study as a starting approximation, the BW correction is negligibly small for the $6p^2P_{3/2}$ state, since the $6p_{3/2}$ orbital (the only one in the considered approximation capable of contributing to the HFS constant) has a negligible amplitude inside the nucleus. At the same time, in the framework of this approximation, the HFS constant is rather large: 1415 MHz (see

Table 2.5. Calculated values of the hyperfine structure constant (in MHz) of the neutral thallium atom ^{205}Tl in the $6p^2P_{3/2}$ electronic state using various nuclear models and electron theory methods. The contribution of the BW effect $-A^{\rm BW}$ is given in parentheses.

Method	PMD	Ball	WS
DHF	1415	1415	1415
CCSD	6	40	36
		(+34)	(+30)
CCSD(T)	244	273	269
		(+29)	(+25)
+Basis corr	+4	–	–
+CCSDT − CCSD(T)	−49	–	–
+CCSDT(Q) − CCSDT	+14	–	–
+Gaunt	+1	–	–
Total[a]	214	243	239

[a]Instead of missing corrections, the values of contributions obtained in the point dipole model were used (given in the first column).

Table 2.5). However, when correlation effects, including spin polarization of $1s..6s$ electrons, are taken into account, the picture changes. At this point, $s_{1/2}-$ and $p_{1/2}-$ functions can contribute to the BW correction and the HFS constant. As can be seen from the Table 2.5, the contribution of correlation effects, defined as the difference between the hyperfine structure constants obtained using the CCSD(T) and DHF methods, reduces the value at the DHF level by a factor of about 6. Also from Table 2.5 follows, that the absolute value of the correlation contribution to the HFS constant ΔA_{corr} decreases as one moves from the PMD model to models with finite magnetization distribution: $\Delta A_{corr}[\text{PMD}] = -1171$ MHz, $\Delta A_{corr}[\text{ball}] = -1142$ MHz, and $\Delta A_{corr}[\text{WS}] = -1146$ MHz. Note that the BW contribution is 29 MHz in the uniformly magnetized ball model and 25 MHz in the WS model, i.e., it reduces the absolute value of ΔA_{corr} in both models. This is similar to the pattern most often observed, where the BW correction decreases the absolute value of the HFS constant. However, to calculate the BW correction ε, the total value of the hyperfine structure constant is needed, i.e., the sum of the contribution at the DHF

level and the contribution of correlation effects, as is done everywhere in the present study. As noted above, for the $6p^2P_{3/2}$ state these contributions have opposite signs and largely compensate each other, which leads to a small value of the hyperfine structure constant and a huge value of the BW correction ε. According to the definition, the BW correction ε is inversely proportional to the HFS constant. Thus, in the limiting case of absolutely exact cancellation of the $6p_{3/2}$ orbital contribution and the correlation contribution, the BW correction would formally turn out to be infinite.

The results of calculations using the uniformly magnetized ball model and the WS model agree with the experimental value of 265.0383(1) MHz obtained in Ref. [120]. The uncertainty due to the choice of the magnetization distribution model can be estimated as the difference between the results in these models. It amounts to only a few MHz. Based on previous studies for heavy neutral systems [3], we expect the contribution of QED effects to be no more than a few percent. However, a theoretical study of the QED contribution to the HFS constant for the $6p^2P_{3/2}$ state of the Tl atom is of considerable interest. Taking into account the contribution of perturbative quadruple cluster amplitudes, as well as the correction for the incompleteness of the basis set, the total theoretical uncertainty can be estimated at the level of 10% of the final value. However, we also note that the total theoretical uncertainty is approximately 2% of the total contribution of correlation effects.

Table 2.6. Final values of the hyperfine structure constants in the PMD approximation for ^{205}Tl (in MHz) in comparison with previous studies.

	$6p^2P_{1/2}$	$6p^2P_{3/2}$
Ref. [148]	21053	–
Ref. [149]	21390	353
Ref. [147]	21430	317
This work	21488	214

Table 2.7. The calculated values of the BW correction ε (in %) to the HFS constants of the $6p^2P_{1/2}$ and $6p^2P_{3/2}$ states in ^{205}Tl.

Nuclear model	Ball	WS
$6p^2P_{1/2}$	0.7	0.6
$6p^2P_{3/2}$	−14	−12

Let us now proceed to the consideration of the hyperfine magnetic anomaly. The dependence of this quantity on the parameters of the nuclear model can be demonstrated most easily on the example of the model of a uniformly magnetized ball. For this purpose, we have performed a series of calculations of the magnetic anomaly $^{205}\Delta^{203}$ for the electronic states $6p^2P_{1/2}$ and $7s^2S_{1/2}$, varying the model root-mean-square magnetic radii r_m of the isotopes under consideration. In the calculations carried out for ^{203}Tl and ^{205}Tl, the experimental charge radii were used. The anomalies were calculated within the CCSD(T) method using the LBas basis set. The QED effects were not taken into account. Based on the results for hydrogen-like thallium, it can be assumed that the difference between the unknown QED corrections x_{rad} (see equation (2.1)) to the hyperfine constants is negligible for the isotopes considered. Therefore, the QED contribution to the anomaly can be neglected. The obtained dependencies of $^{205}\Delta^{203}$ on the difference of the squares of the model magnetic radii $^{205}r_m^2 - {}^{203}r_m^2$ are shown in the graphs 2.2(a) and 2.2(b). It should be noted that in this case r_m is only a parameter of the model. In addition to the theoretical dependence, the plots also show the experimental values of the hyperfine anomaly. They were obtained using the measured in Refs. [119,150] HFS constants of the electronic states $6p^2P_{1/2}$ and $7s^2S_{1/2}$, as well as the magnetic moment ratio from the Ref. [27]. The uncertainty of the magnetic anomaly $^{205}\Delta^{203}$ experimental value is of the order of 0.3% for the $6p^2P_{1/2}$ state and 24% for the $7s^2S_{1/2}$ state. In the graphs 2.2(a) and 2.2(b), the solid horizontal line indicates the experimental value and the dashed horizontal line indicates its uncertainty. By considering the intersection of the calculated dependence approximated by linear

functions with the horizontal dashed lines, one can extract the difference of the squares of the model magnetic radii $^{205}r_m^2 - {}^{203}r_m^2$ and its uncertainty. As noted above, the experimental value of the anomaly for the $7s^2S_{1/2}$ state is known with a significant uncertainty (see Fig. 2.2(b)). However, the value of the difference of the squared model magnetic radii $^{205}r_m^2 - {}^{203}r_m^2$, determined above from the data for the $6p^2P_{1/2}$ state, allows one to predict the value of the anomaly $^{205}\Delta^{203}[7s^2S_{1/2}] = -3.54(14)\cdot 10^{-4}$ with a smaller uncertainty. This value can be verified after a more precise experiment is conducted. The main conclusion that can be drawn from the consideration of Figs. 2.2(a) and 2.2(b) is that the magnetic anomaly indeed strongly depends on the parameters of the nuclear model used. Let us now proceed to the consideration of the anomaly ratio for the two states and the differential anomaly.

Table 2.8 presents the results of the calculation of the hyperfine magnetic anomalies ratios $^{205}k^x[7s^2S_{1/2}, 6p^2P_{1/2}]$, where x is ^{203}Tl, ^{193}Tl^m, or ^{191}Tl^m. These values were obtained using different methods of electronic structure calculation and three models of magnetization distribution over the nucleus: the uniformly magnetized ball model [34] and the single-particle UD and WS models. In the uniformly magnetized ball model, its radius was chosen to be equal to the charge radius. The values obtained in the different models are in fairly good agreement with each other. This fact confirms the considerations given above in subsection 2.1.3. Thus, the theoretically calculated ratio of hyperfine magnetic anomalies for a pair of electronic states can be used to determine the magnetic moments of short-lived isotopes. We also note that for stable thallium isotopes the effects of charge and magnetization distributions give comparable contributions to the anomalies, and therefore to their ratio. Nevertheless, for isotopes with different nuclear structure, e.g., with different valence nucleon states, the main contribution to the anomaly is contributed by the BW effect.

Table 2.9 presents the obtained values of the differential magnetic anomalies $^{205}\theta^x[7s^2S_{1/2}, 6p^2P_{1/2}]$ [see Eq. (2.32)], where x is ^{203}Tl, ^{193}Tl^m, or ^{191}Tl^m. For the

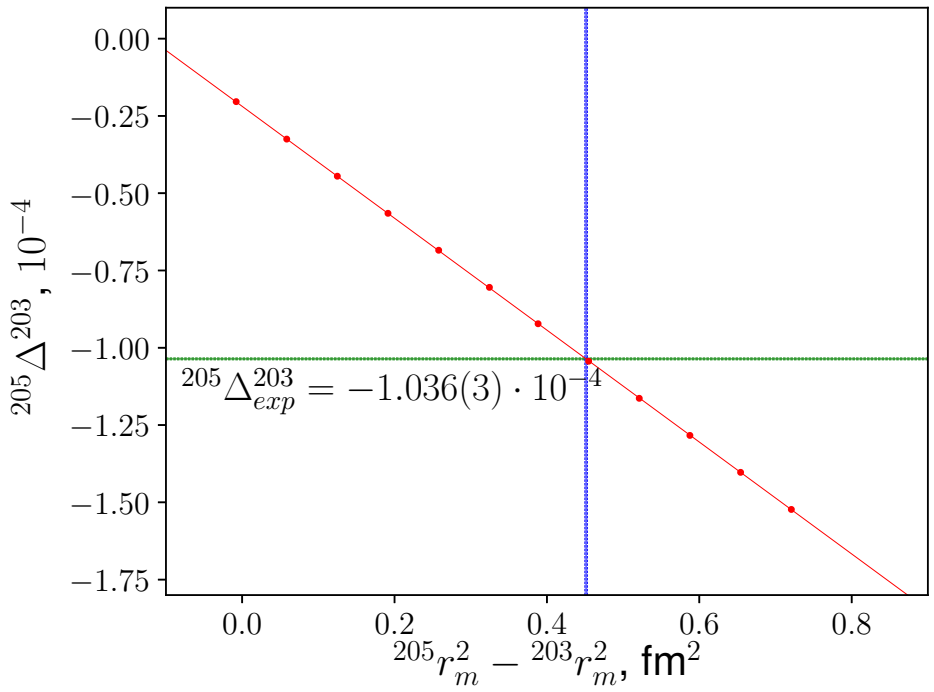

(a)

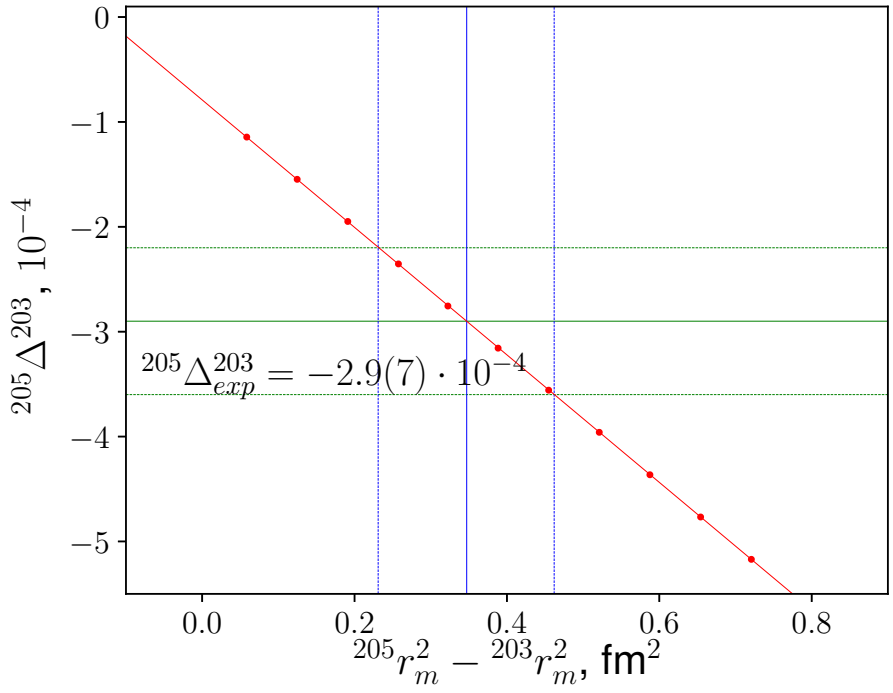

(b)

Figure 2.2. Calculated dependence of hyperfine magnetic anomalies $^{205}\Delta^{203}$ of (a) $6p^2P_{1/2}$ and (b) $7s^2S_{1/2}$ states on the difference of the squared model magnetic radii $^{205}r_m^2 - {}^{203}r_m^2$. Solid and dashed horizontal lines indicate the experimental value with its uncertainty [119, 150]; calculated values are indicated by dots and vertical lines show the fixed values of the difference of the squared model magnetic radii with the uncertainty.

Table 2.8. The ratio of the hyperfine magnetic anomalies $^{205}k^{x}[7s^2S_{1/2}, 6p^2P_{1/2}]$, where x is ^{203}Tl, ^{193}Tl^m, or ^{191}Tl^m. For the Ball and UD models the rms magnetic radius was chosen to be equal to the experimental rms charge radius.

Nucleus	Method	Ball	UD	WS
^{203}Tl	DHF	3.77	3.77	3.85
	CCSD	3.38	3.38	3.44
	CCSD(T)	3.47	3.47	3.54
^{193}Tl^m	DHF	3.73	3.55	3.54
	CCSD	3.36	3.23	3.22
	CCSD(T)	3.45	3.32	3.31
^{191}Tl^m	DHF	3.74	3.55	3.54
	CCSD	3.36	3.23	3.22
	CCSD(T)	3.46	3.32	3.31

calculations, as in the previous case, three models of the magnetization distribution over the nucleus were used: the model of a uniformly magnetized ball and the single-particle UD and WS models. The calculated values of the differential anomaly for the short-lived isotopes ^{193}Tl^m and ^{191}Tl^m are slightly smaller than the estimate $^{205}\theta^{x(I=9/2)}[7s^2S_{1/2}, 6p^2P_{1/2}] = -1.2 \cdot 10^{-2}$ obtained in Ref. [33]. This difference can be explained by the use of the effective value of the orbital g-factor of the valence nucleon $g_L = 1.16$ from Ref. [151] in Ref. [33]. At the same time, in the present work we used the value $g_L = 1.0$. To test this assumption, calculations were performed at the DHF level using the effective value of g_L from the article [151] and the corresponding value of g_S obtained using the Eqs. (2.9) and (2.10). The following results were obtained: $^{205}\theta^{x(I=9/2)}[7s^2S_{1/2}, 6p^2P_{1/2}] = -1.13 \cdot 10^{-2}$ and $^{205}\theta^{x(I=9/2)}[7s^2S_{1/2}, 6p^2P_{1/2}] = -0.95 \cdot 10^{-2}$ for the single-particle UD and WS models, respectively. Thus, the calculation results confirm the assumption.

As follows from Table 2.9, the accuracy of the differential magnetic anomaly calculation depends on the level of accounting for interelectron correlation effects less than for the ratio of magnetic anomalies. For stable thallium isotopes, i.e., for the differential magnetic anomaly $^{205}\theta^{203}[7s^2S_{1/2}, 6p^2P_{1/2}]$, the experimental values and the calculation results give the same order of magnitude. However, for the

Table 2.9. Differential hyperfine magnetic anomalies $^{205}\theta^{x}[7s^2S_{1/2}, 6p^2P_{1/2}]$, where x is ^{203}Tl, ^{193}Tl^m or ^{191}Tl^m, 10^{-4}. For the Ball and UD models, the rms magnetic radius was chosen to be equal to the experimental rms charge radius. The last column shows the experimental values [33, 119, 150].

Nucleus	Method	Ball	UD	WS	Experiment
^{203}Tl	DHF	−1.09	−1.09	−0.86	−1.9(8)
	CCSD	−1.05	−1.05	−0.83	
	CCSD(T)	−1.06	−1.06	−0.84	
^{193}Tl^m	DHF	−5.14	−93	−69	−129(62)
	CCSD	−4.92	−90	−66	
	CCSD(T)	−4.98	−91	−67	
^{191}Tl^m	DHF	−6.06	−96	−72	−154(60)
	CCSD	−5.80	−92	−69	
	CCSD(T)	−5.87	−93	−70	

short-lived isotopes ^{193}Tl^m and ^{191}Tl^m, the single-particle models of the nucleus allow one to obtain results much more accurately than the model of a uniformly magnetized ball. This fact can be explained as follows. The stable isotopes ^{205}Tl and ^{203}Tl have a similar nuclear structure with the valence nucleon in the $s_{1/2}$ state with zero orbital momentum (see Table 2.2). In this case, the single-particle UD model reduces to the model of a uniformly magnetized ball. This is not the case with the short-lived isotopes ^{193}Tl^m and ^{191}Tl^m with the valence nucleon state having nonzero orbital momentum. As a result, from Table 2.9 follows that it is necessary to use more complex models than the uniformly magnetized ball model to consider pairs of nuclei with different structure.

Table 2.10 presents the magnetic moments values obtained using the Eqs. (2.30) – (2.33) with the ratio of anomalies calculated in this work (see Table 2.8) and the experimental values of HFS constants from the paper [33]. For isotopes ^{193}Tl^m and ^{191}Tl^m, the anomaly ratios coincide within a given uncertainty. The remaining isotopes in Table 2.10 have a similar nuclear structure since they also have one valence proton in the $1h_{9/2}$ state. Therefore, the same anomaly ratio value, 3.31(10), was used for other isotopes. Following the work [33], we used the mean weighted value of experimental differential anomaly $^{205}\theta^{x(I=9/2)}[7s^2S_{1/2}, 6P_{1/2}] = -1.53(37) \cdot 10^{-2}$

in determination of the magnetic moments of the considered isotopes. The values obtained using this approach are presented in the third column of Table 2.10. Comparing these values with the results of the work [33] one can notice a good agreement between them. However, due to the difference in the used value of the anomaly ratio, the values are still different. In the present study, we used the one-particle model with the WS potential to determine the magnetic moments, and in the paper [33] the one-particle model with a uniform valence nucleon distribution from the paper [117] was used. Alternatively, one can use an approach in which the differential anomaly is determined for each isotope separately using the Eq. (2.32). For this purpose, we used the experimental values of the HFS constants $A_{205}[7s^2S_{1/2}] = 12296.1(7)$ from Ref. [150], $A_{205}[6p^2P_{1/2}] = 21310.835(5)$ from Ref. [119], and the hyperfine constants for short-lived thallium isotopes from Ref. [33]. The last column of Table 2.10 presents the results obtained with this approach. The obtained values of the magnetic moments agree well with the values $\mu(^{193}\mathrm{Tl}^m) = 3.84(3)\mu_N$ and $\mu(^{191}\mathrm{Tl}^m) = 3.79(2)\mu_N$ determined by the author of the dissertation in Ref. [34] using the same approach and the value of the anomaly ratio calculated in the model of a uniformly magnetized ball. Note that the main source of the uncertainty in the determination of magnetic moments is the experimental uncertainty in the measurement of the HFS constants of short-lived isotopes. Thus, using the theoretical data obtained in the present work, the values of magnetic moments can be refined after more accurate experiments.

In addition to the neutron-deficient Tl isotopes discussed above, measurements of the hyperfine constants for the isotopes $^{207}\mathrm{Tl}^g$ and $^{209}\mathrm{Tl}$ were carried out in work [80]. Since they have a similar nuclear structure to $^{203}\mathrm{Tl}$ with a valence proton in the $3s_{1/2}$ state, the value of the anomaly ratio $^{205}k^{203}[7s^2S_{1/2}, 6p^2P_{1/2}] = 3.54(14)$ calculated in this study (see Table 2.8) was used to interpret the experimental data. Using it, the magnetic moment values $\mu(^{207}\mathrm{Tl}^g) = 1.868(6)\mu_N$ and $\mu(^{209}\mathrm{Tl}) = 1.735(28)\mu_N$ were determined in Ref. [80].

Table 2.10. Magnetic moments $\mu(\mu_N)$ for short-lived thallium isotopes with $I = 9/2$ obtained using the theoretically calculated anomaly ratio in the WS model. In the last two columns, the first uncertainty corresponds to the experiment, and the second uncertainty corresponds to the accuracy of the theoretical calculation of the magnetic anomalies ratio.

Nucleus	Ref. [33]	This work[a]	This work[b]
$^{187}\mathrm{Tl}^m$	3.707(22)	3.710(22)(2)	3.687(38)(2)
$^{189}\mathrm{Tl}^m$	3.756(22)	3.758(22)(2)	3.764(42)(2)
$^{191}\mathrm{Tl}^m$	3.781(22)	3.783(22)(2)	3.785(24)(2)
$^{193}\mathrm{Tl}^m$	3.824(22)	3.827(22)(2)	3.841(25)(2)

[a]Values are obtained using the averaged differential anomaly value.
[b]Values are obtained using individual experimental values of differential anomalies.

2.3. Contribution of the finite magnetization distribution to the NMR shielding constant for the molecular anion $\mathbf{ReO_4^-}$

In the present thesis, the influence of the finite magnetization distribution over the nucleus on the shielding constant for the molecular anion $\mathrm{ReO_4^-}$ was investigated. For this purpose, the substitution given by the Eq. (2.26) in the hyperfine interaction operator (2.25) in the framework of the single-particle WS model discussed in subsection 2.1.1 was used. This involved the use of methods and computer code developed by the author of this thesis. Modeling of the electronic structure and calculation of other contributions to the shielding constant were performed by L. V. Skripnikov. The obtained results are given in Table 2.11. For both considered isotopes ^{185}Re and ^{187}Re, the contribution of the nuclear magnetization distribution was found to be almost the same and it does not differ in Table 2.11. As can be seen, the effect of the finite nuclear magnetization distribution (-73 ppm or 1.8% of the final value of σ) is more important than the solvent effect for the system under consideration. To the best of our knowledge, no previous attempts have been made to account the effect of the finite nuclear magnetization distribution on the shielding

Table 2.11. Calculated values of various contributions to the rhenium nucleus shielding constant σ for ReO_4^- in ppm.

Contribution	Value
Diamagnetic:	
QZQZ–LAO/PBE0	7633
Paramagnetic:	
TZTZ/108e–CCSD	−3741
TZTZ/108e–CCSD(T) − 108e–CCSD	350
DZDZ/24e–CCSDT − 24e–CCSD(T)	−81
Basis corr.	−10
Gaunt	15
Solvent effect, from Ref. [28]	−25
Finite magn. distribution (WS)	−73
Total	4069

constants in many-electron molecules using the relativistic coupled cluster method. However, studies with precision calculations have been carried out for hydrogen-like ions [152, 153].

Using the calculated value of the shielding constant with the finite magnetization distribution correction, the magnetic moments of rhenium isotopes were determined in Ref. [81]: $\mu(^{185}\mathrm{Re}) = 3.1567(3)(12)\mu_N$, $\mu(^{187}\mathrm{Re}) = 3.1891(3)(12)\mu_N$, where the first uncertainty is experimental and the second uncertainty is due to the theoretical uncertainty in the calculation of the shielding constant.

Chapter 3.

Isotope shift in atomic spectra

Chapter 3 is devoted to the study of isotope shifts in the optical spectra of neutral atoms. The chapter begins with a brief theoretical overview. Next, we proceed with testing of computer programs [83, 84] developed to calculate isotope shift parameters. To perform the tests, calculations were carried out for several lithium-like ions. The obtained parameter values are in good agreement with the results of the work [154]. In the following, we describe how all-electron calculations of the isotope shift parameters were performed for the $6s^2S_{1/2} \to 6p^2P_{1/2}$ transition of the neutral Au atom. The parameter values obtained in these calculations were then used to determine the rms charge radii from experimental data on isotope shift frequencies for a chain of short-lived isotopes of the Au atom. These results were first published in Ref. [85].

This chapter concludes with a consideration of isotope shifts in the Tl atom. Using the same approach as for the Au atom, the isotope shift parameters were calculated for the transitions $6p^2P_{3/2} \to 7s^2S_{1/2}$, $6p^2P_{1/2} \to 6d^2D_{3/2}$ and $6p^2P_{1/2} \to 7s^2S_{1/2}$ of the Tl atom. These parameters were then used to interpret the experiment. The details of the calculations and the results obtained were first published in Ref. [82].

3.1. General theoretical information

In this thesis, we used the following expression to parameterize the isotope shift of the transition energy $\Delta\nu^{A',A} = \nu^{A'} - \nu^{A}$:

$$\Delta\nu^{A',A} = (k_{\mathrm{NMS}} + k_{\mathrm{SMS}})(\frac{1}{M^{A'}} - \frac{1}{M^{A'}}) + \delta\left\langle r^2\right\rangle^{A',A}, \tag{3.1}$$

where k_{NMS}, k_{SMS} denote the normal and specific mass shift constants, F is the field shift constant, M^{A} and $M^{A'}$ are the masses of isotopes with mass numbers A and A', $\delta\left\langle r^2\right\rangle^{A',A} = \left\langle r^2\right\rangle^{A'} - \left\langle r^2\right\rangle^{A}$ is the difference of the mean-squared charge radii of the considered isotopes. It should be noted that such nuclear physical effects as deformation and polarization of the nucleus [154–156] can lead to the appearance of additional terms in the expression (3.1). Generally, the contribution of these terms is rather small and therefore we do not consider them in this study.

To calculate the field shift constant F, it is necessary to calculate the derivative $F = \partial\nu/\partial\left\langle r^2\right\rangle$. The mass shift constants k_{NMS} and k_{SMS} can be calculated using the following relativistic operators [157–160]:

$$H_{\mathrm{NMS}} = \frac{1}{2M}\sum_i(\boldsymbol{p}_i^2 - \frac{\alpha Z}{r_i}\left[\boldsymbol{\alpha}_i + \frac{(\boldsymbol{\alpha}_i\cdot\boldsymbol{r}_i)\boldsymbol{r}_i}{r_i^2}\right]\cdot\boldsymbol{p}_i), \tag{3.2}$$

$$H_{\mathrm{SMS}} = \frac{1}{2M}\sum_{i\neq k}(\boldsymbol{p}_i\cdot\boldsymbol{p}_k - \frac{\alpha Z}{r_i}\left[\boldsymbol{\alpha}_i + \frac{(\boldsymbol{\alpha}_i\cdot\boldsymbol{r}_i)\boldsymbol{r}_i}{r_i^2}\right]\cdot\boldsymbol{p}_k), \tag{3.3}$$

where Z is the charge of the nucleus, $\boldsymbol{\alpha}_i$ are the Dirac matrices acting on the i-th electron, and $\boldsymbol{r}_i$ is the position of the i-th electron. Note that H_{SMS} is a two-electron operator. This fact complicates practical calculations.

3.2. Testing of the developed calculation methods

In Ref. [154], different contributions to the mass shift constant for lithium-like ions were calculated. The so-called nonrelativistic (NR) and relativistic (R) parts were separated: $k_{\mathrm{NMS}} = k_{\mathrm{NRNMS}} + k_{\mathrm{RNMS}}$ and $k_{\mathrm{SMS}} = k_{\mathrm{NRSMS}} + k_{\mathrm{RSMS}}$. These constants can be calculated using the following operators included in the expressions (3.2) and (3.3):

$$H_{\mathrm{NRNMS}} = \frac{1}{2M}\sum_i \boldsymbol{p}_i^2, \tag{3.4}$$

$$H_{\mathrm{RNMS}} = \frac{1}{2M}\sum_i (-\frac{\alpha Z}{r_i}\left[\boldsymbol{\alpha}_i + \frac{(\boldsymbol{\alpha}_i\cdot\boldsymbol{r}_i)\boldsymbol{r}_i}{r_i^2}\right]\cdot\boldsymbol{p}_i), \tag{3.5}$$

$$H_{\mathrm{NRSMS}} = \frac{1}{2M}\sum_{i\neq k} (\boldsymbol{p}_i\cdot\boldsymbol{p}_k), \tag{3.6}$$

$$H_{\mathrm{RSMS}} = \frac{1}{2M}\sum_{i\neq k} (-\frac{\alpha Z}{r_i}\left[\boldsymbol{\alpha}_i + \frac{(\boldsymbol{\alpha}_i\cdot\boldsymbol{r}_i)\boldsymbol{r}_i}{r_i^2}\right]\cdot\boldsymbol{p}_k), \tag{3.7}$$

To verify the programs developed in this study, we performed test calculations separately with each operator (3.4) – (3.7) for different lithium-like ions and compared the obtained values with the results of Ref. [154]. Table 3.1 presents the comparison for the constant k_{NRNMS}, Table 3.2 for k_{RNMS}, Table 3.3 for k_{NRSMS}, and Table 3.4 for k_{RSMS}. In parentheses below the values calculated in this paper, the deviations with respect to the results of the work [154] in percent are given. As it can be seen, the maximum deviation is less than 2% in standard calculations and less than 1% with Gaunt interaction correction taking into account. This small difference can be explained by the fact that in the work [154] the Breit interaction was fully taken into account. Moreover, in calculations we used a finite Gaussian basis set based on Dyall [98,100,161] basis sets (which was not specifically optimized for the calculation of lithium-like ions) and a Gaussian nuclear charge distribution model [162]. At

the same time, a basis set of B-splines [154] and the Fermi model of the charge distribution over the nucleus were applied in Ref. [163]. Summarizing the above, we can conclude that the program code developed for the calculation of mass shift constants works correctly and can be used for calculations in neutral atoms.

Table 3.1. Calculated values of the k_{NRNMS} constant (in THz·u) for various lithium-like ions.

$2s_{1/2} - 2p_{1/2}$	Si^{11+}	Ar^{15+}	Zn^{27+}	Nd^{57+}	Hg^{77+}	Th^{87+}	U^{89+}
This work	−3.737	−5.867	−21.538	−336.87	−1533.37	−3176.0	−3672.7
	(0.6%)	(0.9%)	(1.5%)	(0.9%)	(0.4%)	(−0.1%)	(−0.2%)
This work, Gaunt	−3.771	−5.947	−21.960	−340.57	−1541.59	−3186.3	−3683.3
	(−0.3%)	(−0.4%)	(−0.4%)	(−0.2%)	(−0.1%)	(−0.4%)	(−0.5%)
Ref. [154]	−3.759	−5.923	−21.862	−339.91	−1539.8	−3173.8	−3664.8

Table 3.2. Calculated values of the k_{RNMS} constant (in THz·u) for various lithium-like ions.

$2s_{1/2} - 2p_{1/2}$	Si^{11+}	Ar^{15+}	Zn^{27+}	Nd^{57+}	Hg^{77+}	Th^{87+}	U^{89+}
This work	0.563	1.609	13.811	323.5	1572.7	3356.8	3906.7
	(0.2%)	(0.0%)	(0.1%)	(0.1%)	(0.0%)	(−0.2%)	(−0.3%)
This work, Gaunt	0.563	1.608	13.804	323.1	1570.1	3350.0	3898.6
	(0.2%)	(0.0%)	(0.1%)	(0.2%)	(0.2%)	(0.0%)	(−0.1%)
Ref. [154]	0.564	1.609	13.819	323.79	1573.3	3349.5	3894.4

Table 3.3. Calculated values of the k_{NRSMS} constant (in THz·u) for various lithium-like ions.

$2s_{1/2} - 2p_{1/2}$	Si^{11+}	Ar^{15+}	Zn^{27+}	Nd^{57+}	Hg^{77+}	Th^{87+}	U^{89+}
This work	−41.706	−74.573	−236.159	−1229.95	−2830.61	−4274.4	−4651.4
	(0.0%)	(0.0%)	(−0.1%)	(−0.2%)	(−0.3%)	(−0.4%)	(−0.4%)
This work, Gaunt	−41.654	−74.453	−235.531	−1223.57	−2811.51	−4242.4	−4615.9
	(0.1%)	(0.1%)	(0.2%)	(0.3%)	(0.3%)	(0.4%)	(0.4%)
Ref. [154]	−41.701	−74.544	−235.921	−1227.04	−2821.08	−4257.6	−4632.5

Table 3.4. Calculated values of the k_{RSMS} constant (in THz·u) for various lithium-like ions.

$2s_{1/2} - 2p_{1/2}$	Si^{11+}	Ar^{15+}	Zn^{27+}	Nd^{57+}	Hg^{77+}	Th^{87+}	U^{89+}
This work	0.726	2.170	19.394	409.92	1689.00	3240.5	3687.8
	(0.7%)	(0.0%)	(−0.1%)	(−0.3%)	(−0.4%)	(−0.5%)	(−0.5%)
This work, Gaunt	0.725	2.167	19.347	407.97	1678.51	3218.2	3661.9
	(0.8%)	(0.1%)	(0.1%)	(0.2%)	(0.2%)	(0.2%)	(0.2%)
Ref. [154]	0.731	2.169	19.369	408.63	1681.66	3224.2	3668.6

3.3. Au atom

3.3.1. Calculation details

The first step of the study involved a full-electron calculation using the CCSD(T) method [89, 90] with the Dirac – Coulomb Hamiltonian and the Gaussian model of the nuclear charge distribution. In this case, the LHbas basis set, an extended version of Dyall AE4Z [95, 97], was used to compute the constants F and k_{NMS}. Table 3.5 gives the total number of basis functions of different types included in this set, as well as the composition of other sets used in the calculations. Due to its greater computational difficulty, the Mbas basis set – an extended version of Dyall AE3Z [95, 97], but with fewer functions than LHbas, was used for the all-electron calculation of the constant k_{SMS}. In all the calculations of the Au atom described above, the energy of the virtual orbitals was limited to the value 10000 E_h.

Further, corrections for higher order correlation effects were calculated using the CCSDT(Q) [110, 111, 140] method with Mbas basis set. In this calculation, 19 valence electrons were included ($1s - 4f$ electrons were frozen) and the constraint on the energy of the virtual orbitals was set to 20 E_h. Since the main calculation of k_{SMS} was performed in a smaller basis set than in the case of k_{NMS} and F, the corresponding correction to the obtained value must be estimated in order to achieve a comparable level of accuracy. For this purpose, we computed the difference between the values obtained in the full-electron calculations by the CCSD method with the Lbas and Mbas basis sets. Similar to the LHbas basis set, Lbas is an extended version

of Dyall AE4Z, but contains fewer high angular momentum functions (see Table 3.5). The Gaunt interaction correction for all considered constants was calculated as a difference of values obtained by the DHF method with the Dirac – Coulomb and Dirac – Coulomb – Gaunt Hamiltonians. To estimate the uncertainties of the performed calculations, we also carried out calculations using the Sbas basis set, which is an extended version of the Dyall AE2Z [95, 97].

Table 3.5. The composition of the basis sets used in calculations of the electronic structure of the Au atom. The basis sets are given in the descending order of their quality.

Basis set	Functions
LHbas	40s, 36p, 19d, 14f, 10g, 7h, 4i
Lbas	40s, 36p, 19d, 14f, 10g, 5h, 1i
Mbas	36s, 30p, 15d, 11f, 5g, 1h
Sbas	30s, 25p, 12d, 9f, 1g

3.3.2. Results

The result of the calculation of the field shift constant F and the estimation of the obtained uncertainty for the considered transition $6s^2S_{1/2} \to 6p^2P_{1/2}$ of Au atom are presented in Table 3.6. As can be seen, the iterative consideration of triple amplitudes within the CCSDT method gives a significant contribution (about 2.6% of the total value) compared to the perturbative consideration by the CCSD(T) method. Nevertheless, as follows from the results of the perturbative calculation of the correction for quadruple amplitudes CCSDT(Q), which amounted to about 1.2%, convergence in the level of accounting for the interelectron correlation was finally achieved. The contribution of the Gaunt interelectron interaction is less than 1% of the total value.

Table 3.7 presents the results of the calculation of the constants k_{NMS}, k_{SMS}, and $k_{\mathrm{MS}} = k_{\mathrm{NMS}} + k_{\mathrm{SMS}}$, as well as the estimate of the obtained uncertainties. As can be easily seen, for both constants k_{NMS} and k_{SMS}, corrections for the iterative accounting

Table 3.6. Calculated value and uncertainty of the field shift constant F (in GHz/fm^2) for the $6s^2S_{1/2} \to 6p^2P_{1/2}$ transition in the Au atom.

Transition	$6s^2S_{1/2} \to 6p^2P_{1/2}$
Contributions:	
$79e-$CCSD(T)	-41.9
$19e-$CCSDT $-$ $19e-$CCSD(T)	$+1.0$
$19e-$CCSDT(Q) $-$ $19e-$CCSDT	$+0.5$
Basis set correction	–
Gaunt	$+0.3$
Uncertainties:	
Correlation (valence electrons)	0.5
Correlation (core electrons)	0.1
Basis set	0.6
Basis and correlation interference	0.1
Gaunt	0.3
Charge distribution model	0.4
QED	0.4
Total	$-40.1(11)$

of the triple cluster amplitudes relative to the peturbative one give a significant contribution to the final values (see line "$19e-$CCSDT $-$ $19e-$CCSD(T)"). The contribution of the quadruple cluster amplitudes to $k_{\rm SMS}$, calculated as the difference between the values obtained using the CCSDT(Q) and CCSDT methods, is also not negligible. At the same time, in the case of the constant $k_{\rm NMS}$, this contribution turns out to be quite small relative to the final theoretical value. The situation with the contribution of the interelectron Gaunt interaction is similar. In the case of the constant $k_{\rm NMS}$ the correction for this interaction is not large, but for the constant $k_{\rm SMS}$ it gives a significant contribution to the final value.

The following contributions were considered in the determination of the final calculation uncertainty of the constants F, $k_{\rm NMS}$, $k_{\rm SMS}$, and $k_{\rm MS} = k_{\rm NMS} + k_{\rm SMS}$.

1. The uncertainty due to the finite size of the basis set. In the case of constants F and k_{NMS}, it was estimated as the difference of the results obtained using

Table 3.7. Calculated values and uncertainties of $k_{\rm NMS}$ and $k_{\rm SMS}$ (in GHz·u) and their sum $k_{\rm MS}$ for the $6s^2S_{1/2} \to 6p^2P_{1/2}$ transition in the Au atom.

Transition	$6s^2S_{1/2} \to 6p^2P_{1/2}$		
	$k_{\rm NMS}$	$k_{\rm SMS}$	$k_{\rm MS}$
	Contributions:		
$79e$ – CCSD(T)	723	221	944
$19e$ – CCSDT − $19e$ – CCSD(T)	−124	−37	−161
$19e$ – CCSDT(Q) − $19e$ – CCSDT	−4	−31	−35
Basis set correction	–	−28	−28
Gaunt	+5	−22	−17
Uncertainties:			
Correlation (valence electrons)	4	31	
Correlation (core electrons)	32	77	
Basis set	10	28	
Basis and correlation interference	21	19	
Gaunt	5	22	
Total	600(40)	103(93)	703(101)

the CCSD(T) method with the LHBas and MBas basis sets. For the constant k_{SMS}, this contribution was estimated as the difference of the values obtained using the CCSD method with the LBas and MBas basis sets. In Tables 3.6 and 3.7, the contribution from this source of uncertainty is given in the row "Basis set".

2. The uncertainty in taking into account correlation effects using the CCSDT(Q) method for 19 valence electrons. As an estimate of the magnitude of this uncertainty, we used the difference between the values obtained using the CCSDT(Q) and CCSDT methods in calculations with 19 electrons and using the MBas basis set. In Tables 3.6 and 3.7, the row "Correlation (valence electrons)" corresponds to this source of uncertainty.

3. The uncertainty of accounting for correlation effects for the 60 inner-core $1s...4f$ electrons of the Au atom. To estimate this value, the difference of contributions of noniterative triple amplitudes (T) obtained in calculations

with all 79 electrons and with 19 valence electrons was calculated. This difference corresponds to the contribution of the triple amplitudes of the core electrons to the considered constants. In Tables 3.6 and 3.7, the contribution from this source of uncertainty is presented in the row "Correlation (core electrons)".

4. The uncertainty due to the interference of the basis set size and accounting for correlation effects. To estimate this quantity, we calculated the difference of higher order correlation contributions in the MBas and SBas basis sets. In Tables 3.6 and 3.7, the contribution of this effect is presented in the row "Basis and correlation interference".

5. The Gaunt interaction contribution given in Tables 3.6 and 3.7 was completely included in the final uncertainty (i.e., we assumed that this contribution was calculated with 100% uncertainty).

6. In the case of the constant F the uncertainty due to the model of the charge distribution over the nucleus used in the calculations was also taken into account. For this purpose at the DHF level, the calculations with the Gaussian and Fermi charge distributions were carried out. The uncertainty obtained as the difference of these values is given in Table 3.6.

7. Finally, following Ref. [82] we included QED effects of $\approx$1% in the uncertainty of constant F.

To obtain the final uncertainty, we calculated the square root of the sum of the squares of all the uncertainties described above.

Using the constants given in Tables 3.6 and 3.7, the experimental data obtained in Ref. [85] for the isotope chain of the Au atom were interpreted. Table 3.8 presents the measured isotope shifts (IS) $\delta\nu_{A,197}$ and the derived values of $\delta\langle r^2\rangle_{A,197}$.

Table 3.8. Values of IS ($\delta\nu_{A,197}$) and $\delta\langle r^2\rangle_{A,197}$ relative to ^{197}Au extracted from experimental data assuming different I values. The I values in parentheses represent cases where the value is not certain or was not measured directly. Statistical experimental uncertainties are given in parentheses, while systematic uncertainties stemming from the atomic calculations are given in curly brackets.

A	I	$\delta\nu_{A,197}$, MHz	$\delta\langle r^2\rangle_{A,197}$, fm^2
^{176}Au^{ls}	(3)	43340(640)	-1.091(16){31}
	(4)	42860(660)	−1.079(16){31}
	(5)	42520(700)	−1.071(16){31}
^{176}Au^{hs}	(8)	42580(310)	−1.072(8){31}
	(9)	43070(370)	−1.085(9){31}
^{177}Au^{g}	1/2	39290(220)	−0.990(5){29}
^{177}Au^{m}	(11/2)	37860(250)	−0.954(6){28}
^{178}Au^{g}	(2)	24650(260)	−0.624(7){18}
	(3)	23800(260)	−0.603(7){18}
^{178}Au^{m}	(7)	9790(140)	−0.254(3){8}
	(8)	10300(140)	−0.266(3){9}
^{179}Au	1/2	31570(200)	−0.796(5){23}
^{180}Au	(1)	10650(200)	−0.274(5){9}
^{181}Au	(3/2)	7820(230)	−0.203(6){7}
^{182}Au	(2)	7160(200)	−0.186(5){6}
^{183}Au	(5/2)	5620(120)	−0.147(3){5}^{a}
^{187}Au^{m}	(9/2)	5380(160)	−0.139(4){4}^{b}
^{191}Au^{m}	(11/2)	7950(180)	−0.201(4){6}
^{193}Au^{m}	11/2	4780(180)	−0.121(4){4}
^{195}Au^{m}	11/2	1760(220)	−0.045(5){1}

^{a}Our value differs from $\delta\langle r^2\rangle_{A,197}(^{183}\text{Au}) = -0.130(9)$ [164], partly due to the different atomic parameters of the IS used.
$^b\delta\langle r^2\rangle_{A,197}(^{187}\text{Au}^m)$ was calculated using the new atomic parameters of the IS, $\delta\nu_{A,197}(^{187}\text{Au}^m)$ was found in Ref. [165].

3.4. Tl atom

Using the same computational scheme, program code, and method of theoretical uncertainty estimation as for the gold atom, the isotope shift constants for the thallium atom were calculated in Ref. [82]. The final results of these calculations are summarized in Table 3.9 (numerical calculations were performed by G. Penyazkov).

Table 3.9. The final values of the mass shift constants k_{NMS}, k_{SMS}, their sum $k_{\rm MS}$ (in GHz·u), and the field shift constant F (in GHz/fm^2).

	k_{NMS}	k_{SMS}	k_{MS}	F
$6p^2P_{3/2} \to 7s^2S_{1/2}$ (535 nm)	−323(10)	188(35)	−135(36)	16.15(32)
$6p^2P_{1/2} \to 6d^2D_{3/2}$ (277 nm)	−605(14)	30(69)	−575(71)	9.50(44)
$6p^2P_{1/2} \to 7s^2S_{1/2}$ (378 nm)	−421(27)	145(46)	−275(54)	15.22(30)

Using the constants given in Table 3.9, one can interpret the isotope shifts measured earlier and recalculate the differences of the rms charge radii $\delta\langle r^2\rangle$. However, in the case of the 277 nm transition, instead of the theoretical value of the constant F [9. 50(44) GHz/fm^2], one can use the calculated value for the 535 nm transition and the ratio of constants F for the two transitions $k_{\rm expt} = F_{277\ \rm nm}/F_{535\ \rm nm}$ determined from experimental data using the King plot [138]: $F_{277\ \rm nm} = F_{535\ \rm nm}k_{\rm expt} = 9.32(23)$ GHz/fm^2. Such approach allows one to achieve higher accuracy in this case and therefore it was applied to determine $\delta\langle r^2\rangle$. The obtained values are presented in Table 3.10. The experimental uncertainty is denoted by parentheses. The uncertainty due to the inaccuracy of the calculation of the field and mass shift constants is given in curly brackets. In addition, Table 3.10 summarizes the results obtained with old values of constants from Refs. [138, 166].

As follows from Table 3.10, for the most exotic isotopes (A<186), the theoretical uncertainty becomes comparable to the experimental one. Generally, the theoretical uncertainty does not exceed 2.6%. Such a level of accuracy in the study of isotope shifts in heavy atoms is at least as good as that achieved for radium [156] and francium [177] atoms. The values of $\delta\langle r^2\rangle$ obtained in this work differ from those

Table 3.10. The $\delta\langle r^2\rangle$ values for the Tl isotope chain determined from the experimental IS data for the three transitions considered in the articles [138, 166] and in this thesis. The uncertainty given in parentheses is due to the experimental uncertainty of IS value measurement, and the uncertainty given in curly brackets is theoretical. In the presence of different experimental data for the same isotope, the data with the smallest uncertainty were selected.

A	I	$\delta\langle r^2\rangle$, fm^2 [138, 166]	$\delta\langle r^2\rangle$, fm^2	A	I	$\delta\langle r^2\rangle$, fm^2 [138, 166]	$\delta\langle r^2\rangle$, fm^2
208g	5	0.183(13){13}	0.1919(130){38}[a]	192m	7	−0.6358(6){450}	−0.6681(6){130}[i]
207g	1/2	0.1048(2){70}	0.1100(2){22}[b]	191g	1/2	−0.6544(7){460}	−0.6878(7){140}[i]
205g	1/2	0	0	191m	9/2	−0.4899(6){340}	−0.5158(6){100}[i]
204g	2	−0.0635(71){40}	−0.0667(74){13}[c]	190g	2	−0.7063(4){490}	−0.7424(4){150}[i]
203g	1/2	−0.10321(2){700}	−0.10840(3){220}[d]	190m	7	−0.7223(5){510}	−0.7591(5){150}[i]
202g	2	−0.1834(71){130}	−0.1926(74){38}[c]	189m	9/2	−0.5543(41){390}	−0.5837(43){120}[e]
201g	1/2	−0.2077(9){150}	−0.2182(9){43}[e]	188m	7	−0.8134(5){570}	−0.8549(5){170}[i]
200g	2	−0.2979(71){210}	−0.3129(74){62}[c]	187m	9/2	−0.616(31){43}	−0.650(32){17}[h]
199g	1/2	−0.3116(71){220}	−0.3275(74){65}[c]	186m1	7	−0.9324(15){650}	−0.9799(15){200}[k]
198g	2	−0.4035(71){290}	−0.4239(74){84}[f]	186m2	10	−0.719(23){50}	−0.758(24){20}[h]
198m	7	−0.3804(71){270}	−0.3998(74){80}[g]	185g	1/2	−0.938(41){66}	−0.987(43){25}[h]
197g	1/2	−0.4119(71){290}	−0.4330(74){86}[f]	185m	9/2	−0.731(29){51}	−0.770(30){20}[h]
197m	9/2	−0.272(26){19}	−0.2871(270){75}[h]	184m1	2	−0.979(32){69}	−1.031(32){27}[l]
196g	2	−0.4795(5){340}	−0.5036(5){100}[i]	184m2	7	−0.976(24){68}	−1.027(26){27}[l]
196m	7	−0.4544(6){320}	−0.4773(6){95}[i]	184m3	10	−0.777(20){54}	−0.820(23){21}[l]
195g	1/2	−0.4820(71){340}	−0.5068(75){100}[j]	183g	1/2	−1.033(15){72}	−1.086(17){28}[l]
195m	9/2	−0.324(11){23}	−0.3419(120){90}[h]	183m	9/2	−0.775(15){54}	−0.818(17){22}[l]
194g	2	−0.5551(39){50}	−0.5831(5){120}[i]	182m1	4	−1.120(18){78}	−1.179(19){30}[l]
194m	7	−0.5481(5){380}	−0.5759(5){110}[i]	182m2	7	−1.123(30){78}	−1.182(33){30}[l]
193g	1/2	−0.5716(11){400}	−0.6007(12){120}[e]	181	1/2	−1.174(16){82}	−1.236(17){32}[l]
193m	9/2	−0.4111(10){290}	−0.4329(11){87}[e]	180	4	−1.254(22){88}	−1.319(24){34}[l]
192g	2	−0.6296(4){440}	−0.6616(4){130}[i]	179	1/2	−1.274(29){89}	−1.340(31){35}[l]

[a] IS experimental data from Ref. [167]
[b] IS experimental data from Ref. [168]
[c] IS experimental data from Ref. [169]
[d] IS experimental data from Ref. [170]
[e] IS experimental data from Ref. [171]
[f] IS experimental data from Ref. [172]
[g] IS experimental data from Ref. [173]
[h] IS experimental data from Ref. [138]
[i] IS experimental data from Ref. [174]
[j] IS experimental data from Ref. [175]
[k] IS experimental data from Ref. [176]
[l] IS experimental data from Ref. [166]

given in the literature by an order of magnitude of 5%. From the formal point of view, this difference fits into the theoretical uncertainty $\delta\langle r^2\rangle$ in Refs. [138, 166]. However, the theoretical uncertainty (7%) reported in these papers [138, 166] was based on estimates from general considerations and did not have the same theoretical justification as in this study. Moreover, a significant difference in the computational results (up to 30%, see Table 3.9) may indicate a significant underestimation of the theoretical uncertainty. It should also be noted that in Refs. [138,166] it was decided to neglect the specific mass shift constant for the $6p^2P_{3/2} \rightarrow 7s^2S_{1/2}$ transition in determination of $\delta\langle r^2\rangle$. However, Table 3.9 shows that value of k_{SMS} is significant for this transition and should be taken into account to achieve a high level of accuracy.

Chapter 4.

Search for $\mathcal{T}$, $\mathcal{P}$-violating interactions induced by axionlike particles in molecules

In Chapter 4 axionlike particle (ALP)-mediated $\mathcal{T}$, $\mathcal{P}$-violating interactions in molecules are considered. The molecular parameters of these interactions for the HfF^+ cation were calculated in the course of this study. They were used to reinterpret the results of an experiment searching for the electric dipole moment (EDM) of the electron [69]. As a result, new constraints on the product of constants of the considered interactions were established. The obtained results were first published in Refs. [86, 87].

4.1. General theoretical information

The interaction between the atomic nucleus nucleons and electrons induced by the exchange of ALPs can be both preserving and violating the $\mathcal{T}$,$\mathcal{P}$-parity. The subject of study in this thesis is the $\mathcal{T}$,$\mathcal{P}$-violating interaction. In the case of ALP exchange with mass m_a, the interaction potential between a nucleon and an electron can be written as follows [58, 178]:

$$V_{eN}(\boldsymbol{r}-\boldsymbol{R}) = +i\frac{g_N^s g_e^p}{4\pi}\frac{e^{-m_a|\boldsymbol{r}-\boldsymbol{R}|}}{|\boldsymbol{r}-\boldsymbol{R}|}\gamma_0\gamma_5, \tag{4.1}$$

where the nucleon N can be a proton or a neutron, g_N^s is the scalar interaction constant of the nucleon with the ALP, g_e^p is the pseudoscalar interaction constant of the electron with the ALP, $\boldsymbol{R}$ is the nucleon position, $\boldsymbol{r}$ is the electron position, and Dirac γ matrices act on the four-component electron wave function. In previous works [58, 70–72], the point nucleus approximation in the ALP-induced electron-

nucleus interaction operator was used for the calculations (the electron wave function itself was calculated for the case of a finite nucleus):

$$V_{eN}(r) = +i\frac{g_N^s g_e^p}{4\pi}\frac{e^{-m_a r}}{r}\gamma_0\gamma_5. \tag{4.2}$$

In the present thesis, we managed to go beyond this approximation and perform calculations directly with the operator (4.1), taking into account the effect of the finite nucleus size. For this purpose, we modified the calculation methods originally developed for the $\mathcal{T}$,$\mathcal{P}$-violating electron-electron interaction induced by the ALP exchange. The potential of this interaction can be written as follows [58, 178]:

$$V_{ee}(\boldsymbol{r}_1, \boldsymbol{r}_2) = +i\frac{g_e^s g_e^p}{4\pi}\frac{e^{-m_a|\boldsymbol{r}_1-\boldsymbol{r}_2|}}{|\boldsymbol{r}_1-\boldsymbol{r}_2|}\gamma_0\gamma_5\ , \tag{4.3}$$

where g_e^s is the scalar constant of the electron-ALP interaction, $\boldsymbol{r}_1$ and $\boldsymbol{r}_2$ are the positions of electrons, and the Dirac γ-matrices act on the wave function of the second electron.

By summing the expression (4.1) over all particles, one can find the total $\mathcal{T}$,$\mathcal{P}$-violating ALP-mediated interaction between the selected nucleus and electrons of the linear molecule under consideration. The total interaction can be characterized by a single parameter completely determined by the electronic structure of the molecule [70, 179]:

$$W_{\rm ax}^{(eN)}(m_a) = \frac{1}{\Omega}\frac{1}{\bar{g}_N^s g_e^p}\langle\Psi|\sum_{i=1}^{N_{\rm e}}\sum_{N}\int d\boldsymbol{R}\rho(\boldsymbol{R})V_{eN}(\boldsymbol{r}_i-\boldsymbol{R})|\Psi\rangle, \tag{4.4}$$

where $\rho(\boldsymbol{R})$ is the normalized to unity nuclear density, Ψ is the electron wave function of the linear molecule under consideration, Ω is the projection of the total electron angular momentum on the axis of the molecule, N_e is the number of electrons, and the index i runs over all electrons. In this study, it is assumed that

the difference in the distribution of protons and neutrons can be neglected. Note that $\bar{g}^s_N$ is the ALP-nucleon interaction coupling constant averaged over all nucleons of the nucleus: $\bar{g}^s_N = (N_n g^s_n + Z g^s_p)/A$, where g^s_n and g^s_p are the scalar ALP-proton and ALP-neutron interaction coupling constants, respectively, N_n is the number of neutrons, Z is the charge of the nucleus, and $A = N_n + Z$ is the mass number.

In a similar way, the electron-electron interaction can be characterized by a single molecular parameter:

$$W^{(ee)}_{\rm ax}(m_a) = \frac{1}{\Omega}\frac{1}{g^s_e g^p_e}\langle\Psi|\sum_{i,j=1}^{N_e}{}' V_{ee}(\boldsymbol{r}_i, \boldsymbol{r}_j)|\Psi\rangle. \tag{4.5}$$

In this sum, only terms with $i \neq j$ should be taken into account, which is indicated by the prime index above the sum sign.

Using the notations introduced above, the electron level energy shift caused by the $\mathcal{T}$,$\mathcal{P}$-violating interaction (4.1) can be written in the following form:

$$\delta E = \bar{g}^s_N g^p_e \Omega W^{(eN)}_{\rm ax}(m_a), \tag{4.6}$$

and the energy shift induced by the $\mathcal{T}$,$\mathcal{P}$-violating interaction (4.3) can be written as:

$$\delta E = g^s_e g^p_e \Omega W^{(ee)}_{\rm ax}(m_a). \tag{4.7}$$

Let us consider separately two limiting cases for the considered interactions. This will be useful for the analysis of the obtained results.

Low mass limit. As can be easily seen, at $m_a = 0$ the exponent in the interaction potentials (4.1) and (4.3) can be replaced by unity. In the case of small but non-zero masses such replacement, obviously, will be only approximate. The conditions under which this approximation will be sufficiently accurate can be estimated as follows. As the mass of the ALP decreases, the characteristic radius of the Yukawa-type

interaction $R_{\rm Yu} = 1/m_a$(relativistic units) $= \hbar/m_a c$ will increase [58]. When it becomes much larger than the size of the molecule itself, further increase in size will make almost no difference to the interaction inside the molecule. In the localization region of the electron wave function, the argument of the exponential function $m_a r \approx 0$, and hence $exp(m_a r) \approx 1$. The characteristic molecular distance, which determines the scale of the electronic problem, can be taken to be 1 Bohr. A Yukawa interaction with such a characteristic radius corresponds to an ALP mass $m_a \approx 4$ keV. Thus, one can expect that at $m_a < 1$ keV the values of the parameters $W_{\rm ax}^{(eN)}$ and $W_{\rm ax}^{(ee)}$ are almost independent of m_a.

High mass limit. At $m_a \to +\infty$, the dependence on r of the potential (4.1) approaches the δ-function [72] up to a constant factor:

$$\frac{e^{-m_a r}}{4\pi r}. \to \frac{1}{m_a^2}\delta(\boldsymbol{r}). \tag{4.8}$$

To approach the limit, the characteristic radius of the Yukawa interaction should be smaller than the nuclear scale of 1 Fm, which corresponds to $m_a \approx 0.2$ GeV. Therefore, one can expect the approximation to be valid at $m_a \geq 1$ GeV. Since the interaction at such large masses becomes almost point-like, it becomes possible to use the following approximation in Eq. (4.4):

$$\int d\boldsymbol{R}\rho(\boldsymbol{R})V_{eN}(\boldsymbol{r}_i - \boldsymbol{R}) \approx +i\frac{g_N^s g_e^p}{m_a^2}\rho(r_i)\gamma_0\gamma_5. \tag{4.9}$$

In the Eq. (4.5), one can also passage to the limit (4.8). As a result, approximate expressions for the parameters $W_{\rm ax}^{(eN)}$ and $W_{\rm ax}^{(ee)}$ can be obtained (see also Refs. [58, 70]): $W_{\rm ax}^{(eN)}(m_a) \simeq \widetilde{W}^{eN} m_a^{-2}$ and $W_{\rm ax}^{(ee)}(m_a) \simeq \widetilde{W}^{ee} m_a^{-2}$, where the new parameters $\widetilde{W}^{eN}$ and $\widetilde{W}^{ee}$ are independent of m_a. The parameterization of the energy shift due

to electron-nuclear interaction can be written in the following form [71]:

$$\delta E \approx \frac{\bar{g}_N^s g_e^p}{m_a^2} \Omega \widetilde{W}^{eN}, \tag{4.10}$$

where

$$\widetilde{W}^{eN} = \lim_{m_a \to +\infty} m_a^2 W_{\text{ax}}^{(eN)}(m_a). \tag{4.11}$$

A similar parameterization can be written for the electron-electron interaction:

$$\delta E \approx \frac{g_e^s g_e^p}{m_a^2} \Omega \widetilde{W}^{ee}, \tag{4.12}$$

where

$$\widetilde{W}^{ee} = \lim_{m_a \to +\infty} m_a^2 W_{\text{ax}}^{(ee)}(m_a). \tag{4.13}$$

In addition, it should be noted that at large ALP masses the $W_{\text{ax}}^{(eN)}$ parameter can be expressed using the parameter of the electron-nuclear scalar-pseudoscalar interaction. This fact follows directly from the expression for the scalar-pseudoscalar interaction potential [5] (see also Eq. (4.9)):

$$V_{S-PS} = iZk_{S-PS} \frac{G_F}{\sqrt{2}} \rho(\boldsymbol{r}) \gamma_0 \gamma_5, \tag{4.14}$$

where k_{S-PS} is the dimensionless interaction coupling constant, Z is the charge of the nucleus, G_F is the Fermi constant ($2.2225 \cdot 10^{-14}$ in atomic units). The energy shift corresponding to this interaction can be parameterized as follows:

$$\delta E = \Omega k_{S-PS} W_{S-PS}, \tag{4.15}$$

where

$$W_{S-PS} = \frac{1}{\Omega} \langle \Psi | \frac{1}{k_{S-PS}} \sum_{i=1}^{N_e} V_{S-PS}(\boldsymbol{r}_i) | \Psi \rangle. \tag{4.16}$$

In summary, in the limiting case of high mass ALPs, the relation between the molecular parameters can be expressed by a simple formula:

$$W_{\rm ax}^{(eN)}(m_a \to \infty) = \frac{A\sqrt{2}}{Z}\frac{1}{G_F m_a^2} W_{S-PS}. \tag{4.17}$$

4.2. Practical implementation of calculation methods

The methods developed in Ref. [86] for the calculation of $W_{\rm ax}^{(ee)}(m_a)$ were modified to account for the effect of finite nucleus size in the calculation of the molecular parameter $W_{\rm ax}^{(eN)}(m_a)$. Indeed, both problems require the computation of "primitive integrals" of the form $\langle ab|e^{-m_a r_{12}}/r_{12}|cd\rangle$, where a, b, c, d are Gaussian functions of the form $x^n y^m z^k e^{-\beta r^2}$. The parameter $\beta > 0$ determines the diffusivity of this basis function, the numbers n, m, k are non-negative integers, and their sum is equal to the total angular momentum of the function. In the calculation of the parameter $W_{\rm ax}^{(ee)}(m_a)$, all four functions a, b, c, d arise from the finite basis decomposition of the molecular bispinors. In the case of computing $W_{\rm ax}^{(eN)}(m_a)$, only two Gaussians are associated with the electron wave function, and two others are modeling the distribution of nucleons over the nucleus. This is the result because we use a Gaussian model of the charge distribution over the nucleus $\rho = ce^{-\alpha r^2}$ [142] and assume that the neutron distribution coincides fairly well with the proton distribution. Consequently, the "primitive integrals" appearing in the calculation of $W_{\rm ax}^{(eN)}(m_a)$ can be written in the following form: $\langle a\gamma|e^{-m_a r_{12}}/r_{12}|c\gamma\rangle$, where $\gamma = \sqrt{\rho}$. For more generality, however, let us consider in detail the implementation of the calculation method for "primitive integrals" of the form $\langle ab|e^{-m_a r_{12}}/r_{12}|cd\rangle$. In the case of a diatomic molecule, the basis functions a, b, c, d can be centered on different nuclei, which complicates such a calculation (see in Ref. [72] a solution of the one-center problem with Gaussian-type functions).

The computation of the Yukawa integrals $\langle ab|e^{-m_a r_{12}}/r_{12}|cd\rangle$ is a generalization

of the Coulomb integrals $\langle ab|1/r_{12}|cd\rangle$ computation problem. The computational algorithm used to solve the latter most often involves the calculation of the Boys function [180, 181]:

$$F_m(T) = \int_0^1 dt t^{2m} e^{-Tt^2}. \tag{4.18}$$

To compute integrals $\langle ab|e^{-m_a r_{12}}/r_{12}|cd\rangle$, it turns out to be sufficient to replace the Boys function with a more complicated special function [182]:

$$G_m(T,U) = \int_0^1 dt t^{2m} e^{-Tt^2+U(1-\frac{1}{t^2})}. \tag{4.19}$$

This makes it possible to use many generalizations of the classical algorithms for the calculation of two-electron Coulomb integrals: McMurchie – Davidson [183], Obara – Saika [184], Pople – Hehre [185], Head – Gordon – Pople [186], PRISM of Gill et al. [187] and others [188–191]. In the presented thesis, we used a computational algorithm implemented in the LIBINT library [192] to compute the Yukawa integrals. The approach used in the library is analogous to the quadrature method of Rys – Dupuis et al. [193–195], later elaborated by Lindh et al. [196]. The advantage of this approach in comparison with other numerical methods is the possibility to perform calculations of integrals with orbitals having high angular momentum. Nevertheless, in order to use it in practical calculations, a number of modifications had to be made in the library code. Initially, the algorithm we need was implemented to perform electronic structure calculations using explicitly correlated methods [182, 197–201]. The variation range of variables T and U allowed in this case turned out to be too small for our purposes [192]. In this thesis, the range has been significantly extended.

As mentioned above, the main method of integrals calculation in the original version of the LIBINT library is a tailored Gaussian quadrature [198]. For this purpose, precomputed data is used, allowing calculations to be carried out in the range $0 \leq T \leq T_{max}$ and $U_{min} \leq U \leq 10^3$, where $T_{max} = 1024$ and $U_{min} = 10^{-7}$. In

case $T > T_{max}$ or $U < U_{min}$, "Scheme 1" of the paper [197] is applied, which consists of calculating

$$G_{-1} = \frac{e^{-T}}{4}\sqrt{\frac{\pi}{U}}\left[e^{k^2}\mathrm{erfc}(k) + e^{\lambda^2}\mathrm{erfc}(\lambda)\right], \tag{4.20}$$

$$G_0 = \frac{e^{-T}}{4}\sqrt{\frac{\pi}{T}}\left[e^{k^2}\mathrm{erfc}(k) - e^{\lambda^2}\mathrm{erfc}(\lambda)\right], \tag{4.21}$$

where erfc is the complementary error function,

$$k = -\sqrt{T} + \sqrt{U}, \tag{4.22}$$

$$\lambda = \sqrt{T} + \sqrt{U}, \tag{4.23}$$

and sequentially applying upward recurrence relations to compute the remaining values of G_m:

$$G_m = \frac{1}{2T}[(2m-1)G_{m-1} + 2UG_{m-2} - e^{-T}]. \tag{4.24}$$

In the modification of the library, we added code that implements computations using upward recurrence relations at $T = 0$ (see Ref. [197]). The first element is calculated using the following formula:

$$G_0 = 1 - e^U\sqrt{\pi U}\mathrm{erfc}(\sqrt{U}). \tag{4.25}$$

The remaining elements are determined using recurrence relations:

$$G_m(0,U) = \frac{1}{2m+1}[1 - 2UG_{m-1}(0,U)]. \tag{4.26}$$

Furthermore, we found numerical instabilities at small T in "Scheme 1". They are generated by the appearance of T in the denominator in the Eq. (4.24). To solve this problem, we have added code that implements "Scheme 3" (see paper [197]) for $T < 0.1$ at $U < U_{min}$. According to this method, $G_m(T,U)$ can be computed by

summing a series:

$$G_m(T,U) = \sum_{k=0}^{\infty} \frac{(-T)^k}{k!} G_{m+k}(0,U). \tag{4.27}$$

In practice, we restricted ourselves to considering terms up to and including $k = 8$, and the values of $G_m(0,U)$ were determined using Eqs. (4.25) and (4.26).

We used the identity (4.8) to verify the calculations in the limiting case of extremely high ALP masses. In this case, as a numerical implementation of the delta function, we used the procedure for computing the expectation value of the operator $c \cdot e^{-\alpha r^2}$, where c is the normalization factor and the parameter α should be chosen much larger than any exponential parameter β of primitive Gaussian basis functions. The application of such a method allowed us to use the implementation of the algorithm for the calculation of the corresponding two-electron integrals already existing in the LIBINT library.

Finally, after the calculation of primitive integrals $\langle ab|e^{-m_a r_{12}}/r_{12}|cd\rangle$, a 4-index transformation [202] from the basis of primitive Gaussian functions to the basis of molecular orbitals, taking into account the structure of γ matrices, was performed to calculate $W_{\mathrm{ax}}^{(ee)}$. The program code necessary for this was developed by D. E. Maison [71]. In the case of the $W_{\mathrm{ax}}^{(eN)}$ constant calculation, a similar transformation from the basis of primitive Gaussian functions to the basis of molecular orbitals was also performed.

4.3. Molecular cation HfF^+

4.3.1. Calculation details

The molecular parameters $W_{\mathrm{ax}}^{(eN)}$ and $W_{\mathrm{ax}}^{(ee)}$ can be non-zero only if there are unpaired electrons in the studied electronic state. In the presented thesis, we consider the $^3\Delta_1$ electronic state of the molecular cation HfF^+ on which the electron EDM measurement experiment was performed. In this state there are only two unpaired

electrons localized mainly on the Hf nucleus. Their states approximately correspond to the $5d$ and $6s$ orbitals of the Hf^{++} ion. It can be assumed that in the case of high ALP mass, due to the small radius of interactions (4.1) and (4.3), the contributions from the two-center integrals to the parameters $W_{\rm ax}^{(eN)}$ and $W_{\rm ax}^{(ee)}$ would be negligible. This assumption turns out to be correct. It follows from our direct calculation for $m_a = 10^4$ eV that the contribution from the two-center integrals is negligibly small in this case. This makes it possible to simplify a significant part of the calculations. Therefore, for $m_a \geq 10^5$ eV we used this method.

The electronic structure of the molecular cation HfF^+ was modeled using the Dirac – Coulomb Hamiltonian. We used the experimental distance [203] between the Hf and F nuclei in all calculations. As the model of the charge distribution over the nucleus, we used a Gaussian model, which is well suited for molecular problems [142].

The calculation of the $W_{\rm ax}^{(eN)}$ parameter in the point nucleus approximation was performed by D. E. Maison using the CCSD(T) method with various corrections (see detailed description in Ref. [86]). Consideration of the finite nucleus size effect was performed by the author of this thesis. The correlation calculation of the correction for this effect was performed within the CCSD(T) method with the same basis set as in the calculation in the point nucleus approximation. The program code developed to calculate the matrix elements of the operator using the relation (4.4) was modified to calculate the $W_{\rm ax}^{(ee)}$ constant.

The calculation of the $W_{\rm ax}^{(ee)}$ parameter with account of interelectron correlation effects turned out to be much more complicated than the calculation of $W_{\rm ax}^{(eN)}$, since the operator (4.3) is two-electron. Therefore, the required calculations were performed using the CCSD(T) method and the SBas basis set consisting of the AE2Z basis sets [96, 99, 100] on both atoms. In this case, the contribution of all electrons was taken into account in the correlation calculation. Nevertheless, the application of such an approach allowed us to obtain sufficiently accurate results in the case of the YbOH molecule [71]. The matrix elements of the interaction operator (4.3) were

calculated by the author of the present study. Correlation calculations of the $W_{\rm ax}^{(ee)}$ parameter were performed by D. E. Maison. Note also that the only attempt to calculate the $W_{\rm ax}^{(ee)}$ constant at the consideration of the effect (4.7) in molecules was undertaken in Ref. [71]. However, the problem was considered within the framework of the approximation according to which the exponent in the Eq. (4.3) can be approximated by the first two terms of the Taylor series expansion (i.e., in the case of low mass of the ALP).

4.3.2. Results

Table 4.1 summarizes the results of the calculation of the molecular parameters of $W_{\rm ax}^{(eN)}$ for different ALP masses. As can be seen, in the point nucleus approximation the $W_{\rm ax}^{(eN)}(m_a)$ function changes sign between $m_a = 10^4$ eV and $m_a = 10^5$ eV, as in the case of the YbOH molecule [71]. Note also that the values of the parameter $W_{\rm ax}^{(eN)}(m_a)$ for the molecular cation HfF^+ considered in this work are approximately twice smaller than the values of $W_{\rm ax}^{(eN)}(m_a)$ for the YbOH molecule for all considered ALP masses. This fact can be related to the different values of Ω in the Eq. (4.4): $\Omega = 1/2$ for YbOH, while for HfF^+ $\Omega = 1$. Nevertheless, for both molecules the energy shift (4.6) is comparable.

Table 4.1 also presents the calculated values of the finite nucleus size correction. They were calculated with a Gaussian distribution of nucleons in Eq. (4.4) with the rms radius equal to the rms charge radius of the nucleus. As can be easily seen, the effect is negligible for light ALPs and becomes significant for heavy ALPs ($m_a \geq 10^7$ eV). The largest effect, about 15%, was found for the ALP mass $m_a = 10^{10}$ eV and it remains unchanged for higher ALP masses. The obtained results can be explained using considerations similar to those given for the limit cases in section 4.1. The characteristic radius of the Yukawa interaction $R_{\rm Yu} = 1/m_a$(relativistic units) $= \hbar/m_a c$ substantially exceeds the molecule size in the case of light ALPs [58]. For

example, the characteristic atomic scale of 1 Bohr corresponds to $m_a \approx 4$ keV. The details of the nucleon distribution for such an interaction are insignificant. In contrast, for heavier ALPs, the characteristic interaction range becomes comparable to the size of the nucleus. For example, the nuclear scale of 1 Fm corresponds to $m_a \approx 0.2$ GeV. In this case it is necessary to take into account the effect of the finite size of the atomic nucleus.

Table 4.1. Calculated values of molecular parameters $W_{\rm ax}^{(eN)}(m_a)$ for different ALP masses. The second column presents the results with potential (4.2) obtained using the CCSD(T) method with various corrections (see details in Ref. [86]). The "**Correction**" column contains the calculated correction for the difference between the interaction (4.1) and (4.2) (see details in Ref. [87]). It was used to calculate the values of $W_{\rm ax}^{(eN)}(m_a)$ in the second to last column. The last column contains the limits on the product of constants $|\bar{g}_N^s g_e^p|$ obtained using the experimental data from the paper [69] and the values of $W_{\rm ax}^{(eN)}(m_a)$ in the second to last column.

m_a, eV	$W_{\rm ax}^{(eN)}(m_a)$, $m_e c/\hbar$		$W_{\rm ax}^{(eN)}(m_a)$, $m_e c/\hbar$	$\lvert\bar{g}_N^s g_e^p\rvert$
	Interaction (4.2)	Correction, %	Interaction (4.1)	Limit, $\hbar c$
1	$+1.67 \cdot 10^{-5}$	0	$+1.67 \cdot 10^{-5}$	$1.11 \cdot 10^{-20}$
10	$+1.67 \cdot 10^{-5}$	0	$+1.67 \cdot 10^{-5}$	$1.11 \cdot 10^{-20}$
10^2	$+1.66 \cdot 10^{-5}$	0	$+1.66 \cdot 10^{-5}$	$1.11 \cdot 10^{-20}$
10^3	$+1.54 \cdot 10^{-5}$	0	$+1.54 \cdot 10^{-5}$	$1.19 \cdot 10^{-20}$
10^4	$+3.30 \cdot 10^{-6}$	0	$+3.30 \cdot 10^{-6}$	$5.25 \cdot 10^{-20}$
10^5	$-1.15 \cdot 10^{-5}$	0	$-1.15 \cdot 10^{-5}$	$1.66 \cdot 10^{-20}$
10^6	$-6.41 \cdot 10^{-6}$	0	$-6.41 \cdot 10^{-6}$	$2.97 \cdot 10^{-20}$
10^7	$-2.85 \cdot 10^{-7}$	-1	$-2.82 \cdot 10^{-7}$	$6.74 \cdot 10^{-19}$
10^8	$-5.30 \cdot 10^{-9}$	-9	$-4.81 \cdot 10^{-9}$	$3.95 \cdot 10^{-17}$
10^9	$-5.85 \cdot 10^{-11}$	-13	$-5.09 \cdot 10^{-11}$	$3.73 \cdot 10^{-15}$
10^{10}	$-5.87 \cdot 10^{-13}$	-13	$-5.10 \cdot 10^{-13}$	$3.73 \cdot 10^{-13}$

Table 4.2 presents the results of the calculation of the parameter $W_{\rm ax}^{(ee)}(m_a)$ for different ALP masses. Correlation effects give the largest contribution for heavy ALPs. In the case of light ALPs with masses less than $m_a = 10^2$ eV, the values of $W_{\rm ax}^{(ee)}(m_a)$ are almost identical. Furthermore, in this case, $W_{\rm ax}^{(ee)}$ is about a factor of two smaller than $W_{\rm ax}^{(ee)}$ for the YbOH [71] molecule at the same ALP masses. This may be related to different values of Ω of the considered states of YbOH and HfF^+ molecules, as in the case of the parameter $W_{\rm ax}^{(eN)}(m_a)$. As one moves from light to

heavy ALPs, first the value of $W_{\rm ax}^{(ee)}(m_a)$ changes slightly at $m_a = 10^3$ eV, then decreases by a factor of almost 3 for $m_a = 10^4$ eV, and finally changes sign.

Table 4.2. Calculated values of molecular parameters $W_{\rm ax}^{(ee)}(m_a)$ for different ALP masses at different levels of the electronic structure theory. The last column presents the constraints on the product of constants $|g_e^s g_e^p|$ obtained using the experimental data from the Ref. [69].

m_a, eV	$W_{\rm ax}^{(ee)}(m_a)$, $m_e c/\hbar$			$\lvert g_e^s g_e^p \rvert$
	DHF	CCSD	CCSD(T) (**Total**)	Limit, $\hbar c$
1	$+6.35 \cdot 10^{-6}$	$+8.83 \cdot 10^{-6}$	$+8.63 \cdot 10^{-6}$	$2.16 \cdot 10^{-20}$
10	$+6.35 \cdot 10^{-6}$	$+8.83 \cdot 10^{-6}$	$+8.63 \cdot 10^{-6}$	$2.16 \cdot 10^{-20}$
10^2	$+6.34 \cdot 10^{-6}$	$+8.81 \cdot 10^{-6}$	$+8.61 \cdot 10^{-6}$	$2.16 \cdot 10^{-20}$
10^3	$+5.67 \cdot 10^{-6}$	$+7.81 \cdot 10^{-6}$	$+7.64 \cdot 10^{-6}$	$2.44 \cdot 10^{-20}$
10^4	$+1.98 \cdot 10^{-6}$	$+2.49 \cdot 10^{-6}$	$+2.46 \cdot 10^{-6}$	$7.57 \cdot 10^{-20}$
10^5	$+7.73 \cdot 10^{-8}$	$+1.64 \cdot 10^{-7}$	$+1.59 \cdot 10^{-7}$	$1.17 \cdot 10^{-18}$
10^6	$-4.01 \cdot 10^{-9}$	$-5.77 \cdot 10^{-9}$	$-5.67 \cdot 10^{-9}$	$3.28 \cdot 10^{-17}$
10^7	$-6.83 \cdot 10^{-11}$	$-1.11 \cdot 10^{-10}$	$-1.08 \cdot 10^{-10}$	$1.72 \cdot 10^{-15}$
10^8	$-6.90 \cdot 10^{-13}$	$-1.12 \cdot 10^{-12}$	$-1.09 \cdot 10^{-12}$	$1.70 \cdot 10^{-13}$
10^9	$-6.94 \cdot 10^{-15}$	$-1.12 \cdot 10^{-14}$	$-1.09 \cdot 10^{-14}$	$1.69 \cdot 10^{-11}$
10^{10}	$-6.97 \cdot 10^{-17}$	$-1.12 \cdot 10^{-16}$	$-1.10 \cdot 10^{-16}$	$1.67 \cdot 10^{-9}$

The most accurate constraint on the EDM of the electron was obtained in the experiment [69] with HfF^+ molecular cation: $|d_{\rm e}| = 4.1 \times 10^{-30} e{\cdot}$cm. Using the relations (4.6) – (4.7) and the calculated in Refs. [12,16,204,205] value of the effective field $E_{\rm eff} = W_d|\Omega| \approx 23$ GV/cm, it is possible to set a constraint $\delta E \approx 23$ μHz on the energy of the $\mathcal{T}$,$\mathcal{P}$-violating of the effects. By applying the relations (4.6) and (4.7), this constraint can be interpreted in terms of constraints on the product of the ALP interaction coupling constants. The obtained constraints for the corresponding ALP masses are given in the last columns of Tables 4.1 and 4.2.

In Ref. [16] the value of the scalar-pseudoscalar interaction molecular parameter $|W_{S-PS}| = 20.1$ kHz was calculated. According to the relation (4.17), this corresponds to the parameter $|W_{\rm ax}^{(eN)}(m_a = 10^{10}{\rm eV})| = 4.93 \cdot 10^{-13} m_e c/\hbar$. This value is in a good agreement with the final value of $|W_{\rm ax}^{(eN)}(m_a = 10^{10}{\rm eV})| = 5.10 \cdot 10^{-13} m_e c/\hbar$ obtained in the present work.

In the limiting cases of light and heavy ALPs, the same constraints can be used simultaneously for a wide range of ALP masses. For convenience, the constraints for these limiting cases are given separately in Table 4.3. For light ALPs, the constraints on the products of the constants $\bar{g}_N^s g_e^p$ and $g_e^s g_e^p$ obtained by reinterpreting the experimental data from Ref. [69] are an order of magnitude better than those established in Ref. [58] based on the experiment with the ThO molecule [206]. For heavy ALPs, the constraints on $\bar{g}_N^s g_e^p$ established in this study are slightly better, and on $g_e^s g_e^p$ are 3 times better compared to the constraints [58] from the ThO [206] experiment.

Table 4.3. A brief summary of the obtained constraints on the product of coupling constants for the limiting cases of light and heavy ALPs.

Limit	Constraint
$\lvert\bar{g}_N^s g_e^p\rvert/(\hbar c)$, $m_a \ll 1$ keV	1.1×10^{-20}
$\lvert g_e^s g_e^p\rvert/(\hbar c)$, $m_a \ll 1$ keV	2.2×10^{-20}
$\lvert\bar{g}_N^s g_e^p\rvert/(\hbar c m_a^2)$, $m_a \geq 1$ GeV	$3.2 \cdot 10^{-15}$ GeV^{-2}
$\lvert g_e^s g_e^p\rvert/(\hbar c m_a^2)$, $m_a \geq 1$ GeV	$1.7 \cdot 10^{-11}$ GeV^{-2}

Following the method applied in the paper [57] one can obtain very stringent indirect estimates on the product $g_N^s g_e^p$ by combining independent constraints on g_N^s and g_e^p from completely different sources. Such sources could be, for example, laboratory experiments and astrophysical observations of stellar energy losses. In particular, the constraint on $g_N^s g_e^p$ obtained from these sources for very light ALPs $m_a < 10^{-14}$ eV is about 17 orders of magnitude better than that determined by other methods. Nevertheless, as noted in Ref. [57], there may be mechanisms that can spoil the astrophysical constraints, and hence laboratory experiments on Earth are essential. In the macroscopic laboratory experiment QUAX-$g_p g_s$ [207], which aimed to measure the long-range forces induced by the ALPs, very strict constraints on the product $g_N^s g_e^p$ were obtained. The best result $g_N^s g_e^p < 4.3 \cdot 10^{-30} \hbar c$ [207] was obtained for the range of ALP masses $7 \cdot 10^{-7} \div 4 \cdot 10^{-6}$ eV. This constraint is about ten orders of magnitude better than that obtained in this work for light ALPs (see Table 4.3).

In this case, the range of ALP masses corresponds to a macroscopic interaction range of the order of 0.1 m. At the same time, for interaction ranges smaller than 1 mm ($m_a > 10^{-3}$ eV), the constraint obtained in this thesis is orders of magnitude better. It should be noted that in the present study we consider the interaction between particles (electrons and nuclei) at the atomic rather than at the macroscopic level. A similar pattern is observed in comparison with other macroscopic experiments [208–212]. For example, the torsion pendulum Eöt-Wash experiment provides a much better constraint on $g_N^s g_e^p$ for light ALPs ($m_a < 10^{-7}$ eV), but not for heavy ones. The situation with laboratory constraints on the product $g_e^s g_e^p$ is similar: there are more stringent constraints for light ALPs from other sources. For example, from the results of work [213] follows many orders of magnitude more stringent constraint for interaction distances larger than 1 cm, which corresponds to light ALPs with masses $m_a < 10^{-6}$ eV, but not for heavy ALPs. A similar situation is observed in comparison with the spherical superconducting torsion balance experiment [214]. A compilation of various existing experimental constraints is shown in Fig. 2 of Ref. [57] and Fig. 2 of Ref. [58]. As can be seen, the combination of experimental data obtained using the HfF^+ cation [69] and the molecular parameters calculated in the present study allows one to refine the laboratory constraints on the product of the ALP interaction coupling constants for ALP masses $m_a \geq 10^{-2}$ eV.

Conclusion

In this research, new methods of quantum mechanical study of atomic-molecular systems were implemented to analyze the properties of nuclei. In the problem of the Bohr – Weisskopf correction to the hyperfine structure of neutral atoms and molecules, it was shown that the calculations can be performed using a finite Gaussian basis set, which allows the use of modern quantum-chemical software packages. For this purpose, however, separate programs have been developed to calculate the matrix elements of the finite magnetization distribution contribution to the hyperfine structure constant. The results obtained using these programs were applied to refine the magnetic moments of short-lived Tl isotopes. In the future, the method developed in this study can be applied to determine the magnetic moments of short-lived isotopes of other nuclei.

In addition, the approach developed for the calculation of the Bohr – Weisskopf correction was applied to evaluate the contribution of the finite magnetization distribution to the shielding constant of the nuclear magnetic moment in the NMR experiment with the molecular anion ReO_4^-. To the best of our knowledge, for molecular systems this effect has been evaluated for the first time simultaneously with a precision calculation of the electronic structure using the coupled cluster method. The approach developed in this study can be applied to the interpretation of other NMR experiments on the measurement of nuclear magnetic moments.

One more part of the work was the solution of the problem of isotope shifts in the optical spectra of neutral atoms. In the process of its solution, programs were developed to calculate the parameters characterizing isotope shifts and required to determine the rms charge radii of nuclei from experimental data. Using these programs, experiments with Au and Tl atoms were interpreted. At the moment, similar experiments are planned for other atoms. The method of calculation and uncertainty estimation developed in this work can be applied to the interpretation

of these experiments.

In addition to the problems described above, we considered the interpretation of molecular experiments to search for the electron EDM in terms of the ALP-mediated $\mathcal{T}$, $\mathcal{P}$-violating interactions. New methods have been developed to calculate the molecular parameters that describe these interactions. Using them, we interpreted data from the experiment on the HfF^+ molecular cation and refined constraints on the products of interaction coupling constants for intermediate-mass ALPs and heavy ALPs. The approach applied in this work can be used for the interpretation of future experiments.

Acknowledgements

The author expresses great gratitude to his supervisor Leonid Skripnikov for his comprehensive assistance and support in performing research. In addition, the author thanks A. E. Barzakh, D. E. Maison, G. Penyazkov, A. V. Oleinichenko, Yu. A. Demidov, I. A. Mitroplosky as well as the teams of the Quantum Physics and Chemistry Department of the Advanced Development Division, NRC "Kurchatov Institute" – PNPI and the Department of Quantum Mechanics of the Faculty of Physics of Saint Petersburg State University.

This work has been carried out using computing resources of the federal collective usage center Complex for Simulation and Data Processing for Mega-science Facilities at NRC "Kurchatov Institute", http://ckp.nrcki.ru/. In addition, the computing resources of the Quantum Physics and Chemistry Department of the Advanced Development Division, NRC "Kurchatov Institute" – PNPI was used to carry out some calculations. The research was supported by grants from the Russian Science Foundation (project No. 19-72-10019, No. 18-12-00227), the Russian Foundation for Basic Research (project No. 20-32-70117) and the "Basis" Foundation (project No. 21-1-2-47-2), as well as by the President of Russian Federation Grant MK-2230.2018.2.

List of abbreviations and designations

ALP	axionlike particle
HFS	hyperfine structure
QED	quantum electrodynamics
BW	Bohr – Weisskopf effect
BR	Breit – Rosenthal effect
PMD	point magnetic dipole
WS	Woods – Saxon model
UD	uniform distribution
NMR	nuclear magnetic resonance
IS	isotope shift
EDM	electric dipole moment
DHF	Dirac – Hartree – Fock method
NMS	normal mass shift
SMS	specific mass shift
SO	spin-orbit interaction
ppm	parts per million
CCSD	Coupled cluster method with single and double excitations
CCSD(T)	Coupled cluster method with single, double as well as perturbative consideration of triple excitations
CCSDT	Coupled cluster method with single, double and triple excitations
CCSDT(Q)	Coupled cluster method with single, double, triple and perturbative consideration of quadruple excitations

References

1. Search for new physics with atoms and molecules / M. S. Safronova, D. Budker, D. DeMille et al. // Rev. Mod. Phys. — 2018. — Jun. — Vol. 90. — P. 025008.
2. Porsev S. G., Beloy K., Derevianko A. Precision Determination of Electroweak Coupling from Atomic Parity Violation and Implications for Particle Physics // Phys. Rev. Lett. — 2009. — May. — Vol. 102. — P. 181601.
3. Ginges J. S. M., Volotka A. V., Fritzsche S. Ground-state hyperfine splitting for Rb, Cs, Fr, Ba^+, and Ra^+ // Phys. Rev. A. — 2017. — Vol. 96, no. 6. — P. 062502.
4. Fleig T., Skripnikov L. V. P,T-Violating and Magnetic Hyperfine Interactions in Atomic Thallium // Symmetry. — 2020. — Vol. 12, no. 4. — P. 498.
5. Ginges J. S. M., Flambaum V. V. Violations of fundamental symmetries in atoms and tests of unification theories of elementary particles // Phys. Rep. — 2004. — Vol. 397. — P. 63–154.
6. Kozlov M. G., Labzowsky L. N. Parity Violation Effects in Diatomics // J. Phys. B. — 1995. — Vol. 28, no. 9. — P. 1933–1961.
7. Quiney H. M., Skaane H., Grant I. P. Hyperfine and P,T-odd effects in YbF $^2\Sigma$ // J. Phys. B. — 1998. — Vol. 31. — P. L85–95.
8. P,T-parity violation effects in polar heavy-atom molecules / A. V. Titov, N. S. Mosyagin, A. N. Petrov et al. // Progr. Theor. Chem. Phys. — 2006. — Vol. 15. — P. 253–283.
9. Skripnikov L. V., Titov A. V. Theoretical study of ThF^+ in the search for T, P-violation effects: Effective state of a Th atom in ThF^+ and ThO compounds // Phys. Rev. A. — 2015. — Apr. — Vol. 91. — P. 042504.
10. Skripnikov L. V., Titov A. V. Theoretical study of thorium monoxide for the electron electric dipole moment search: Electronic properties of $H^3\Delta_1$ in ThO // J. Chem. Phys. — 2015. — Vol. 142, no. 2. — P. 024301.

11. Relativistic coupled-cluster calculation of the electron-nucleus scalar-pseudoscalar interaction constant W_s in YbF / A. Sunaga, M. Abe, M. Hada, B. P. Das // Phys. Rev. A. — 2016. — Apr. — Vol. 93. — P. 042507.
12. Fleig T. $\mathcal{P},\mathcal{T}$-odd and magnetic hyperfine-interaction constants and excited-state lifetime for HfF^+ // Phys. Rev. A. — 2017. — Oct. — Vol. 96. — P. 040502(R).
13. Hyperfine structure constants on the relativistic coupled cluster level with associated uncertainties / P. A. B. Haase, E. Eliav, M. Iliaš, A. Borschevsky // J. Phys. Chem. A. — 2020. — Vol. 124, no. 16. — P. 3157–3169.
14. Skripnikov L. V. Nuclear magnetization distribution effect in molecules: Ra^+ and RaF hyperfine structure // J. Chem. Phys. — 2020. — Vol. 153, no. 11. — P. 114114.
15. Search for parity- and time-and-parity–violation effects in lead monofluoride (PbF): *Ab initio* molecular study / L. V. Skripnikov, A. D. Kudashov, A. N. Petrov, A. V. Titov // Phys. Rev. A. — 2014. — Dec. — Vol. 90. — P. 064501.
16. Skripnikov L. V. Communication: Theoretical study of HfF^+ cation to search for the $\mathcal{T},\mathcal{P}$-odd interactions // J. Chem. Phys. — 2017. — Vol. 147, no. 2. — P. 021101.
17. TaN molecule as a candidate for the search for a T,P-violating nuclear magnetic quadrupole moment / L. V. Skripnikov, A. N. Petrov, N. S. Mosyagin et al. // Phys. Rev. A. — 2015. — Jul. — Vol. 92. — P. 012521.
18. Skripnikov L. V., Maison D. E., Mosyagin N. S. Scalar-pseudoscalar interaction in the francium atom // Phys. Rev. A. — 2017. — Feb. — Vol. 95. — P. 022507.
19. Zakharova A., Petrov A. $\mathcal{P},\mathcal{T}$-odd effects for the RaOH molecule in the excited vibrational state // Phys. Rev. A. — 2021. — Mar. — Vol. 103. — P. 032819.
20. Petrov Alexander, Zakharova Anna. Sensitivity of the YbOH molecule to P T-odd effects in an external electric field // Physical Review A. — 2022. —

Vol. 105, no. 5. — P. L050801.

21. Sushkov O. P., Flambaum V. V. Parity breaking effects in diatomic molecules // Sov. Phys. – JETP. — 1978. — Vol. 48. — P. 608–613.
22. Sushkov O. P., Flambaum V. V., Khriplovich I. B. Possibility of investigation of P- and T-odd nuclear forces in atomic and molecular experiments // Sov. Phys. – JETP. — 1984. — Vol. 87, no. 5. — P. 1521–1540.
23. Sensitivity of condensed-matter P-and T-violation experiments / D. Budker, S. K. Lamoreaux, A. O. Sushkov, O. P. Sushkov // Physical Review A. — 2006. — Vol. 73, no. 2. — P. 022107.
24. Towards a test of QED in investigations of the hyperfine splitting in heavy ions / V. M. Shabaev, A. N. Artemyev, V. A. Yerokhin et al. // Phys. Rev. Lett. — 2001. — Vol. 86, no. 18. — P. 3959–3962.
25. High precision hyperfine measurements in Bismuth challenge bound-state strong-field QED / J. Ullmann, Z. Andelkovic, C. Brandau et al. // Nat. Commun. — 2017. — Vol. 8. — P. 15484.
26. New Nuclear Magnetic Moment of ^{209}Bi: Resolving the Bismuth Hyperfine Puzzle / L. V. Skripnikov, S. Schmidt, J. Ullmann et al. // Phys. Rev. Lett. — 2018. — Feb. — Vol. 120. — P. 093001.
27. Stone N. J. Table of nuclear magnetic dipole and electric quadrupole moments // Table of nuclear magnetic dipole and electric quadrupole moments, INDC(NDS)–0658, International Atomic Energy Agency (IAEA). — 2014.
28. Antušek A., Repisky M. NMR absolute shielding scales and nuclear magnetic dipole moments of transition metal nuclei // PCCP. — 2020. — Vol. 22. — P. 7065–7076.
29. Nuclear magnetic dipole moment of ^{209}Bi from NMR experiments / A. Antušek, M. Repisky, M. Jaszuński et al. // Phys. Rev. A. — 2018. — Nov. — Vol. 98. — P. 052509.
30. Persson J. R. Extraction of hyperfine anomalies without precise values of the

nuclear magnetic dipole moment // Eur. Phys. J. A. — 1998. — May. — Vol. 2, no. 1. — P. 3–4.

31. Cheal B., Flanagan K. T. Progress in laser spectroscopy at radioactive ion beam facilities // J. Phys. G: Nucl. Part. Phys. — 2010. — Vol. 37, no. 11. — P. 113101.
32. The nuclear magnetic moment of ^{208}Bi and its relevance for a test of bound-state strong-field QED / S. Schmidt, J. Billowes, M. L. Bissell et al. // Phys. Lett. B. — 2018. — Vol. 779. — P. 324 – 330.
33. Hyperfine structure anomaly and magnetic moments of neutron deficient Tl isomers with I= 9/2 / A. E. Barzakh, L. Kh. Batist, D. V. Fedorov et al. // Phys. Rev. C. — 2012. — Vol. 86, no. 1. — P. 014311.
34. Prosnyak S. D., Maison D. E., Skripnikov L. V. Hyperfine structure in thallium atom: Study of nuclear magnetization distribution effects // J. Chem. Phys. — 2020. — Vol. 152, no. 4. — P. 044301.
35. Roberts B. M., Ginges J. S. M. Nuclear Magnetic Moments of Francium-207–213 from Precision Hyperfine Comparisons // Phys. Rev. Lett. — 2020. — Aug. — Vol. 125. — P. 063002.
36. Hyperfine anomaly in gold and magnetic moments of $I^\pi = 11/2^-$ gold isomers / A. E. Barzakh, D. Atanasov, A. N. Andreyev et al. // Phys. Rev. C. — 2020. — Mar. — Vol. 101. — P. 034308.
37. Prosnyak S. D., Skripnikov L. V. Effect of nuclear magnetization distribution within the Woods-Saxon model: Hyperfine splitting in neutral Tl // Phys. Rev. C. — 2021. — Mar. — Vol. 103. — P. 034314.
38. Unexpectedly large charge radii of neutron-rich calcium isotopes / R. F. Garcia Ruiz, M. L. Bissell, K. Blaum et al. // Nat. Phys. — 2016. — Vol. 12, no. 6. — P. 594–598.
39. Measurement and microscopic description of odd–even staggering of charge radii of exotic copper isotopes / R. P. De Groote, J. Billowes, C. L. Binnersley

et al. // Nat. Phys. — 2020. — Vol. 16, no. 6. — P. 620–624.

40. Charge radii of exotic potassium isotopes challenge nuclear theory and the magic character of N= 32 / Á Koszorús, X. F. Yang, W. G. Jiang et al. // Nat. Phys. — 2021. — Vol. 17, no. 4. — P. 439–443.
41. Laser Spectroscopy of Neutron-Rich ^{207,208}Hg Isotopes: Illuminating the Kink and Odd-Even Staggering in Charge Radii across the $N = 126$ Shell Closure / T. Day Goodacre, A. V. Afanasjev, A. E. Barzakh et al. // Phys. Rev. Lett. — 2021. — Jan. — Vol. 126. — P. 032502.
42. Heyde K., Wood J. L. Nuclear shapes: from earliest ideas to multiple shape coexisting structures // Physica Scripta. — 2016. — Vol. 91, no. 8. — P. 083008.
43. Sudden change in the nuclear charge distribution of very light mercury isotopes / J. Bonn, G. Huber, H. J. Kluge et al. // Phys. Lett. B. — 1972. — Vol. 38, no. 5. — P. 308–311.
44. Isotope shift of ^{182}Hg and an update of nuclear moments and charge radii in the isotope range ^{181}Hg – ^{206}Hg / G. Ulm, S. K. Bhattacherjee, P. Dabkiewicz et al. // Zeitschrift für Physik A Atomic Nuclei. — 1986. — Vol. 325. — P. 247–259.
45. Characterization of the shape-staggering effect in mercury nuclei / B. A. Marsh, T. Day Goodacre, S. Sels et al. // Nature Physics. — 2018. — Vol. 14, no. 12. — P. 1163–1167.
46. Shape staggering of midshell mercury isotopes from in-source laser spectroscopy compared with density-functional-theory and Monte Carlo shell-model calculations / S. Sels, T. Day Goodacre, B. A. Marsh et al. // Phys. Rev. C. — 2019. — Apr. — Vol. 99. — P. 044306.
47. Charge Radius of Neutron-Deficient ^{54}Ni and Symmetry Energy Constraints Using the Difference in Mirror Pair Charge Radii / S. V. Pineda, K. König, Dominic M. Rossi et al. // Phys. Rev. Lett. — 2021. — Vol. 127, no. 18. — P. 182503.

48. Angeli I., Marinova K. P. Table of experimental nuclear ground state charge radii: An update // At. Data Nucl. Data Tables. — 2013. — Vol. 99, no. 1. — P. 69 – 95.
49. Peccei R. D., Quinn Helen R. CP Conservation in the Presence of Pseudoparticles // Phys. Rev. Lett. — 1977. — Jun. — Vol. 38. — P. 1440–1443.
50. Wilczek F. Problem of Strong $\mathcal{P}$ and $\mathcal{T}$ Invariance in the Presence of Instantons // Phys. Rev. Lett. — 1978. — Vol. 40, no. 5. — P. 279.
51. Weinberg S. A new light boson? // Phys. Rev. Lett. — 1978. — Vol. 40, no. 4. — P. 223.
52. Svrcek P., Witten E. Axions in string theory // J. High Energy Phys. — 2006. — Vol. 2006, no. 06. — P. 051.
53. String axiverse / A. Arvanitaki, S. Dimopoulos, S. Dubovsky et al. // Phys. Rev. D. — 2010. — Vol. 81, no. 12. — P. 123530.
54. Abbott L. F., Sikivie P. A cosmological bound on the invisible axion // Phys. Lett. B. — 1983. — Vol. 120, no. 1-3. — P. 133–136.
55. Preskill J., Wise M. B., Wilczek F. Cosmology of the invisible axion // Phys. Lett. B. — 1983. — Vol. 120, no. 1-3. — P. 127–132.
56. Dine M., Fischler W. The not-so-harmless axion // Phys. Lett. B. — 1983. — Vol. 120, no. 1-3. — P. 137–141.
57. O'Hare C. A. J., Vitagliano E. Cornering the axion with CP-violating interactions // Phys. Rev. D. — 2020. — Dec. — Vol. 102. — P. 115026.
58. Stadnik Y. V., Dzuba V. A., Flambaum V. V. Improved Limits on Axionlike-Particle-Mediated P,T-Violating Interactions between Electrons and Nucleons from Electric Dipole Moments of Atoms and Molecules // Phys. Rev. Lett. — 2018. — Jan. — Vol. 120. — P. 013202. — see also https://arxiv.org/abs/1708.00486v3 (2020).
59. Rosenthal J. E., Breit G. The isotope shift in hyperfine structure // Phys. Rev. — 1932. — Vol. 41, no. 4. — P. 459.

60. Bohr A., Weisskopf V. F. The influence of nuclear structure on the hyperfine structure of heavy elements // Phys. Rev. — 1950. — Vol. 77, no. 1. — P. 94.
61. Sen'kov R. A., Dmitriev V. F. Nuclear magnetization distribution and hyperfine splitting in Bi^{82+} ion // Nucl. Phys. A. — 2002. — Vol. 706, no. 3. — P. 351 – 364.
62. Hyperfine Structure of ^{67}Ga and ^{72}Ga / V. J. Ehlers, Y. Kabasakal, H. A. Shugart, O. Tezer // Phys. Rev. — 1968. — Vol. 176, no. 1. — P. 25.
63. Isotope shift factors for the Cd^+ $5s\,^2S_{1/2} \rightarrow 5p\,^2P_{3/2}$ transition and determination of Cd nuclear charge radii / J. Z. Han, C. Pan, K. Y. Zhang et al. // Phys. Rev. Res. — 2022. — Jul. — Vol. 4. — P. 033049.
64. Large Shape Staggering in Neutron-Deficient Bi Isotopes / A. Barzakh, A. N. Andreyev, C. Raison et al. // Phys. Rev. Lett. — 2021. — Nov. — Vol. 127. — P. 192501.
65. Otten E. W. Nuclear Radii and Moments of Unstable Isotopes // Treatise on Heavy Ion Science: Volume 8: Nuclei Far From Stability / Ed. by D. Allan Bromley. — Boston, MA : Springer US, 1989. — P. 517–638. — ISBN: 978-1-4613-0713-6.
66. Salpeter E. E. Some atomic effects of an electronic electric dipole moment // Phys. Rev. — 1958. — Vol. 112, no. 5. — P. 1642–1648.
67. Sandars P. G. H. The electric dipole moment of an atom // Phys. Lett. — 1965. — Vol. 14, no. 3. — P. 194–196.
68. Flambaum V. V. Electron electric dipole moment enhancement in heavy atoms // Yad. Fiz. — 1976. — Vol. 24, no. 2. — P. 383–386.
69. An improved bound on the electron's electric dipole moment / T. S. Roussy, L. Caldwell, T. Wright et al. // Science. — 2023. — Vol. 381, no. 6653. — P. 46–50.
70. Electronic structure of the ytterbium monohydroxide molecule to search for axionlike particles / D. E. Maison, V. V. Flambaum, N. R. Hutzler, L. V. Skrip-

nikov // Phys. Rev. A. — 2021. — Feb. — Vol. 103. — P. 022813.

71. Axion-mediated electron–electron interaction in ytterbium monohydroxide molecule / D. E. Maison, L. V. Skripnikov, A. V. Oleynichenko, A. V. Zaitsevskii // J. Chem. Phys. — 2021. — Vol. 154, no. 22. — P. 224303.
72. Maison D. E., Skripnikov L. V. Static electric dipole moment of the francium atom induced by axionlike particle exchange // Phys. Rev. A. — 2022. — Mar. — Vol. 105. — P. 032813.
73. Peccei Roberto D. The Strong CP Problem and Axions // Axions: Theory, Cosmology, and Experimental Searches / Ed. by M. Kuster, G. Raffelt, B. Beltrán. — Berlin, Heidelberg : Springer Berlin Heidelberg, 2008. — P. 3–17.
74. Adams C. B., Aggarwal N., Agrawal A. et al. Axion Dark Matter. — 2023. — 2203.14923.
75. Kim J. E., Carosi G. Axions and the strong CP problem // Rev. Mod. Phys. — 2010. — Mar. — Vol. 82. — P. 557–601.
76. Kelly K. J., Kumar S., Liu Z. Heavy axion opportunities at the DUNE near detector // Phys. Rev. D. — 2021. — May. — Vol. 103. — P. 095002.
77. Giannotti M., Nita R., Welch E. Phenomenological Implications of Heavy Axion Models // AIP Conf. Proc. — 2010. — Vol. 1274, no. 1. — P. 20–25.
78. Certificate of state registration of the computer program No. 2019613002 Russian Federation. Program for calculation of matrix elements of the Bohr – Weisskopf correction of the hyperfine splitting in atoms in the model of a uniformly magnetized nucleus : No. 2019611924 : submitted 27.02.2019 : published 05.03.2019, Bull. No. 3 / Prosnyak S. D. ; Right holder NRC “Kurchatov Institute” – PNPI. – Registered in the Register of computer programs.
79. Certificate of state registration of the computer program No. 2020666971 Russian Federation. Program for calculation of matrix elements of the magnetization distribution correction to the hyperfine structure of heavy

atoms in the one-particle nucleus model with Woods – Saxon potential : No. 2020666553 : submitted 07.12.2020 : published 18.12.2020, Bull. No. 12 / Prosnyak S. D. ; Right holder NRC "Kurchatov Institute" – PNPI. – Registered in the Register of computer programs.

80. Magnetic moments of thallium isotopes in the vicinity of magic N= 126 / Z. Yue, A. N. Andreyev, A. E. Barzakh et al. // Phys. Lett. B. — 2024. — Vol. 849. — P. 138452.
81. Skripnikov L. V., Prosnyak S. D. Refined nuclear magnetic dipole moment of rhenium: ^{185}Re and ^{187}Re // Phys. Rev. C. — 2022. — Vol. 106, no. 5. — P. 054303.
82. Refined theoretical values of field and mass isotope shifts in thallium to extract charge radii of Tl isotopes / G. Penyazkov, S. D. Prosnyak, A. E. Barzakh, L. V. Skripnikov // J. Chem. Phys. — 2023. — Vol. 158, no. 11.
83. Certificate of state registration of the computer program No. 2024610108 Russian Federation. Program for calculation of matrix elements of normal mass shift operator : No. 2023688619 : submitted 18.12.2023 : published 10.01.2024, Bull. No. 1 / Prosnyak S. D. ; Right holder NRC "Kurchatov Institute" – PNPI. – Registered in the Register of computer programs.
84. Certificate of state registration of the computer program No. 2024612074 Russian Federation. Program for calculating the specific mass shift correction to the nuclear recoil operator : No. 2023688647 : submitted 18.12.2023 : published 29.01.2024, Bull. No. 2 / Prosnyak S. D. ; Right holder NRC "Kurchatov Institute" – PNPI. – Registered in the Register of computer programs.
85. Deformation versus Sphericity in the Ground States of the Lightest Gold Isotopes / J. G. Cubiss, A. N. Andreyev, A. E. Barzakh et al. // Phys. Rev. Lett. — 2023. — Nov. — Vol. 131. — P. 202501.
86. Prosnyak S. D., Maison D. E., Skripnikov L. V. Updated Constraints

on $\mathcal{T}$,$\mathcal{P}$-Violating Axionlike-Particle-Mediated Electron-Electron and Electron-Nucleus Interactions from HfF^+ Experiment // Symmetry. — 2023. — Vol. 15, no. 5. — P. 1043.

87. Prosnyak S. D., Skripnikov L. V. Axion-mediated electron-nucleus and electron-electron interactions in the barium monofluoride molecule // Physical Review A. — 2024. — Vol. 109, no. 4. — P. 042821.
88. Saue T., Jensen H. J. A. Quaternion symmetry in relativistic molecular calculations: The Dirac–Hartree–Fock method // J. Chem. Phys. — 1999. — Vol. 111, no. 14. — P. 6211–6222.
89. Bartlett R. J., Musiał M. Coupled-cluster theory in quantum chemistry // Rev. Mod. Phys. — 2007. — Vol. 79, no. 1. — P. 291–352.
90. Visscher L., Lee T. J., Dyall K. G. Formulation and implementation of a relativistic unrestricted coupled-cluster method including noniterative connected triples // J. Chem. Phys. — 1996. — Vol. 105, no. 19. — P. 8769–8776.
91. Cohen H. D., Roothaan C. C. J. Electric dipole polarizability of atoms by the Hartree—Fock method. I. Theory for closed-shell systems // J. Chem. Phys. — 1965. — Vol. 43, no. 10. — P. S34–S39.
92. Mayer I. Simple theorems, proofs, and derivations in quantum chemistry. — Springer Science & Business Media, 2013.
93. Dyall K. G., Fægri Jr K. Introduction to relativistic quantum chemistry. — Oxford University Press, 2007.
94. Shavitt I., Bartlett R. J. Many-body methods in chemistry and physics: MBPT and coupled-cluster theory. — Cambridge university press, 2009.
95. Dyall K. G. Relativistic and nonrelativistic finite nucleus optimized double zeta basis sets for the 4p, 5p and 6p elements // Theor. Chem. Acc. — 1998. — Vol. 99, no. 6. — P. 366–371.
96. Dyall K. G. Relativistic double-zeta, triple-zeta, and quadruple-zeta basis sets for the 5d elements Hf–Hg // Theor. Chem. Acc. — 2004. — Vol. 112. —

P. 403–409.

97. Dyall K. G. Relativistic quadruple-zeta and revised triple-zeta and double-zeta basis sets for the 4p, 5p, and 6p elements // Theor. Chem. Acc. — 2006. — Vol. 115, no. 5. — P. 441–447.
98. Dyall K. G. Core correlating basis functions for elements 31–118 // Theor. Chem. Acc. — 2012. — Vol. 131, no. 5. — P. 1217.
99. Dyall K. G., Gomes A. S. P. Revised relativistic basis sets for the 5d elements Hf–Hg // Theor. Chem. Acc. — 2010. — Vol. 125. — P. 97–100.
100. Dyall K. G. Relativistic double-zeta, triple-zeta, and quadruple-zeta basis sets for the light elements H–Ar // Theor. Chem. Acc. — 2016. — Apr. — Vol. 135, no. 5. — P. 128.
101. V. Skripnikov L., S. Mosyagin N., V. Titov A. Relativistic coupled-cluster calculations of spectroscopic and chemical properties for element 120 // Chem. Phys. Lett. — 2013. — Vol. 555. — P. 79–83.
102. Principles of direct 4-component relativistic SCF: application to caesium auride / B. T Saue, K. Fægri, T. Helgaker, O. Gropen // Mol. Phys. — 1997. — Vol. 91, no. 5. — P. 937–950.
103. The DIRAC code for relativistic molecular calculations / T. Saue, R. Bast, A. S. P. Gomes et al. // J. Chem. Phys. — 2020. — Vol. 152, no. 20. — P. 204104.
104. Lindgren I., Mukherjee D. On the connectivity criteria in the open-shell coupled-cluster theory for general model spaces // Phys. Rep. — 1987. — Vol. 151, no. 2. — P. 93–127.
105. Kaldor U. The Fock space coupled cluster method: theory and application // Theor. Chim. Acta. — 1991. — Vol. 80, no. 6. — P. 427–439.
106. Multireference nature of chemistry: The coupled-cluster view / D. I. Lyakh, M. Musiał, V. F. Lotrich, R. J. Bartlett // Chem. Rev. — 2012. — Vol. 112, no. 1. — P. 182–243.

107. Relativistic Fock-Space Coupled Cluster Method: Theory and Recent Applications / E. Eliav, A. Borschevsky, A. Zaitsevskii et al. ; Ed. by Manuel Yáñez, Russell J. Boyd. — First Edition edition. — Oxford : Elsevier, 2024. — P. 79–93. — ISBN: 978-0-12-823256-9.

108. DIRAC, a relativistic ab initio electronic structure program, Release DIRAC15 (2015), written by R. Bast, T. Saue, L. Visscher, and H. J. Aa. Jensen, with contributions from V. Bakken, K. G. Dyall, S. Dubillard, U. Ekstroem, E. Eliav, T. Enevoldsen, E. Fasshauer, T. Fleig, O. Fossgaard, A. S. P. Gomes, T. Helgaker, J. Henriksson, M. Ilias, Ch. R. Jacob, S. Knecht, S. Komorovsky, O. Kullie, J. K. Laerdahl, C. V. Larsen, Y. S. Lee, H. S. Nataraj, M. K. Nayak, P. Norman, G. Olejniczak, J. Olsen, Y. C. Park, J. K. Pedersen, M. Pernpointner, R. Di Remigio, K. Ruud, P. Salek, B. Schimmelpfennig, J. Sikkema, A. J. Thorvaldsen, J. Thyssen, J. van Stralen, S. Villaume, O. Visser, T. Winther, and S. Yamamoto (see http://www.diracprogram.org).

109. MRCC. — M. Kállay, P. R. Nagy, D. Mester, Z. Rolik, G. Samu, J. Csontos, J. Csóka, P. B. Szabó, L. Gyevi-Nagy, B. Hégely, I. Ladjánszki, L. Szegedy, B. Ladóczki, K. Petrov, M. Farkas, P. D. Mezei, and á. Ganyecz: The MRCC program system: Accurate quantum chemistry from water to proteins, J. Chem. Phys. 152, 074107 (2020); MRCC, a quantum chemical program suite written by M. Kállay, P. R. Nagy, D. Mester, Z. Rolik, G. Samu, J. Csontos, J. Csóka, P. B. Szabó, L. Gyevi-Nagy, B. Hégely, I. Ladjánszki, L. Szegedy, B. Ladóczki, K. Petrov, M. Farkas, P. D. Mezei, and Á. Ganyecz. See www.mrcc.hu.

110. Kállay M., Surján P. R. Higher excitations in coupled-cluster theory // J. Chem. Phys. — 2001. — Vol. 115, no. 7. — P. 2945–2954.

111. Kállay M., Szalay P. G., Surján P. R. A general state-selective multireference coupled-cluster algorithm // J. Chem. Phys. — 2002. — Vol. 117, no. 3. — P. 980–990.

112. Oleynichenko A. V., Zaitsevskii A., Eliav E. Towards high performance rel-

ativistic electronic structure modelling: the EXP-T program package // Supercomputing / Ed. by Vladimir Voevodin, Sergey Sobolev. — Vol. 1331. — Cham : Springer International Publishing, 2020. — P. 375–386.

113. Oleynichenko A. V., Zaitsevskii A., Eliav E. — 2021. — EXP-T, an extensible code for Fock space relativistic coupled cluster calculations (see `http://www.qchem.pnpi.spb.ru/expt`).
114. Tupitsyn I. I., Deyneka G. B., Bratzev V. F. HFD. — 1977–2002. — HFD, a program for atomic finite-difference four-component Dirac-Hartree-Fock calculations on the base of the HFD code [116].
115. Tupitsyn I. I. HFDB. — 2003. — HFDB, a program for atomic finite-difference four-component Dirac-Hartree-Fock-Breit calculations written on the base of the HFD code [116].
116. Bratzev V. F., Deyneka G. B., Tupitsyn I. I. Application of the Hartree-Fock method to calculation of relativistic atomic wave functions // Bull. Acad. Sci. USSR, Phys. Ser. — 1977. — Vol. 41, no. 12. — P. 173–182.
117. Gustavsson M. G. H., Forssén Christian, Pendrill Ann Marie Mårtensson. Thallium hyperfine anomaly // Hyperfine Interactions. — 2000. — Vol. 127, no. 1-4. — P. 347–352.
118. Ground-state hyperfine splitting of high-Z hydrogenlike ions / V. M. Shabaev, M. Tomaselli, T. Kühl et al. // Phys. Rev. A. — 1997. — Vol. 56, no. 1. — P. 252.
119. Lurio A., Prodell A. G. Hfs Separations and Hfs Anomalies in the $^2P_{\frac{1}{2}}$ State of Ga^{69}, Ga^{71}, Tl^{203}, and Tl^{205} // Phys. Rev. — 1956. — Vol. 101, no. 1. — P. 79.
120. Gould G. hfs Separations and hfs Anomaly in the $6^2P_{\frac{3}{2}}$ Metastable Level of Tl^{203} and Tl^{205} // Phys. Rev. — 1956. — Vol. 101, no. 6. — P. 1828.
121. Shabaev V. M. Hyperfine structure of hydrogen-like ions // J. Phys. B. — 1994. — Vol. 27, no. 24. — P. 5825.

122. Pyykkö P., Pajanne E., Inokuti M. Hydrogen-like relativistic corrections for electric and magnetic hyperfine integrals // Int. J. Quantum Chem. — 1973. — Vol. 7, no. 4. — P. 785–806.

123. Ionesco-Pallas N. J. Nuclear Magnetic Moments from Hyperfine Structure Data // Phys. Rev. — 1960. — Vol. 117, no. 2. — P. 505.

124. Woods R. D., Saxon D. S. Diffuse surface optical model for nucleon-nuclei scattering // Phys. Rev. — 1954. — Vol. 95, no. 2. — P. 577.

125. Rost E. Proton shell-model potentials for lead and the stability of superheavy nuclei // Phys. Lett. B. — 1968. — Vol. 26, no. 4. — P. 184–187.

126. Bohr A. On the Quantization of Angular Momenta in Heavy Nuclei // Phys. Rev. — 1951. — Jan. — Vol. 81. — P. 134–138.

127. Le Bellac M. Hyperfine structure of μ-mesic atoms // Nuclear Physics. — 1963. — Vol. 40. — P. 645–655.

128. Calculation of Francium Hyperfine Anomaly / E. A. Konovalova, Y. A. Demidov, M. G. Kozlov, A. E. Barzakh // Atoms. — 2018. — Vol. 6, no. 3. — P. 39.

129. Zherebtsov O. M., Shabaev V. M. Higher order interelectronic-interaction correctionsto the ground-state hyperfine splitting in lithiumlike ions // Can. J. Phys. — 2000. — Vol. 78, no. 7. — P. 701–709.

130. Tupitsyn I. I., Loginov A. V., Shabaev V. M. Calculations of hyperfine splitting constants taking into account the volume distribution of the nuclear magnetic moment. I. Computational procedure as applied to hydrogen-like ions // Opt. Spectrosc. — 2002. — Vol. 93, no. 3. — P. 357–367.

131. Ground-state hyperfine structure of H-, Li-, and B-like ions in the intermediate-Z region / A. V. Volotka, D. A. Glazov, I. I. Tupitsyn et al. // Phys. Rev. A. — 2008. — Dec. — Vol. 78. — P. 062507.

132. Effects of finite size nuclei in relativistic four-component calculations of hyperfine structure / E. Malkin, M. Repiský, S. Komorovský et al. // J. Chem.

Phys. — 2011. — Vol. 134, no. 4. — P. 044111.

133. Roberts B. M., Ginges J. S. M. Hyperfine anomaly in heavy atoms and its role in precision atomic searches for new physics // Phys. Rev. A. — 2021. — Aug. — Vol. 104. — P. 022823.
134. Sapirstein J., Cheng K. T. Calculation of radiative corrections to hyperfine splittings in the neutral alkali metals // Phys. Rev. A. — 2003. — Feb. — Vol. 67. — P. 022512.
135. Calculation of thallium hyperfine anomaly / E. A. Konovalova, M. G. Kozlov, Yu. A. Demidov, A. E. Barzakh // Rad. Appl. — 2017. — Vol. 2. — P. 181–185. — URL: arXiv:1703.10048.
136. Ginges J. S. M., Volotka A. V. Testing atomic wave functions in the nuclear vicinity: The hyperfine structure with empirically deduced nuclear and quantum electrodynamic effects // Phys. Rev. A. — 2018. — Vol. 98, no. 3. — P. 032504.
137. Kozlov M. G., Porsev S. G., Johnson W. R. Parity nonconservation in thallium // Phys. Rev. A. — 2001. — Vol. 64, no. 5. — P. 052107.
138. Changes in the mean-square charge radii and magnetic moments of neutron-deficient Tl isotopes / A. E. Barzakh, L. Kh. Batist, D. V. Fedorov et al. // Phys. Rev. C. — 2013. — Vol. 88, no. 2. — P. 024315.
139. Magnetic moment of ^{207}Pb and the hyperfine splitting of $^{207}Pb^{81+}$ / V. Fella, L. V. Skripnikov, W. Nörtershäuser et al. // Phys. Rev. Res. — 2020. — Mar. — Vol. 2. — P. 013368.
140. Kállay M., Gauss J. Approximate treatment of higher excitations in coupled-cluster theory // J. Chem. Phys. — 2005. — Vol. 123, no. 21. — P. 214105.
141. Skripnikov L. V. Combined 4-component and relativistic pseudopotential study of ThO for the electron electric dipole moment search // J. Chem. Phys. — 2016. — Vol. 145, no. 21. — P. 214301.
142. Visscher L., Dyall K. G. Dirac–Fock atomic electronic structure calculations

using different nuclear charge distributions // At. Data Nucl. Data Tables. — 1997. — Vol. 67, no. 2. — P. 207–224.

143. Hyperfine structure of hydrogenlike thallium isotopes / Peter Beiersdorfer, Steven B Utter, Keith L Wong et al. // Phys. Rev. A. — 2001. — Vol. 64, no. 3. — P. 032506.
144. Hyperfine structure of heavy hydrogen-like ions / P. Beiersdorfer, J. R. Crespo López-Urrutia, S. B. Utter et al. // Nuclear Instruments and Methods in Physics Research Section B: Beam Interactions with Materials and Atoms. — 2003. — Vol. 205. — P. 62–65.
145. Shabaev V. M. (private communication) // private communication. — 2019.
146. Vacuum-polarization corrections to the hyperfine splitting in heavy ions and to the nuclear magnetic moments / A. N. Artemyev, V. M. Shabaev, G. Plunien et al. // Phys. Rev. A. — 2001. — Vol. 63, no. 6. — P. 062504.
147. Mårtensson-Pendrill Ann-Marie. Magnetic moment distributions in Tl nuclei // Phys. Rev. Lett. — 1995. — Vol. 74, no. 12. — P. 2184.
148. Reappraisal of the electric dipole moment enhancement factor for thallium / H. S. Nataraj, B. K. Sahoo, B. P. Das, D. Mukherjee // Phys. Rev. Lett. — 2011. — Vol. 106, no. 20. — P. 200403.
149. Safronova U. I., Safronova M. S., Johnson W. R. Excitation energies, hyperfine constants, $E1$, $E2$, and $M1$ transition rates, and lifetimes of $6s^2nl$ states in Tl I and Pb II // Phys. Rev. A. — 2005. — Vol. 71, no. 5. — P. 052506.
150. Absolute frequency measurement of the $6P_{1/2} \rightarrow 7S_{1/2}$ transition in thallium / Tzu-Ling Chen, Isaac Fan, Hsuan-Chen Chen et al. // Phys. Rev. A. — 2012. — Vol. 86, no. 5. — P. 052524.
151. Hyperfine Anomaly Measurements in Francium Isotopes and the Radial Distribution of Neutrons / J. S. Grossman, L. A. Orozco, M. R. Pearson et al. // Phys. Rev. Lett. — 1999. — Aug. — Vol. 83. — P. 935–938.
152. QED Theory of the Nuclear Magnetic Shielding in Hydrogenlike Ions /

V. A. Yerokhin, K. Pachucki, Z. Harman, C. H. Keitel // Phys. Rev. Lett. — 2011. — Jul. — Vol. 107. — P. 043004.

153. QED calculation of the nuclear magnetic shielding for hydrogenlike ions / V. A. Yerokhin, K. Pachucki, Z. Harman, C. H. Keitel // Phys. Rev. A. — 2012. — Feb. — Vol. 85. — P. 022512.
154. Relativistic calculations of the isotope shifts in highly charged Li-like ions / N. A. Zubova, Y. S. Kozhedub, V. M. Shabaev et al. // Phys. Rev. A. — 2014. — Dec. — Vol. 90. — P. 062512.
155. Laser spectroscopy for the study of exotic nuclei / X. F. Yang, S. J. Wang, S. G. Wilkins, R. F. Garcia Ruiz // Prog. Part. Nucl. Phys. — 2022. — P. 104005.
156. Charge radii of radium isotopes / L. W. Wansbeek, S. Schlesser, B. K. Sahoo et al. // Phys. Rev. C. — 2012. — Jul. — Vol. 86. — P. 015503.
157. Shabaev V. M. Mass corrections in a strong nuclear field // Theor. Math. Phys. — 1985. — Vol. 63, no. 3. — P. 588.
158. Palmer C. W. P. Reformulation of the theory of the mass shift // J. Phys. B. — 1987. — nov. — Vol. 20, no. 22. — P. 5987–5996.
159. Shabaev V. M. Nuclear recoil effect in the relativistic theory of multiply charged ions // Sov. J. Nucl. Phys. — 1988. — Vol. 47. — P. 69.
160. Shabaev V. M., Artemyev A. N. Relativistic nuclear recoil corrections to the energy levels of multicharged ions // J. Phys. B: Atom. Mol. Phys. — 1994. — Vol. 27, no. 7. — P. 1307.
161. Dyall K. G. Relativistic double-zeta, triple-zeta, and quadruple-zeta basis sets for the 4s, 5s, 6s, and 7s elements // J. Phys. Chem. A. — 2009. — Vol. 113, no. 45. — P. 12638–12644.
162. The use of gaussian nuclear charge distributions for the calculation of relativistic electronic wavefunctions using basis set expansions / O. Visser, P. J. C. Aerts, D. Hegarty, W. C. Nieuwpoort // Chem. Phys. Lett. — 1987. —

Vol. 134, no. 1. — P. 34–38.

163. Johnson W. R., Blundell S. A., Sapirstein J. Finite basis sets for the Dirac equation constructed from B splines // Phys. Rev. A. — 1988. — Jan. — Vol. 37. — P. 307–315.

164. Observation of strongly deformed ground-state configurations in ^{184}Au and ^{183}Au by laser spectroscopy / U. Krönert, S. Becker, G. Bollen et al. // Zeitschrift für Physik A Atomic Nuclei. — 1988. — Vol. 331, no. 4. — P. 521–522.

165. Shape coexistence in ^{187}Au studied by laser spectroscopy / A. E. Barzakh, D. Atanasov, A. N. Andreyev et al. // Phys. Rev. C. — 2020. — Vol. 101, no. 6. — P. 064321.

166. Changes in mean-squared charge radii and magnetic moments of $^{179-184}$Tl measured by in-source laser spectroscopy / A. E. Barzakh, A. N. Andreyev, Th. E. Cocolios et al. // Phys. Rev. C. — 2017. — Vol. 95, no. 1. — P. 014324.

167. Resonance ionization spectroscopy in a buffer gas cell with radioactive decay detection, demonstrated using ^{208}Tl / W. Lauth, H. Backe, M. Dahlinger et al. // Phys. Rev. Lett. — 1992. — Mar. — Vol. 68. — P. 1675–1678.

168. Nuclear Magnetic Moment of ^{207}Tl / R. Neugart, H. H. Stroke, S. A. Ahmad et al. // Phys. Rev. Lett. — 1985. — Oct. — Vol. 55. — P. 1559–1562.

169. Hull R. J., Stroke H. H. Hyperfine-Structure Separations, Isotope Shifts, and Nuclear Magnetic Moments of the Radioactive Isotopes Tl^{199}, Tl^{200}, Tl^{201}, Tl^{202}, and Tl^{204} // J. Opt. Soc. Am. — 1961. — Nov. — Vol. 51, no. 11. — P. 1203–1212.

170. Hermann G., Lasnitschka G., Spengler D. Hyperfine structures and level isotope shifts of the $n^2S_{1/2}$ (n= 7–12)- and $n^2D_{3/2,5/2}$ (n= 6–10)-levels of ^{203,205}Tl measured by atomic beam spectroscopy // Z. Phys. D. — 1993. — Vol. 28. — P. 127.

171. Nuclear structure of light thallium isotopes as deduced from laser spectroscopy

on a fast atom beam / J. A. Bounds, C. R. Bingham, H. K. Carter et al. // Phys. Rev. C. — 1987. — Dec. — Vol. 36. — P. 2560–2568.

172. Hyperfine Structure, Nuclear Moments, and Isotope Shifts of ^{197}Tl and ^{198}Tl / S. P. Davis, H. Kleiman, D. Goorvitch, T. Aung // J. Opt. Soc. Am. — 1966. — Nov. — Vol. 56, no. 11. — P. 1604–1606.
173. Goorvitch D., Kleiman H., Davis S. P. The isomer shift of ^{198}Tl // Nucl. Phys. — 1967. — Vol. 99, no. 1. — P. 1–5.
174. Nuclear moments and the change in the mean square charge radius of neutron deficient thallium isotopes / R. Menges, U. Dinger, N. Boos et al. // Z. Phys. A. — 1992. — Vol. 341. — P. 475.
175. Goorvitch D., Davis S. P., Kleiman H. Isotope Shift and Hyperfine Structure of the Neutron-Deficient Thallium Isotopes // Phys. Rev. — 1969. — Dec. — Vol. 188. — P. 1897–1904.
176. Nuclear spectroscopy using lasers at Oak Ridge National Laboratory: experiments with stable (past) and radioactive (future) tandem beams / H. A. Schuessler, E. C. Benck, F. Buchinger, H. K. Carter // Nucl. Instrum. Methods Phys. Res. A. — 1995. — Vol. 352, no. 3. — P. 583–587.
177. Isotope shifts in the $7s \to 8s$ transition of francium: Measurements and comparison to ab initio theory / M. R. Kalita, J. A. Behr, A. Gorelov et al. // Phys. Rev. A. — 2018. — Apr. — Vol. 97. — P. 042507.
178. Moody J. E., Wilczek F. New macroscopic forces? // Phys. Rev. D. — 1984. — Vol. 30, no. 1. — P. 130.
179. Calculation of the spin-rotational Hamiltonian including $\mathcal{P}$- and $\mathcal{P},\mathcal{T}$-odd weak interaction terms for the HgF and PbF molecules / Yu. Yu. Dmitriev, Yu. G. Khait, M. G. Kozlov et al. // Phys. Lett. A. — 1992. — Vol. 167, no. 3. — P. 280–286.
180. Boys S. F. Electronic wave functions-I. A general method of calculation for the stationary states of any molecular system // Proc. Math. Phys. Eng. Sci. —

1950. — Vol. 200, no. 1063. — P. 542–554.

181. Helgaker T., Jorgensen P., Olsen J. Molecular electronic-structure theory. — John Wiley & Sons, 2013.
182. Ten-no S. Initiation of explicitly correlated Slater-type geminal theory // Chem. Phys. Lett. — 2004. — Vol. 398, no. 1. — P. 56–61.
183. McMurchie L. E., Davidson E. R. One- and two-electron integrals over cartesian gaussian functions // J. Comput. Phys. — 1978. — Vol. 26, no. 2. — P. 218–231.
184. Obara S., Saika A. Efficient recursive computation of molecular integrals over Cartesian Gaussian functions // J. Chem. Phys. — 1986. — Vol. 84, no. 7. — P. 3963–3974.
185. Pople J. A., Hehre W. J. Computation of electron repulsion integrals involving contracted Gaussian basis functions // J. Comput. Phys. — 1978. — Vol. 27, no. 2. — P. 161–168.
186. Head-Gordon M., Pople J. A. A method for two-electron Gaussian integral and integral derivative evaluation using recurrence relations // J. Chem. Phys. — 1988. — Vol. 89, no. 9. — P. 5777–5786.
187. Gill P. M. W., Johnson B. G., Pople J. A. Two-electron repulsion integrals over Gaussian s functions // Int. J. Quantum Chem. — 1991. — Vol. 40, no. 6. — P. 745–752.
188. Hamilton T. P., Schaefer H. F. New variations in two-electron integral evaluation in the context of direct SCF procedures // Chem. Phys. — 1991. — Vol. 150, no. 2. — P. 163–171.
189. Ten-no S. An efficient algorithm for electron repulsion integrals over contracted Gaussian-type functions // Chem. Phys. Lett. — 1993. — Vol. 211, no. 2. — P. 259–264.
190. New algorithm for electron repulsion integrals oriented to the general contraction scheme / T. Yanai, K. Ishida, H. Nakano, K. Hirao // Int. J. Quantum

Chem. — 2000. — Vol. 76, no. 3. — P. 396–406.

191. Nakai H., Kobayashi M. New algorithm for the rapid evaluation of electron repulsion integrals: elementary basis algorithm // Chem. Phys. Lett. — 2004. — Vol. 388, no. 1. — P. 50–54.
192. F. Valeev E. Libint: A library for the evaluation of molecular integrals of many-body operators over Gaussian functions. — http://libint.valeyev.net/. — 2022. — version 2.8.0.
193. Dupuis M., Rys J., King H. F. Evaluation of molecular integrals over Gaussian basis functions // J. Chem. Phys. — 1976. — Vol. 65, no. 1. — P. 111–116.
194. King H. F., Dupuis M. Numerical integration using rys polynomials // J. Comput. Phys. — 1976. — Vol. 21, no. 2. — P. 144–165.
195. Rys J., Dupuis M., King H. F. Computation of electron repulsion integrals using the rys quadrature method // J. Comput. Chem. — 1983. — Vol. 4, no. 2. — P. 154–157.
196. Lindh R., Ryu U., Liu B. The reduced multiplication scheme of the Rys quadrature and new recurrence relations for auxiliary function based two-electron integral evaluation // J. Chem. Phys. — 1991. — Vol. 95, no. 8. — P. 5889–5897.
197. Ten-no S. New implementation of second-order Møller-Plesset perturbation theory with an analytic Slater-type geminal // J. Chem. Phys. — 2007. — Vol. 126, no. 1. — P. 014108.
198. Shiozaki T. Evaluation of Slater-type geminal integrals using tailored Gaussian quadrature // Chem. Phys. Lett. — 2009. — Vol. 479, no. 1-3. — P. 160–164.
199. Kumar A., Neese F., Valeev E. F. Explicitly correlated coupled cluster method for accurate treatment of open-shell molecules with hundreds of atoms // J. Chem. Phys. — 2020. — Vol. 153, no. 9. — P. 094105.
200. Size-consistent explicitly correlated triple excitation correction / M. Kállay, R. A. Horváth, L. Gyevi-Nagy, P. R. Nagy // J. Chem. Phys. — 2021. — Vol. 155, no. 3. — P. 034107.

201. Basis Set Limit CCSD(T) Energies for Extended Molecules via a Reduced-Cost Explicitly Correlated Approach / M. Kállay, R. A. Horváth, L. Gyevi-Nagy, P. R. Nagy // J. Chem. Phys. — 2023. — Vol. 19, no. 1. — P. 174–189.

202. A four-index transformation in Dirac's four-component relativistic theory / M. Abe, T. Yanai, T. Nakajima, K. Hirao // Chem. Phys. Lett. — 2004. — Vol. 388, no. 1-3. — P. 68–73.

203. Broadband velocity modulation spectroscopy of HfF^+: Towards a measurement of the electron electric dipole moment / K. C. Cossel, D. N. Gresh, L. C. Sinclair et al. // Chem. Phys. Lett. — 2012. — Vol. 546, no. 0. — P. 1 – 11.

204. Theoretical study of HfF^+ in search of the electron electric dipole moment / A. N. Petrov, N. S. Mosyagin, T. A. Isaev, A. V. Titov // Phys. Rev. A. — 2007. — Vol. 76. — P. 030501(R).

205. Petrov A. N., Mosyagin N. S., Titov A. V. Theoretical study of low-lying electronic terms and transition moments for HfF^+ for the electron EDM search // Phys. Rev. A. — 2009. — Vol. 79. — P. 012505.

206. Improved limit on the electric dipole moment of the electron / V. Andreev, D. G. Ang, D. DeMille et al. // Nature. — 2018. — Vol. 562, no. 7727. — P. 355–360.

207. Improved constraints on monopole–dipole interaction mediated by pseudo-scalar bosons / N. Crescini, C. Braggio, G. Carugno et al. // Phys. Lett. B. — 2017. — Vol. 773. — P. 677–680.

208. Preferred-frame and CP-violation tests with polarized electrons / B. R. Heckel, E. G. Adelberger, C. E. Cramer et al. // Phys. Rev. D. — 2008. — Nov. — Vol. 78. — P. 092006.

209. Search for anomalous spin-dependent forces using stored-ion spectroscopy / D. J. Wineland, J. J. Bollinger, D. J. Heinzen et al. // Phys. Rev. Lett. — 1991. — Sep. — Vol. 67. — P. 1735–1738.

210. Lee J., Almasi A., Romalis M. Improved Limits on Spin-Mass Interactions //

Phys. Rev. Lett. — 2018. — Apr. — Vol. 120. — P. 161801.

211. Improved constraints on an axion-mediated force / S. A. Hoedl, F. Fleischer, E. G. Adelberger, B. R. Heckel // Phys. Rev. Lett. — 2011. — Vol. 106, no. 4. — P. 041801.

212. Light Dark Matter Search with Ionization Signals in XENON1T / E. Aprile, J. Aalbers, F. Agostini et al. // Phys. Rev. Lett. — 2019. — Dec. — Vol. 123. — P. 251801.

213. Limits on spin-mass couplings within the axion window / A. N. Youdin, D. Krause Jr., K. Jagannathan et al. // Phys. Rev. Lett. — 1996. — Vol. 77, no. 11. — P. 2170.

214. New Constraints on Short-Range Forces Coupling Mass to Intrinsic Spin / G. D. Hammond, C. C. Speake, C. Trenkel, A. P. Patón // Phys. Rev. Lett. — 2007. — Feb. — Vol. 98. — P. 081101.